

UNICAMP

UNIVERSIDADE ESTADUAL DE
CAMPINAS

Instituto de Matemática, Estatística e
Computação Científica

GEOVAN CARLOS MENDONÇA CAMPOS

**Numerical analysis of multiscale methods for
elliptic-parabolic problems with application in
the cell dynamics during the formation of
colorectal cancer**

**Análise numérica de métodos multiescala para
problemas elípticos-parabólicos com aplicação na
dinâmica celular durante a formação do câncer
colorretal**

Campinas

2021

Geovan Carlos Mendonça Campos

**Numerical analysis of multiscale methods for
elliptic-parabolic problems with application in the cell
dynamics during the formation of colorectal cancer**

**Análise numérica de métodos multiescala para problemas
elípticos-parabólicos com aplicação na dinâmica celular
durante a formação do câncer colorretal**

Tese apresentada ao Instituto de Matemática, Estatística e Computação Científica da Universidade Estadual de Campinas como parte dos requisitos exigidos para a obtenção do título de Doutor em Matemática Aplicada.

Thesis presented to the Institute of Mathematics, Statistics and Scientific Computing of the University of Campinas in partial fulfillment of the requirements for the degree of Doctor in Applied Mathematics.

Supervisor: Giuseppe Romanazzi

Este exemplar corresponde à versão final da Tese defendida pelo aluno Geovan Carlos Mendonça Campos e orientada pelo Prof. Dr. Giuseppe Romanazzi.

Campinas

2021

Ficha catalográfica
Universidade Estadual de Campinas
Biblioteca do Instituto de Matemática, Estatística e Computação Científica
Ana Regina Machado - CRB 8/5467

C157n Campos, Geovan Carlos Mendonça, 1993-
Numerical analysis of multiscale methods for elliptic-parabolic problems with application in the cell dynamics during the formation of colorectal cancer / Geovan Carlos Mendonça Campos. – Campinas, SP : [s.n.], 2021.

Orientador: Giuseppe Romanazzi.
Tese (doutorado) – Universidade Estadual de Campinas, Instituto de Matemática, Estatística e Computação Científica.

1. Modelagem multiescala. 2. Análise numérica. 3. Diferenças finitas. 4. Cólon (Anatomia) - Câncer. 5. Método dos elementos finitos. I. Romanazzi, Giuseppe, 1976-. II. Universidade Estadual de Campinas. Instituto de Matemática, Estatística e Computação Científica. III. Título.

Informações para Biblioteca Digital

Título em outro idioma: Análise numérica de métodos multiescala para problemas elípticos-parabólicos com aplicação na dinâmica celular durante a formação do câncer colorretal

Palavras-chave em inglês:

Multiscale modeling

Numerical analysis

Finite differences

Colon (Anatomy) - Cancer

Finite element method

Área de concentração: Matemática Aplicada

Títuloção: Doutor em Matemática Aplicada

Banca examinadora:

Giuseppe Romanazzi [Orientador]

José Augusto Mendes Ferreira

Eduardo Cardoso de Abreu

Maicon Ribeiro Correa

Cassio Machiaveli Oishi

Data de defesa: 18-01-2021

Programa de Pós-Graduação: Matemática Aplicada

Identificação e informações acadêmicas do(a) aluno(a)

- ORCID do autor: <https://orcid.org/0000-0003-0726-4669>

- Currículo Lattes do autor: <http://lattes.cnpq.br/1022006224129557>

**Tese de Doutorado defendida em 18 de janeiro de 2021 e aprovada
pela banca examinadora composta pelos Profs. Drs.**

Prof(a). Dr(a). GIUSEPPE ROMANAZZI

Prof(a). Dr(a). JOSÉ AUGUSTO MENDES FERREIRA

Prof(a). Dr(a). EDUARDO CARDOSO DE ABREU

Prof(a). Dr(a). MAICON RIBEIRO CORREA

Prof(a). Dr(a). CASSIO MACHIAVELI OISHI

A Ata da Defesa, assinada pelos membros da Comissão Examinadora, consta no SIGA/Sistema de Fluxo de Dissertação/Tese e na Secretaria de Pós-Graduação do Instituto de Matemática, Estatística e Computação Científica.

Acknowledgements

I would first like to thank my supervisor, Professor Giuseppe Romanazzi, who gave me the opportunity to study and research this such important problem. His motivation, focus and patience have inspired me to keep researching.

I would also like to thank Professor José Augusto Ferreira for his huge contribution. It was a pleasure to be part of his research and even more to learn fascinating tools of numerical analysis. I wish continue learning with him.

In addition, I thank my family, professors and friends. In special Maria Eduarda Berton for her caring, advice and continuing support to complete this thesis.

I am extremely grateful to UNICAMP for providing a high quality teaching.

This study was financed in part by the Coordenação de Aperfeiçoamento de Pessoal de Nível Superior - Brasil (CAPES) - Finance Code 001.

*“I am the Alpha and the Omega, the First and the Last, the Beginning and the End.
(Revelation 22,13)*

Resumo

O cólon humano é propício ao desenvolvimento de câncer devido à possibilidade de ocorrerem mutações na intensa atividade de renovação celular que consiste em um alto número de divisões celulares por dia, localizadas em pequenas cavidades chamadas de criptas. O epitélio do cólon é formado por milhões de criptas e é conhecido que mutações no processo de proliferação (dentro das criptas) podem conduzir à carcinogênese. A dinâmica de células colônicas pode ser modelada usando multiescalas (FIGUEIREDO et al., 2013). Em particular, nós podemos usar uma cripta de referência como um domínio microescala, que é periodicamente distribuído em um domínio macroescala, onde este é associado a uma porção do epitélio do cólon. O modelo final resulta em um sistema de EDPs acoplado formado por um problema elítico e um outro parabólico nos quais as variáveis são a densidade de células proliferativas e a pressão celular exercida.

Apresentamos o processo de homogenização desse sistema de equações supondo a existência de uma expansão assintótica da solução e das demais funções que compõem o problema, veja (CIORANESCU; DONATO, 1999). Aplicamos um método de resolução multiescala baseado em elementos finitos (HMM-FEM) para aproximar a solução homogenizada encontrado em alguns trabalhos como (ABDULLE, 2009; ABDULLE, 2012; ABDULLE; HUBER, 2014). No cenário onde o problema é acoplado e não linear, a implementação de métodos se torna mais robusta computacionalmente, portanto optamos por resolver primeiro o problema elítico e depois o parabólico como uma forma de amenizar essa complexidade.

Em uma única escala, estudamos estabilidade e convergência de um esquema supraconvergente baseado em diferenças finitas centradas para malhas não uniformes que é equivalente à um esquema baseado em elementos finitos. Em um cenário mais simplificado, estudamos convergência e estabilidade do método apresentado. Já para um caso mais geral provamos, para $s = 1, 2$, ordem $O(h^s)$ de convergência para a solução e gradiente se a solução exata está em $H^{1+s}(\Omega)$, veja (FERREIRA; BARBEIRO; GRIGORIEFF, 2005). Para o problema homogenizado, apresentamos uma estratégia supraconvergente que permite aproximar a solução do problema homogenizado acoplado, onde numericamente obtemos uma ordem de convergência quadrática. Por fim, apresentamos um método para resolver problemas multiescala usando dos bons resultados de convergência discutidos acima. Esse modelo é baseado em um problema microescala que posteriormente será usado para construir uma solução macroescala para o sistema homogenizado. Os primeiros indícios de convergência surgem dos resultados numéricos obtidos.

Palavras-chave: Método multiescala. ACF. Câncer colorretal. Simulação numérica.

Abstract

The human colon is prone to develop a cancer due to its cell renovation that consists in a large number of cell divisions per day located in small cavities of the colon epithelium, called crypts. The colon epithelium is filled by millions of crypts, and it is known that mutations in the cell proliferation process (inside the crypts) can lead to the carcinogenesis. Colonic cell proliferation can be modeled by using multiscales ([FIGUEIREDO et al., 2013](#)). In particular, we can use a reference crypt, as a microscale domain, that is periodically distributed in a macroscale domain that is a portion of the colon epithelium. The final model results in a coupled system formed by an elliptic and parabolic equations whose unknowns are the proliferative cell density and the exerted cell pressure.

We present a homogenization for the final PDE model where it is supposed to exist a asymptotic expansion for the exact solution of the problem, see ([CIORANESCU; DONATO, 1999](#)). We apply a multiscale method based on finite elements (HMM-FEM) to approximate the homogenized solution as in ([ABDULLE, 2009](#); [ABDULLE, 2012](#); [ABDULLE; HUBER, 2014](#)). The coupling and the non-linearity of the system implies a more complex implementation and increase the computational effort, thus we first solve the elliptic problem and then the parabolic one to make it easier. As we can see later, that strategy does not affect the convergence rates.

Furthermore, in a single scale, we study a supraconvergent method based on centered finite difference to nonuniform mesh which is equivalent to a fully discrete linear finite element method. Firstly we study convergence and stability of a simpler model and then we prove for $s = 1, 2$ order $O(h^s)$ convergence of solution and gradient if the exact solution is in $H^{1+s}(\Omega)$, see ([FERREIRA; BARBEIRO; GRIGORIEFF, 2005](#)). Numerical results illustrate the methods above. For the multiscale problem, we present a supraconvergent scheme which provides approximations to the coupled system with quadratic convergence rate. This is done by solving the homogenized problem with the supraconvergent method discussed before. Our last contribution is a multiscale model in development which can be useful to solve multiscale problems with the good convergence rates discussed above. That model is based on solving a microscale problem that will be used to construct a macroscale solution for the homogenized system. Numerical results for this model suggest a supraconvergence.

Keywords: Multiscale method. ACF. Colorectal cancer. Numerical simulation.

List of Figures

Figure 1	– Sketch of the two-dimensional model for two epithelial cell populations growing on the surface of a cylindrical crypt, height h and radius βh . The volume fractions of each population are separated by the boundary $Y = C(X, T)$ with normal $N(X, T)$.	20
Figure 2	– Shape of the colonic crypt at different times: $t = 0, 1, 2, 5,$ and 10 respectively.	23
Figure 3	– Colon anatomy	26
Figure 4	– Distribution and shape of crypts. (4(a) can be found in (FIGUEIREDO et al., 2016) and 4(b) in UWA Blue Histology. Copyright Lutz Slomianka 1998-2009.)	27
Figure 5	– Stem cells and its mutations	28
Figure 6	– ACF pictured in a colonoscopy image. The dark blue regions are clusters of deformed and enlarged crypts, called ACF, in the colon epithelium, that appear in the first stage of colon carcinogenesis	29
Figure 7	– A single crypt represented as a two-dimensional surface in \mathbb{R}^3 .	30
Figure 8	– This figure show how the crypts are periodically distributed in our modeled colon epithelium in three dimensions.	30
Figure 9	– 2D domain	34
Figure 10	– Numerical solutions of the multiscale problem.	61
Figure 11	– From top to bottom we have numerical solutions to homogenized problem at the times $t = 0.01, t = 0.04$ and $t = 0.1$.	62
Figure 12	– Convergence rates for HMM approximation (Pressure).	63
Figure 13	– Convergence rates for HMM approximation (Density).	63
Figure 14	– Initial density distribution C_0 defined in (5.54) on the crypt Γ graph of the function f defined in (5.55). Three dimensional plot of the initial density $C_0(x, y)$ in the points $(x, y, f(x, y))$. Two dimensional plot of $C_0(x, y)$ with $(x, y) \in [0, 1]^2$.	75
Figure 15	– Pressure in the points located in the line $y = 0.5$ during the numerical simulation in the time interval $[0, 1]$. Plots are referred to the times $t = 0, 0.1, 0.5, 1$.	76
Figure 16	– Pressure in the points located in the line $y = 0.5$ during the numerical simulation in the time interval $[0, 1]$. Plots are referred to the times $t = 0, 0.1, 0.5, 1$.	77
Figure 17	– Euclidean Norm for the velocity $\ v\ = \xi \ \nabla p\ $ in the points located in the line $y = 0.5$ during the numerical simulation in the time interval $[0, 1]$. Plots are referred to the times $t = 0, 0.1, 0.5, 1$.	77

Figure 18 – Triangles representation	82
Figure 19 – Convergence for ε	110
Figure 20 – Convergence rate for h	110
Figure 21 – From left to right we can see the behavior of the errors for $\varepsilon = 0.05$. . .	111
Figure 22 – From left to right we can see the behavior of the errors for $\varepsilon = 1e - 2$. .	112
Figure 23 – From left to right we can see the behavior of the errors for $\varepsilon = 1e - 3$. .	112
Figure 24 – 24(a) and 24(b) show us the graph of the exact homogenized solution and the numerical solution for pressure and density respectively ($H \sim$ $2e - 03, h = 1e - 04$).	116
Figure 25 – Images 24(a) and 24(b) respectively with zoom applied.	116
Figure 26 – Graph of the exact multiscale solution and the numerical solution for pressure and density respectively ($\varepsilon = 0.1$).	117
Figure 27 – Graph of the exact multiscale solution and the numerical solution for pressure and density respectively ($\varepsilon = 0.01$).	117

List of Tables

Table 1 – Main indicators	18
Table 2 – Main findings	18
Table 3 – Errors and rate of convergence of the HMM method	62
Table 4 – Numerical errors and convergence rates for Example 2	74
Table 5 – Numerical errors and convergence rates for Example 3	74
Table 6 – Numerical errors and convergence rates in Example 4	76
Table 7 – Numerical approximation $p, C(T = 0.01, dt = 5e - 04)$ Example 5	96
Table 8 – Numerical approximation $p, C(T = 0.01, dt = 5e - 04)$ Example 6	97
Table 9 – Numerical approximation $p, C(T = 0.01, dt = 5e - 04)$ Example 7	97
Table 10 – Numerical approximation for homogenized coefficient	105
Table 11 – Numerical approximation for homogenized coefficient	105
Table 12 – Numerical errors	108
Table 13 – Numerical errors	108
Table 14 – Convergence rate for $\varepsilon(H = h = 1e - 04)$	109
Table 15 – Convergence rate for $h(H = 1e - 04, \varepsilon = 1e - 03)$	110
Table 16 – Convergence rate for $H(h = 1e - 04, \varepsilon = 0.05)$	111
Table 17 – Convergence rate for $H(h = 1e - 04, \varepsilon = 0.01)$	112
Table 18 – Convergence rate for $H(h = 1e - 04, \varepsilon = 1e - 3)$	113
Table 19 – Convergence rate for H in $\ \cdot\ _H$ norm($h \sim 1e - 04$)	115
Table 20 – Convergence rate for H in $\ \cdot\ _{H,-}$ norm($h \sim 1e - 04$)	115
Table 21 – Convergence rate for h in $\ \cdot\ _H$ norm($H \sim 2e - 03$)	115
Table 22 – Convergence rate for h in $\ \cdot\ _{H,-}$ norm($H \sim 2e - 03$)	115
Table 23 – Convergence rate for ε in $\ \cdot\ _H$ norm($h \sim 1e - 04, H \sim 2e - 03$)	116
Table 24 – Convergence rate for ε in $\ \cdot\ _{H,-}$ norm($h \sim 1e - 04, H \sim 2e - 03$)	117
Table 25 – Convergence rate for h in $\ \cdot\ _H$ norm($\varepsilon \sim 1e - 06, H \sim 2e - 03$)	118
Table 26 – Convergence rate for h in $\ \cdot\ _H$ norm($\varepsilon \sim 1e - 06, H \sim 2e - 03$)	118
Table 27 – Convergence rate for h in $\ \cdot\ _H$ norm($\varepsilon \sim 1e - 06, h \sim 1e - 04$)	118
Table 28 – Convergence rate for h in $\ \cdot\ _H$ norm($\varepsilon \sim 1e - 06, h \sim 1e - 04$)	118
Table 29 – Numerical approximation for homogenized tensor	123

List of abbreviations and acronyms

ACF	Aberrant Crypt Foci
CRC	Colorectal Cancer
FEM	Finite Elements Method
FDM	Finite Difference Method
HMM	Heterogeneous Multiscale Method
HMM-FEM	Heterogeneous Multiscale Method based on Finite Elements

List of symbols

∇f	Gradient of a function f
u^ε	Multiscale function
u^0	Limit of the sequence $\{u^\varepsilon\}_{\varepsilon>0}$ when $\varepsilon \rightarrow 0$, Homogenized function
\mathcal{A}^ε	Multiscale tensor
\langle , \rangle	Inner product
$\langle \cdot \rangle$	Average or mean operator
\mathcal{A}^0	Homogenized tensor
D_{-x}	The discrete backward operator in x -direction
δ_x	The centered difference operator in x -direction
$\delta_x^{(1/2)}$	The centered difference operator of half step in x -direction
δ_h	The weighted centered difference operator in x -direction
$\square_{i,j}$	Square around (x_i, y_j) with sizes $(x_{i-1/2}, x_{i+1/2}) \times (y_{j-1/2}, y_{j+1/2})$
$\tilde{\square}_{i,j}$	The square $(x_{i-1}, x_i) \times (y_{j-1/2}, y_{j+1/2})$
\triangle	A triangle with a $\pi/2$ angle. In 1D it refers to an interval

Contents

1	INTRODUCTION	17
1.1	Motivation	17
1.2	Review of relevant mathematical models for cell dynamics in a colonic crypt	18
1.2.1	Continuum models for tumor growth based on two families of cells	19
1.2.2	Abnormal cell dynamics	21
1.2.3	Aberrant colonic crypt morphogenesis	22
1.3	Aims and objectives of the thesis	23
1.4	Preliminary results	24
1.5	Overview	24
2	MATHEMATICAL MODEL	25
2.1	Biological background	25
2.1.1	Colon structure	25
2.1.2	Crypts	26
2.1.3	Stem cells	27
2.1.4	Aberrant Crypt Foci (ACF) and development of adenomas	28
2.2	Mathematical model of the crypt geometry, cell proliferation and dynamics in the colonic crypts	29
2.2.1	Crypt geometry	29
2.2.2	3D periodic domain	30
2.2.3	Source terms	31
2.2.4	3D final model	31
2.2.5	Differential model in local coordinates	32
2.2.6	Properties of g and \mathcal{A}	33
2.2.7	2D periodic domain	34
2.2.8	Periodic distribution	34
2.3	Multiscale modeling	36
3	MULTISCALE PROBLEMS AND HOMOGENIZATION	37
3.1	Introduction to homogenization	38
3.2	Homogenization of elliptic equations: some results	38
3.3	Homogenization of parabolic equations: some results (PERSSON et al., 1993)	43
3.4	Homogenization of our multiscale colonic cell problem (2.21)	44
3.4.1	Elliptic equation	44

3.4.2	Parabolic equation	47
4	HETEROGENEOUS MULTISCALE METHOD(HMM)	50
4.1	The HMM framework	50
4.2	Review of HMM-FEM method	51
4.2.1	The macro solver and the needed data	51
4.3	HMM-FEM applied to our problem	53
4.3.1	Approximating \mathcal{A}^0	58
4.3.1.1	Case $\mathcal{A}^\varepsilon(x) = \mathcal{A}(x, \frac{x}{\varepsilon})$	58
4.3.1.2	Case $\mathcal{A}^\varepsilon(x) = \mathcal{A}(\frac{x}{\varepsilon})$ with elements K of same dimension	60
4.4	HMM-FEM approach for multiscale solution	60
4.4.1	Numerical convergence of HMM-FEM to homogenized solution	61
5	SUPRACONVERGENT FDM FOR THE CRYPT CELL DYNAMICS ON NON UNIFORM MESHES	64
5.1	Preliminary results	64
5.2	Convergence analysis and stability	69
5.2.1	Stability for the elliptic equation (5.32) ₁	69
5.2.2	Stability for the parabolic equation (5.32) ₂	70
5.2.3	Convergence	71
5.3	Numerical results	73
6	AN EQUIVALENT FEM WITH SECOND ORDER ACCURACY FOR SOLUTIONS IN $L^\infty([0, T], H^3(\bar{S}))$	78
6.1	Approximating the variational problem	78
6.2	Estimating the method error	84
6.3	Numerical results	95
7	SUPRACONVERGENT MULTISCALE SCHEME	99
7.1	Cell problem	99
7.1.1	The finite difference scheme	100
7.1.2	Equivalent FE method for the cell problem 7.1	101
7.2	Approximating the homogenized coefficient	102
7.3	Approximating the solution of multiscale elliptic problems	106
7.4	Coupled multiscale problem	113
7.5	Comments	119
8	CONCLUSIONS, CONTRIBUTIONS AND FUTURE WORK	120
8.1	Conclusions	120
8.2	Future work	121
8.2.1	Convergence and stability analysis	121

8.2.2	The Hill equation	122
8.2.3	Convergence and stability analysis of the HMM-FEM method applied to a coupled problem	122
8.2.4	2D analysis of supraconvergent multiscale method	122
8.3	Contributions	123
8.3.1	Presentations	123
8.3.2	Project	124
8.3.3	Submissions of articles	124
	 BIBLIOGRAPHY	 125
	 APPENDIX A – RIEMANNIAN MANIFOLD	 129
A.1	Differential model on a manifold	129
A.1.1	Riemannian manifold and metric	129
A.1.2	Differential operators on a Riemannian manifold	130
A.1.2.1	The gradient	130
A.1.2.2	The divergence	131
A.1.2.3	The Laplacian-Beltrami-Operator	131
	 APPENDIX B – BANACH SPACES, SOBOLEV SPACES AND PERIODIC FUNCTION IN SOBOLEV SPACE H^1	 132
B.1	Banach space	132
B.1.1	Dual space	132
B.1.2	Weak convergence	132
B.2	Sobolev space	132
B.2.1	$W_p^k(\Omega)$	132
B.3	Periodic functions in the Sobolev space $H^1(Y)$	133
B.4	Homogenization in one dimensional function space	134
B.5	Some theorems of functional analysis	137
B.6	Supraconvergence and Superconvergence of numerical methods	137

1 Introduction

1.1 Motivation

Colorectal cancer (CRC) is one of the most common cancer in the world and is considered a real public health problem, with over 1.4 million new cases diagnosed each year. Despite improvements in screening for early diagnosis, CRC is responsible for about 700 000 deaths in 2012 (FERLAY et al., 2013). In Brazil, according to estimates of incidence for 2018 from the National Cancer Institute (INCA), 17.380 new cases of cancer of colon and rectum are expected in men and 18.980 in women (INCA, 2018). For 2020, 20540 new cases of colorectal cancer are expected for men and 20470 for women.

In UNICAMP, a CRC screening and prevention program was implemented in 2011 in the Zeferino Vaz Campus. The Program is based on guidance lectures, providing occult blood testing, colonoscopy and surgery when necessary and monitoring of participants. Until February 2017, 22.582 fecal occult blood tests have been made, where about 1.187 people had a positive result (abnormal) and were then recommended for a colonoscopy. 624 polyps (pre-malignant lesions) were found and removed over five years (GARDENAL, 2017; COY, 2013).

There are several risk factors that may increase the chance of a individual developing CRC (SOCIETY, 2018a), such as:

- Family history: People with a first-degree relative who has been diagnosed with CRC are in increased risk. The risk is even higher if that relative was diagnosed with cancer when they were younger than 45.
- Age: Although a person can develop CRC at any age, it is much more common after age 50.
- Lifestyle: A sedentary lifestyle, obesity, lack of exercises, alcohol and smoking are greatly linked with that disease.

An early colon screening can prevent cancer and it is recommended at age 50. One of the several methods for CRC screening is the colonoscopy, that provides a direct visualization of the colonic mucosa and often the terminal ileum. Colonoscopy examination allows early identification of lesions, signs and symptoms, and allows biopsies to be performed. In (MENDES et al., 2018), they present some indicators and findings for the exam in patients aged > 50 years who underwent colonoscopy ($n = 1.614$ exams):

Table 1 – Main indicators

Indications	%
Intestinal bleeding	26.5%
Neoplasia screening	20.7%
Abdominal pain	10.2%
Obstipation	8.2%
History of polyp	7.9%

Table 2 – Main findings

Results	%
Diverticular disease	38.9%
Polyps	38.8%
Normal	23.2%
Angioectasia	4.6%
Neoplasia	4.3%

Source: (MENDES et al., 2018)

We can verify from Table 1 and Table 2 that colonoscopy is an important exam for the diagnosis of various colorectal diseases including the first stages of CRC. In general the current treatment options for CRC are surgery, chemotherapy, and biological therapies (SOCIETY, 2018b). Radiotherapy is not commonly used to treat, although it can be used after surgery to destroy any residual cancer cells.

The Colorectal Cancer is caused by the abnormal growth of epithelial cells which form the lining of colon or rectum. More precisely, the genetic mutations occur inside small cavities, called crypts, located in the colon epithelium. CRC usually begins as a small growth called a polyp which are a protuberance in the intestinal lumen that originates from the mucosa containing dysplastic cells being likely to progress to cancer and it is believed that the precursors of CRC are aberrant crypt foci (ACF) which are clusters of crypts in the colon epithelium, containing cells with a deviant behavior with respect to the normal ones (FIGUEIREDO et al., 2013; LEEUWEN et al., 2006).

The motivation of this thesis is to model and simulate accurately the abnormal cell dynamics in the colon. We propose a cell dynamics model for describing the evolution of abnormal colonic cells in a single crypt and use the periodic crypt distribution in the colon to model such dynamics in the whole colon. The high computational cost of a such numerical method applied in the colon suggested us to implement cheap multiscale methods such as HMM-FEM and and a supraconvergent multiscale method.

In the next section, we present some cell dynamics models related to this work.

1.2 Review of relevant mathematical models for cell dynamics in a colonic crypt

There are many different approaches to modeling cell proliferation and movement such as continuum and cell-based models. According to (MURRAY et al., 2011), continuum models are generally fairly simple, where effects as proliferation, death and other few parameters can be incorporated by introducing a source term into the appropriate mass balance equation. On the other hand, cell-based models are less suited to modeling

cell growth, however they have the ability to track individual cells and are better suited for small number of cells.

We treat in this thesis continuum models for cell dynamics in the colonic crypts based on partial differential equation. A list of models of this type are presented and discussed in this section, where we put on evidence their characteristics and differences also with respect our proposed model (2.4) in Chapter 2.

1.2.1 Continuum models for tumor growth based on two families of cells

King and Franks (KING; FRANKS, 2004) have presented a simple class of models that predicts certain keys stages in the tumor growth. The conservation laws for two types has the following form

$$\begin{cases} \frac{\partial n_1}{\partial t} + \nabla \cdot (n_1 v) &= \nabla \cdot (D_{n_1} \nabla n_1) + K n_1, \\ \frac{\partial n_2}{\partial t} + \nabla \cdot (n_2 v) &= \nabla \cdot (D_{n_2} \nabla n_2) + k n_2, \\ n_1 + n_2 &= 1, \end{cases} \quad (1.1)$$

where n_1, n_2 are respectively the volume fraction of malignant or abnormal cell type and of normal cell type. Cell proliferation and death are modeled by the mitotic rates k, K . Proliferation is associated to positive rates and Death to negative rates. The relation $n_1 + n_2 = 1$ is called overall density condition that assures that no void is allowed between cells. The cell velocity v can be obtained by summing the first two equations in (1.1)

$$\nabla \cdot v = \nabla \cdot (D_{n_1} \nabla n_1 + D_{n_2} \nabla n_2) + K n_1 + k n_2. \quad (1.2)$$

During the tissue growth, elastic effects can be typically neglected and the tissue treated as a fluid. A Darcy constitutive relation has been often adopted in modeling tumor growth, though apparently often more for mathematical simplicity than for physical reasons. We can supplement (1.1) by the constitutive law

$$v = -\frac{\kappa}{\mu} \nabla p. \quad (1.3)$$

where v is the velocity of cells, p is the cell-cell adhesion pressure, μ the viscosity of cells and κ is the motility coefficient. Following the model of King and Franks, in (WALTER, 2009) the mass conservation equations are given by

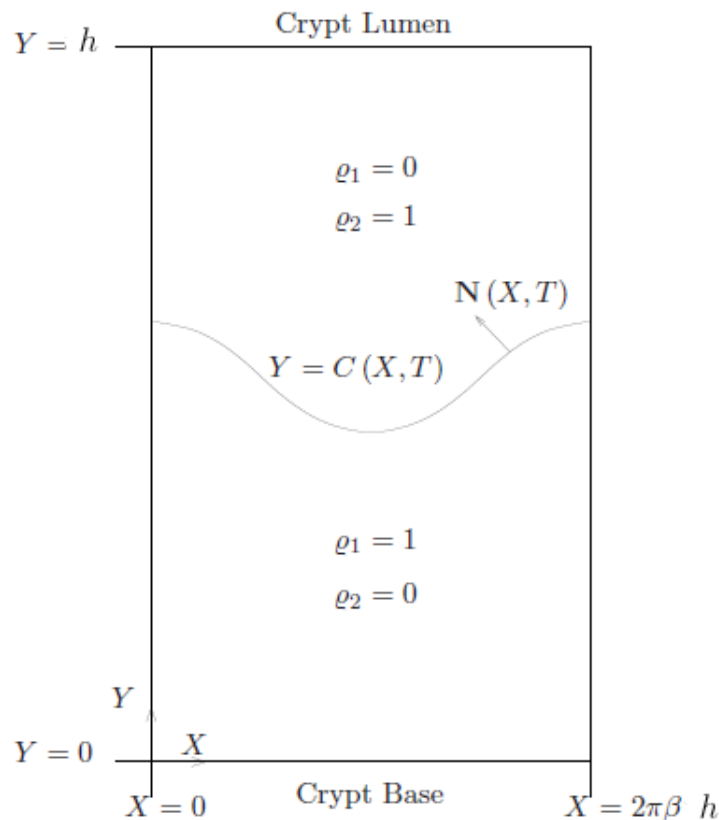
$$\begin{cases} \frac{\partial \varrho_1}{\partial t} + \nabla \cdot (\varrho_1 \hat{V}_1) &= K_1 \varrho_1, \\ \frac{\partial \varrho_2}{\partial t} + \nabla \cdot (\varrho_2 \hat{V}_2) &= K_2 \varrho_2, \\ \varrho_1 + \varrho_2 &= 1, \end{cases} \quad (1.4)$$

where ϱ_1, ϱ_2 are respectively the volume fractions of normal and mutant cell populations, \hat{V}_1, \hat{V}_2 are the cell velocities and K_1, K_2 their net proliferation rates. They suppose that the source terms decrease linearly with distance from the base of the crypt as follows:

$$K_i(X) = k_i \left(1 - \Lambda_i \frac{Y}{h}\right), \quad i = 1, 2. \quad (1.5)$$

where the positive constants k_i are the maximum rate at which the cells of type i proliferate. The crypt is modeled by a 2D surface of a cylinder with height h and radius βh , as show in Figure 1.

Figure 1 – Sketch of the two-dimensional model for two epithelial cell populations growing on the surface of a cylindrical crypt, height h and radius βh . The volume fractions of each population are separated by the boundary $Y = C(X, T)$ with normal $N(X, T)$.



Source: (WALTER, 2009)

Here they consider two cell populations which differ in their proliferation rates and viscosities to develop a continuum model that describes the movement of cells inside a cylindrical crypt. In our model we suppose that families of cells have the same diffusion, that means that have the same behavior in what concern their interaction with other cells. The two families of cells that we consider in our model differ then only for the proliferation rate, as those presented in the next paragraph.

1.2.2 Abnormal cell dynamics

In (FIGUEIREDO et al., 2013) is presented the following elliptic-parabolic coupled model

$$\begin{cases} \frac{\partial C}{\partial t} = \nabla \cdot (\nabla p C) + \nabla \cdot (D_2 \nabla C) + \beta C(1 - C), \\ -\Delta p = \nabla \cdot ((D_2 - D_1) \nabla C) + \alpha(1 - C), \end{cases} \quad (1.6)$$

where D_1, D_2 are diffusion coefficients, C denotes the cells abnormal density, p is the pressure generated by cell-cell adhesion. The proliferative activity is present in the lower two thirds of the crypt of height h , and the activity is larger at the bottom of crypt and decreases upwards towards the orifice of crypt. They define the proliferative rate coefficients α, β as a decreasing function with respect to the height of crypt, thus

$$\alpha(x_3) = \begin{cases} \tau_\alpha(x_3 - \frac{2h}{3})^2 & \text{if } x_3 \leq \frac{2h}{3} \\ 0 & \text{elsewhere,} \end{cases} \quad \beta(x_3) = \begin{cases} \tau_\beta(x_3 - \frac{2h}{3})^2 + \gamma_\beta & \text{if } x_3 \leq \frac{2h}{3} \\ \gamma_\beta & \text{elsewhere.} \end{cases} \quad (1.7)$$

where τ_α is larger than τ_β to guarantee that α is larger than β . In (1.7) γ_β is the positive rate of proliferation for the abnormal cells over the two thirds of the crypt, where normal cells cannot proliferate. A large γ_β characterize cells that very abnormal.

Their multiscale problem is presented in a two dimensional colonic region that is formed by a periodic distribution of a crypt domain. That crypt is represented by a cylinder in \mathbb{R}^3 closed at the bottom and opened at the top. After making a projection of the 3D crypt in a plane and obtaining then a 2D model for crypt, where it is periodically distributed. In this way, they obtain a coupled elliptic-parabolic model in a domain $\Omega \subset \mathbb{R}^2$, which describes the dynamics in space and time of the normal and abnormal cells in the colon.

In (FIGUEIREDO et al., 2016) is considered two population of cells as in (KING; FRANKS, 2004). Based on tumor growth, their model is presented by the following elliptic-parabolic coupled model

$$\begin{cases} \frac{\partial C}{\partial t} = \nabla \cdot (\nabla p C) + \nabla \cdot (D_C \nabla C) + \beta C, \\ -\Delta p = \nabla \cdot ((D_C - D_N) \nabla C) + (\beta - \gamma) C + \gamma, \end{cases} \quad (1.8)$$

where C is the density of abnormal cells, and N is the density of normal cells satisfying the equation

$$\frac{\partial N}{\partial t} = \nabla \cdot (\nabla p N) + \nabla \cdot (D_N \nabla N) + \gamma N, \quad (1.9)$$

with $N + C = 1$. The second equation in (1.8) is obtained summing the parabolic equations associated to N and C . D_C, D_N the diffusion coefficients of abnormal and normal cells, respectively. β is the proliferative rate of abnormal cells and γ is the proliferative rate of

normal cells defined as follows

$$\gamma(x_3) = \begin{cases} \tau_\gamma(x_3 - \frac{2h}{3})^2 & \text{if } x_3 \leq \frac{2h}{3} \\ 0 & \text{elsewhere,} \end{cases} \quad \beta(x_3) = \begin{cases} \tau_\beta(x_3 - \frac{2h}{3})^2 + \gamma_\beta & \text{if } x_3 \leq \frac{2h}{3} \\ \gamma_\beta & \text{elsewhere.} \end{cases} \quad (1.10)$$

Here, they represent a region of the colon epithelium by an heterogeneous domain, obtained by the periodic distribution of a rescaled crypt εP , where εP is a regular flat hexagon with edge size εa . Thus, with that structure they were able to define a 2D heterogeneous periodic model, where the unknown is the pair cell density C^ε and the pressure p^ε . A homogenization technique could be applied to that model considering a sequence indexed by ε , where the objective is to find the limit (C^0, p^0) of the sequence pairs $\{(C^\varepsilon, p^\varepsilon)\}_{\varepsilon>0}$. The homogenized model associated to multiscale problem based on (1.8) is the system

$$\begin{cases} \frac{\partial C^0}{\partial t} - \widetilde{A_{ij}m} \frac{\partial C^0}{\partial x_i} \frac{\partial p^0}{\partial x_j} = D \widetilde{A_{ij}m} \frac{\partial^2 C^0}{\partial x_i \partial x_j} + (\widehat{\beta m} - \widetilde{\gamma m}) C^0 (1 - C^0) \\ - \widetilde{A_{ij}m} \frac{\partial^2 p^0}{\partial x_i \partial x_j} = (\widehat{\beta m} - \widetilde{\gamma m}) C^0 + \widetilde{\gamma m} \end{cases} \quad (1.11)$$

where m is the solution of a cell problem $-\frac{\partial^2(A_{ij}m)}{\partial y_i \partial y_j} = 0$ in P , and A_{ij} define the planification of the crypt. This is a macroscopic model that represents the evolution of ACF at the surface of colon, by using the information of the cell dynamics in the crypts.

Other continuum models can consider other families of cells as differentiated and semi-differentiated as presented in the next paragraph and used along in our model, see chapter (2).

1.2.3 Aberrant colonic crypt morphogenesis

In (FIGUEIREDO et al., 2011) was proposed a hybrid convection-diffusion-shape model for simulating and implemented a method to simulate and predict what has been validated medically, with respect to some aberrant colonic crypt morphogenesis. The model demonstrates crypt fission, in which a single crypt starts dividing into two crypts, when there is an increase of proliferative cells. The problem is modeled by a transport/mass conservation model to describe the dynamics of different types of cells inside a colonic crypt. Using the volume conservation $N_1 + N_2 = 1$ where N_i are the densities of proliferative and apoptotic cells, the final model is given by

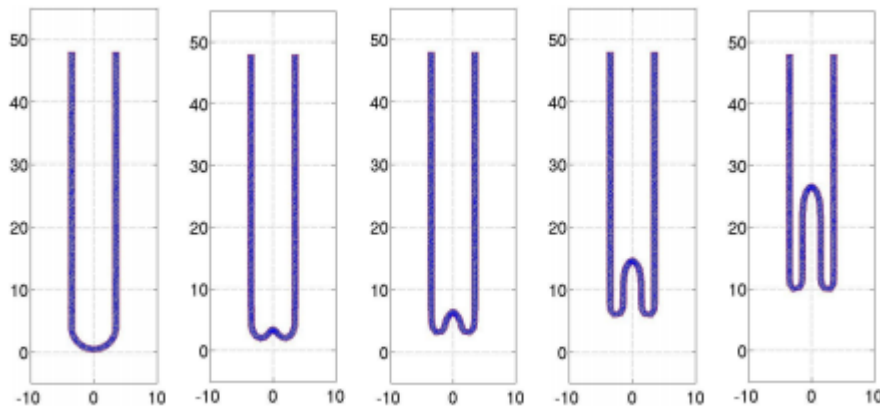
$$\begin{cases} \frac{\partial N}{\partial t} = \nabla \cdot (\nabla p N) + \nabla \cdot (D \nabla N) + \alpha N - \beta N & \text{in } \Omega_c(t) \times [t, t + \Delta_t], \\ -\Delta p = \nabla \cdot (D \nabla N) + \alpha N & \text{in } \Omega_c(t) \times [t, t + \Delta_t], \\ N = 0, p = 1 & \text{in } \Gamma_1 \times (0, T), \\ \frac{\partial N}{\partial n} = 0 & \text{in } (\Gamma_2 \cup \Gamma_3) \times (0, T), \\ N(., 0) = N_0 & \text{in } \Omega_c, \end{cases} \quad (1.12)$$

where Δ_t is a fixed time step used to solve numerically the problem, N is the proliferative cell density and p an internal pressure.

The problem is composed of three parts: the coupled parabolic and elliptic equations, involving the unknowns N and p , and the equation describing the evolution the spatial domain Ω_c . The main purpose of that work was to simulate colonic crypt folding, by means of partial differential equations, more exactly, by using a convection-diffusion-shape model. They used a 2D version of the problem since the histological medical exams are sections of the colon from the mucosa surface until the bottom of the crypts. The set Ω_c stands for the 2D-geometry of the crypt (U-shape) where Γ_1 is its upper boundary, Γ_2 and Γ_3 are respectively, the outer and inner boundaries.

In comparison, this problem considers the same class of cells of this last work but as we will see later, we avoid that kind of boundary conditions considering a manifold PDE model of that problem.

Figure 2 – Shape of the colonic crypt at different times: $t = 0, 1, 2, 5,$ and 10 respectively.



Source: (FIGUEIREDO et al., 2011)

Others models for describing the crypt morphogenesis are based on elastic or viscoelastic relations between colonic cells and epithelial tissue. See (FIGUEIREDO et al., 2019) and references of other models therein.

1.3 Aims and objectives of the thesis

The aim of this work is to describe numerically the dynamics of cancer cells in the colon by means of accurate multiscale methods. In order to perform a numerical analysis of the proposed methods we aim to obtain errors estimates and prove stability and convergence of the proposed methods.

The specific objectives of this work are:

- To prove convergence and stability of the cell proliferation problem in a single scale using a method based on finite differences;
- To study numerically the solutions of the multiscale cell proliferation problem provided by HMM-FEM method;
- To present the numerical properties of a supraconvergent finite difference method applied to multiscale problems.

1.4 Preliminary results

Our first step in the development of this work was use a more realistic surface than the one proposed in (FIGUEIREDO et al., 2013; FIGUEIREDO et al., 2016; FIGUEIREDO et al., 2019) to approximate the crypt's shape, thus we were able to rewrite the main equations in a divergence form which makes the numerical analysis easier. Using the HMM framework, we analyse a suitable homogenized problem and we obtain the numerical convergence of the HMM-FEM numerical solution to the homogenized solution. To prove analytically the convergence and stability in a single scale we use a non uniform space discretization by using finite difference method which we proved the equivalency to a weighted finite elements method. The methods used provide some good error estimates to our problem as we'll see later. At the end of this work we prove convergence and stability to functions in H^{1+s} . All the presented implementations in this work were built in (MATLAB, 2018a).

1.5 Overview

The rest of this manuscript is organized as follows. Chapter 2 presents the biological information of the colon tissue and how it is related with the colorectal cancer and presents a mathematical model in a single crypt. In Chapter 3, we introduce multiscale problems and homogenization. In Chapter 4, we present the HMM method as a framework to designing multiscale methods. In Chapter 5 we present a finite difference method in a non uniform mesh and analyze it numerically, studying its stability and convergence. In Chapter 6, we study a more robust method which provides convergence and stability to H^{1+s} solutions. Finally, in Chapter 7 our purpose is to present a new multiscale scheme that uses the microscale information to solve the homogenized problem and to build then an approximation for the multiscale solution.

2 Mathematical model

The colon (see Figure 3) is a part of the digestive tract located between the small intestine and the rectum. Its principal functions are the absorption of water, minerals, nutrients, and to serve as a storage area for the waste material. Because of its biological nature, the colon has a high level of cellular regeneration and which exposes it to many agents of a physical, chemical, and biological nature, which increases the possibility of developing pathologies, including cancer.

Colorectal cancer is located in the colon or in the rectum digestive tract. It requires years and several genetic mutations of the colonic cells to appear. These mutations lead changes in the cell proliferative behavior and result in a significant deformation of the colorectal crypts.

In the following Section 2.1 we provide some biological information useful to define the mathematical model for the proliferative cells dynamics. In Section 2.2 we model mathematically the geometry domain of a crypt and then also the cell dynamics in a such domain by using a system of partial differential equations.

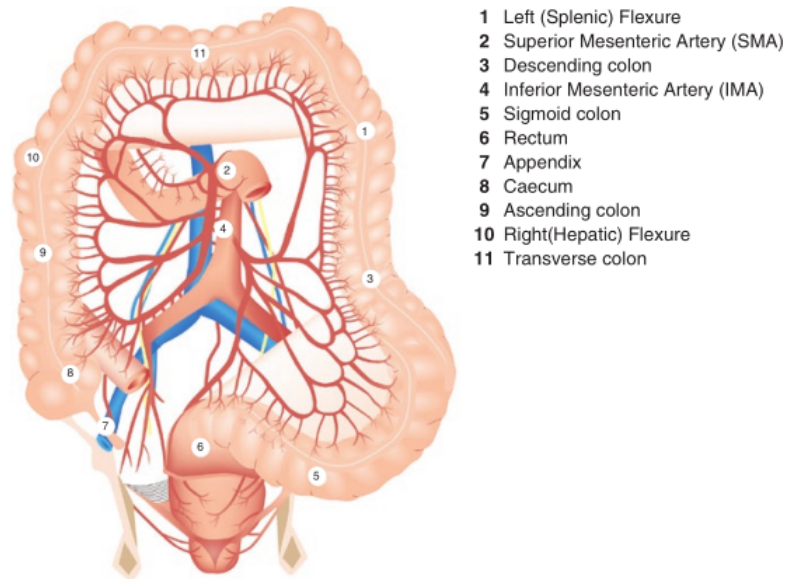
2.1 Biological background

In the following sections we discuss some biological information which allow us to model the crypt's shape 2.1.2 and the proliferative rates.

2.1.1 Colon structure

The anatomical regions of the colon are illustrated in Figure 3. The large intestine is the penultimate stage in the digestive tract, weights only 0.22 kg and is approximately 1.5m long and the diameter varies along its length, the average diameter is around 6 – 8cm (COLLINS, 2016). It extends from the terminal ileum to the anus. The colon is divided into five parts: cecum, ascending colon (measures 12 – 20cm in length), middle or transverse colon (ranging between 40 and 50cm), descending colon (measures 10 – 15cm in length), and the sigmoid colon.

Figure 3 – Colon anatomy



Source: (COLLINS, 2016); Copyright Springer.

The main function of its muscularis externa is to move matter along the large intestine through peristaltic contractions which allows to absorb water and any remaining absorbable nutrients from food. Inside the musculature externa there is the submucosa, which contains vessels that provides the main blood supply for the colon.

2.1.2 Crypts

The epithelial layer of the human colon mucosa is made up of a single sheet of columnar epithelial cells, which form finger-like invaginations called crypts as represented in Figure 4(a). The crypts have epithelial cells that contain digestive enzymes that digest specific foods while they are being absorbed through the epithelium. Thus the colonic crypts are the end absorption functional unit of the intestine. The epithelial cells cover all the colon including the crypts, see Figure 4(b). It is estimated that there are approximately 10^7 crypts in an adult human colon, each crypt containing 1000-4000 epithelial cells. The crypts are about $433\mu m$ in length and approximately $31\mu m$ in diameter (MICHOR et al., 2005).

The epithelial cells are generated at the crypt base and migrate along the crypt axis towards the top orifice. This migration is due to a cell-cell adhesion pressure generated by the cell proliferation. As the cells migrate to the crypt top they differentiate, becomes less proliferative, and when reaching the luminal surface they perform their absorption function and then they are shed into the lumen.

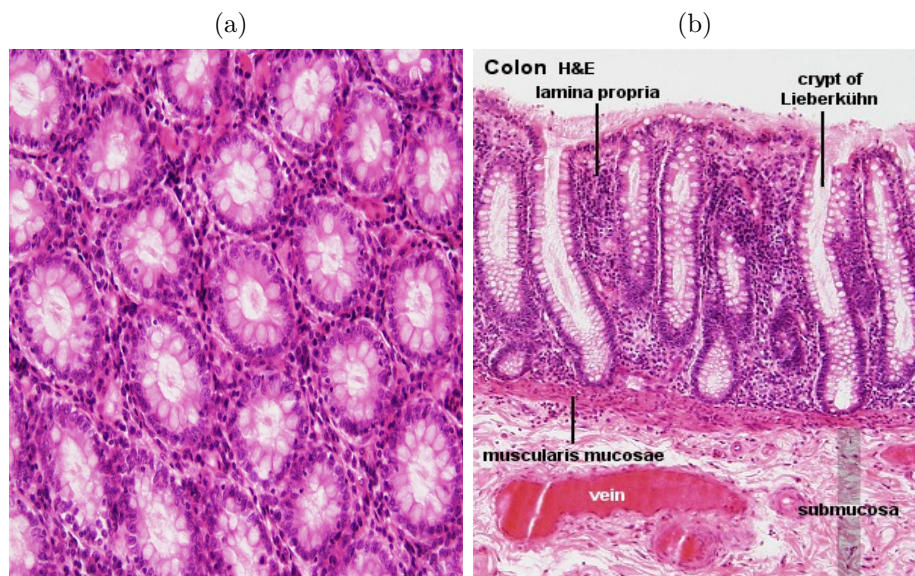


Figure 4 – Distribution and shape of crypts. (4(a) can be found in (FIGUEIREDO et al., 2016) and 4(b) in UWA Blue Histology. Copyright Lutz Slomianka 1998-2009.)

2.1.3 Stem cells

The large intestine and the colon are continuously renewed, in fact billions of cells are lost and created therein on a daily basis. It is widely accepted that cells replacement and production is achieved by stem cells found at the base of crypt. The stem cells are defined as a small population of relatively undifferentiated cells that maintain their size when they divide. The progeny of stem cells (called transit cells) are located above the stem cells along the crypt axis. These transit cells have generate each of the epithelial cells found in colorectal crypts: Colonocytes, the primary absorptive cell; goblet cells, the mucin secreting cell; enteroendocrine cells, the hormone-producing population; and secreting Paneth cells. An average human colonic crypt contains 2000 cells and is believed to have approximately 19 stem cells (KHALEK; GALLICANO; MISHRA, 2010), but this amount can change depending on the crypt location. In the scientific literature it is believed that transit cells undergo 4-6 cell divisions, proliferating less and differentiating as they move upward the crypt. At the top of the crypt there are fully differentiated cells that cannot proliferate anymore.

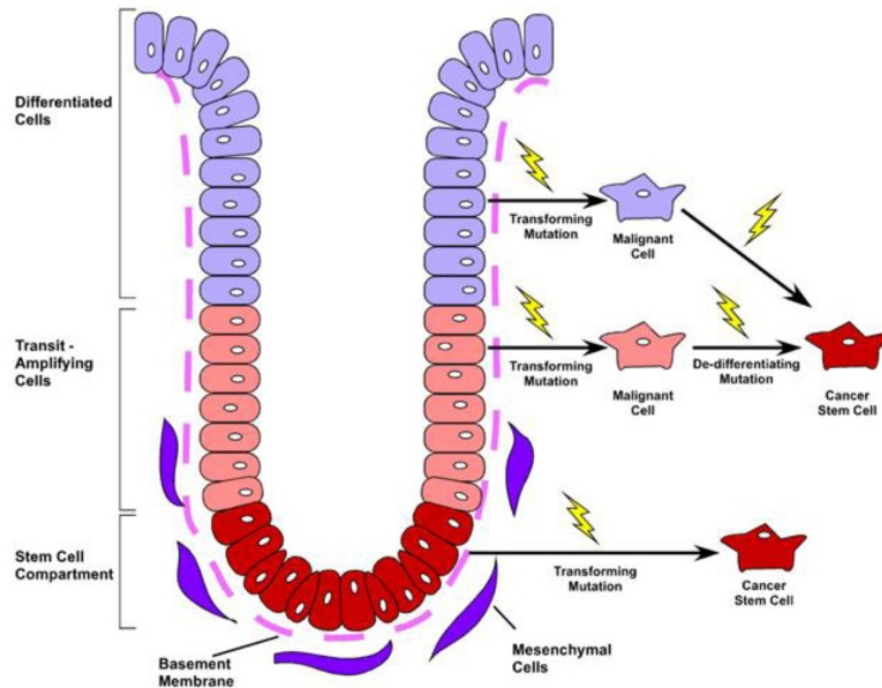


Figure 5 – Stem cells and its mutations

Source: (ANDERSON et al., 2011)

In Figure 5, we have the scheme of a colorectal crypt. Stem cells, at the base (red), proliferate to produce transit cells (pink) and differentiate into differentiated cells (blue). A single transforming mutation in a somatic intestinal stem cell could rise to a CSC (cancer stem cell).

2.1.4 Aberrant Crypt Foci (ACF) and development of adenomas

ACF are focal lesions composed of several enlarged crypts, which are specifically induced by colon carcinogenesis. In Figure 6 we note two ACFs characterized by crypts evidenced by a blue ethylene dye. It is believed that ACF is the earliest expression of this colon carcinogenesis and are the precursors of adenomas. In colon, the adenoma-carcinoma sequence is widely regarded as the main pathway leading to the development of malignancy. Cancer is a multistage process that requires the accumulation of several genetic mutations, each of them alter successively the tissue's normal behavior causing deregulated differentiation and uncontrolled proliferation. A series of pathological alterations are involved in the ACF up to the formation of malignant tumors.

Analysis of colon adenomas has shown that there is an upward expansion of the proliferative compartment towards the surface of crypt in adenomas. Over time the adenoma may accumulate more mutations in critical genes, resulting in malignant transformation to an adenocarcinoma with invasion into the submucosa of the colon.

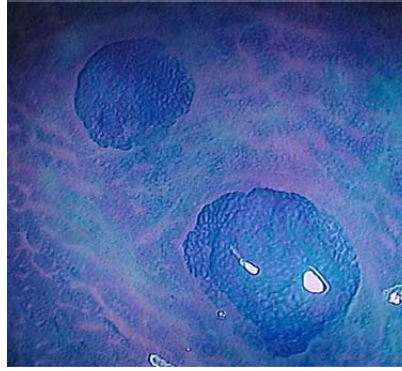


Figure 6 – ACF pictured in a colonoscopy image. The dark blue regions are clusters of deformed and enlarged crypts, called ACF, in the colon epithelium, that appear in the first stage of colon carcinogenesis

Source: (FIGUEIREDO et al., 2016)

2.2 Mathematical model of the crypt geometry, cell proliferation and dynamics in the colonic crypts

From the above literature we are able to model the parameters to build a problem that describe the cell dynamics.

2.2.1 Crypt geometry

As already mentioned the average dimensions of a human colonic crypt are $433 \mu m$ from the bottom to the top, and $31 \mu m$ for the diameter of the top orifice excluding the epithelium (FIGUEIREDO et al., 2016). Since the crypt is our main domain of interest, we choose a surface that approximate its geometry. A single crypt can be represented as the two-dimensional surface Γ generated by the graph of the function $f : [0, 1]^2 \rightarrow \Gamma$, with

$$f(y_1, y_2) = h \left(1 - e^{-\left(\frac{R(y_1, y_2)}{\sigma} \right)^2} \right), \quad (2.1)$$

where $R(y_1, y_2) = \left(y_1 - \frac{1}{2} \right)^2 + \left(y_2 - \frac{1}{2} \right)^2$ and h is the surface height and sigma describe the width of the crypt, that is permit to respect that the height is fourteen times the crypt orifice diameter, see Figure 7.

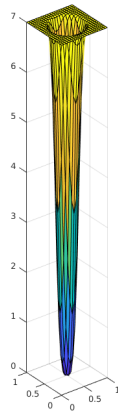


Figure 7 – A single crypt represented as a two-dimensional surface in \mathbb{R}^3 .

2.2.2 3D periodic domain

There are millions of crypts in the human colon epithelium. Based on images provided by colonoscopy, we can see that crypts are almost periodically distributed in the colon, see Figure 6. Therefore to solve and simulate the mathematical problem of cell dynamics in the colon we write our problem in a three-dimensional domain with repeated crypts represented as a surface, see Figure 8, that will represent the external colon epithelium in three dimensions.

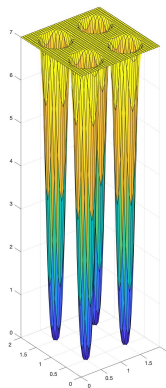


Figure 8 – This figure show how the crypts are periodically distributed in our modeled colon epithelium in three dimensions.

On a such three dimension domain with repeated crypts we will study our multiscale PDE problem in Chapter 3. Before analyzing a such problem we need to define the source terms in the next subsection and present the model in a single crypt in subsection 2.2.4. Then we will rewrite the PDE problem in the two-dimensional manifold, see Section A.1, obtaining a two-dimensional multiscale problem in Section 2.3.

2.2.3 Source terms

Our mathematical model consider only two types of colonic cells: fully differentiated with density N and semi-differentiated cells (also called proliferative or transit cells) with density C . Cells have a proliferative rate that depends on the cell location in the crypt. According to (DRASDO; LOEFFLER, 2001), the proliferative activity is presented in the lower two thirds of the crypt and thus we suppose that the proliferation rate of semi-differentiated cells β_C decrease quadratically with distance from the base to the two thirds of the crypt heights as follows:

$$\beta_C(x, y, z) = \begin{cases} \tau \left(1 - \frac{z}{2h/3}\right)^2 & \text{if } z < \frac{2h}{3} \\ 0 & \text{if } \frac{2h}{3} \leq z \leq h. \end{cases} \quad (2.2)$$

where τ is a positive constant representing the maximum rate at which the cells of type C proliferate.

We also suppose that the rate of transformation (or differentiation) of proliferative semi-differentiated cells C proliferate into fully differentiated cells N is modeled by

$$\alpha_C(x, y, z) = \begin{cases} 0 & \text{if } z < \frac{2h}{3} \\ \tau \left(1 - \frac{z}{2h/3}\right)^2 & \text{if } \frac{2h}{3} \leq z \leq h. \end{cases} \quad (2.3)$$

Furthermore, we assume that the cells verify the overall density hypothesis $N + C = 1$. This is equivalent to suppose that no free-space (no void hypothesis) exists.

2.2.4 3D final model

Let $\Gamma \subset \mathbb{R}^3$ be the surface that models a single crypt, t the time variable belonging to the interval $[0, T]$ with $T > 0$ fixed and $N(x, y, z, t)$ and $C(x, y, z, t)$ are respectively the fully differentiated cells and the semi-differentiated cells densities, at each point (x, y, z) of Γ and at time t . Then, based on models of tumor growth, described by systems of Partial Differential Equations (PDEs) and relying on transport/diffusion/reaction models, we reproduce the following system of PDEs for representing the dynamics of these populations of colonic cells in $\Gamma \times (0, T]$:

$$\begin{cases} \frac{\partial N}{\partial t} + \nabla_{\Gamma} \cdot (v_N N) & = \nabla_{\Gamma} \cdot (D_N \nabla_{\Gamma} N) + \beta_C C \\ \frac{\partial C}{\partial t} + \nabla_{\Gamma} \cdot (v_C C) & = \nabla_{\Gamma} \cdot (D_C \nabla_{\Gamma} C) + \alpha_C C - \beta_C C \\ N + C & = 1. \end{cases} \quad (2.4)$$

We have assumed that (2.4) has Dirichlet boundary conditions with initial conditions $N(\cdot, 0) = N_0, C(\cdot, 0) = C_0$. Here D_N, D_C are the diffusion coefficients of fully and semi-differentiated cells, respectively, β_C is the rate of change of proliferative cells C into fully differentiated N and α_C is the proliferation rate of cells C . The convective velocity of the normal and abnormal cells are denoted by v_N and v_C , respectively. We suppose also that the two populations of cells have the same convective velocity $v_N = v_C = v$, which is defined by $v = -\nabla_\Gamma p$, where p is the cell-cell adhesion pressure and that $D_C = D_N = D$.

Then, by assuming the first two equations in (2.4) and using the overall density hypothesis $N + C = 1$ we obtain the following elliptic-parabolic coupled model whose unknown is the pair (C, p) :

$$\begin{cases} \frac{\partial C}{\partial t} = \nabla_\Gamma \cdot (\nabla_\Gamma p C) + \nabla_\Gamma \cdot (D \nabla_\Gamma C) + \alpha C & \text{in } \Gamma \times (0, T] \\ -\Delta_\Gamma p = \beta C & \text{in } \Gamma \times (0, T] \\ C = p = 0 & \text{on } \partial\Gamma \times (0, T], \end{cases} \quad (2.5)$$

where $\alpha = \alpha_C - \beta_C$ and $\beta = \alpha_C$. Note that

$$\alpha(x, y, z) = \begin{cases} -\tau \left(1 - \frac{z}{2h/3}\right)^2 & \text{if } z \leq \frac{2h}{3} \\ \tau \left(1 - \frac{z}{2h/3}\right)^2 & \text{if } \frac{2h}{3} \leq z \leq h. \end{cases} \quad (2.6)$$

The operator Δ_Γ is the so called *Laplace-Beltrami* operator, which is a generalization to non-flat Riemannian manifolds. The Laplacian operator appears in differential equations describing various physical phenomena, such as heat diffusion, wave propagation, etc.

2.2.5 Differential model in local coordinates

Let $\Gamma \subset \mathbb{R}^3$ be a surface that models a single crypt and a chart $\{Y, \varphi\}$, see Appendix A.1. We can rewrite the system (2.5) in local coordinates (y_1, y_2) as the following problem

$$\begin{cases} |g| \frac{\partial \bar{C}}{\partial t} = \nabla \cdot (\mathcal{A} \nabla \bar{p} \bar{C}) + \nabla \cdot (\bar{D} \mathcal{A} \nabla \bar{C}) + |g| \bar{\alpha} \bar{C} & \text{in } Y \times (0, T] \\ -\nabla \cdot (\mathcal{A} \nabla \bar{p}) = |g| \bar{\beta} \bar{C} & \text{in } Y \times (0, T] \\ \bar{C} = \bar{p} = 0 & \text{on } \partial Y \times (0, T], \end{cases} \quad (2.7)$$

where $|g| = \sqrt{\det g}$, $\mathcal{A} = (g)^{-1} \sqrt{\det g}$ and g is the metric induced by \mathbb{R}^3 . Now, the unknown functions (\bar{C}, \bar{p}) are defined in $Y \times (0, T]$, where $\bar{C} = C \circ \varphi$ and $\bar{p} = p \circ \varphi$. For more details see A.1.

System (2.7) provided with initial condition of C admits a unique solution. This can be proved using the same proof used in (FIGUEIREDO et al., 2016).

2.2.6 Properties of g and \mathcal{A}

The quadratic form I_p on $T_p\Gamma$, the tangent plane of Γ at p (see appendix A.1), is called the first fundamental form of the regular surface $\Gamma \subset \mathbb{R}^3$ at $p \in \Gamma$. Therefore, the first fundamental form is merely the expression of how the surface Γ inherits the natural inner product of \mathbb{R}^3 . Geometrically the first fundamental form allows us to make measurements on the surface.

We shall now express the first fundamental form in the basis $\{\varphi_{y_1}, \varphi_{y_2}\}$ associated to $\varphi(y_1, y_2)$ at p . Since a tangent vector $w \in T_p\Gamma$ is a tangent vector to a parameterized curve $\alpha(s) = \varphi(u(s), v(s))$, $s \in (-\varepsilon, \varepsilon)$, with $p = \alpha(0) = \varphi(u_0, v_0)$, we obtain

$$\begin{aligned} I_p(\alpha'(0)) &= \langle \alpha'(0), \alpha'(0) \rangle_p \\ &= \langle \varphi_{y_1} u' + \varphi_{y_2} v', \varphi_{y_1} u' + \varphi_{y_2} v' \rangle_p \\ &= E(u')^2 + 2F u' v' + G(v')^2, \end{aligned}$$

where the values of the functions involved are computed for $s = 0$, and

$$E(y_1, y_2) = \langle \varphi_{y_1}, \varphi_{y_1} \rangle_p \quad (2.8)$$

$$F(y_1, y_2) = \langle \varphi_{y_1}, \varphi_{y_2} \rangle_p \quad (2.9)$$

$$G(y_1, y_2) = \langle \varphi_{y_2}, \varphi_{y_2} \rangle_p. \quad (2.10)$$

By letting p run in the coordinate neighborhood corresponding to $\varphi(y_1, y_2)$ we obtain functions $E(y_1, y_2), F(y_1, y_2), G(y_1, y_2)$ which are differentiable in that neighborhood.

Then, the symmetric positive definite matrix g is defined as

$$g = \begin{bmatrix} E(y_1, y_2) & F(y_1, y_2) \\ F(y_1, y_2) & G(y_1, y_2) \end{bmatrix}. \quad (2.11)$$

In the case of Γ is obtained by a graph of function f , therefore

$$g = \begin{bmatrix} 1 + (f_{y_1})^2 & f_{y_1} f_{y_2} \\ f_{y_1} f_{y_2} & 1 + (f_{y_2})^2 \end{bmatrix}. \quad (2.12)$$

Then, the functions that depend of g in (2.7) are

$$|g| = \sqrt{1 + (f_{y_1})^2 + (f_{y_2})^2} \geq 1 \quad \forall (y_1, y_2) \in Y, \quad (2.13)$$

and

$$\mathcal{A} = g^{-1} \sqrt{\det g} = \begin{bmatrix} \frac{1 + (f_{y_2})^2}{\sqrt{1 + (f_{y_1})^2 + (f_{y_2})^2}} & -\frac{f_{y_1} f_{y_2}}{\sqrt{1 + (f_{y_1})^2 + (f_{y_2})^2}} \\ -\frac{f_{y_1} f_{y_2}}{\sqrt{1 + (f_{y_1})^2 + (f_{y_2})^2}} & \frac{1 + (f_{y_1})^2}{\sqrt{1 + (f_{y_1})^2 + (f_{y_2})^2}} \end{bmatrix}. \quad (2.14)$$

We can check easily that the eigenvalues of \mathcal{A} are

$$\lambda = \frac{1}{\sqrt{1 + (f_{y_1})^2 + (f_{y_2})^2}}, \quad \Lambda = \frac{1 + (f_{y_1})^2 + (f_{y_2})^2}{\sqrt{1 + (f_{y_1})^2 + (f_{y_2})^2}}, \quad (2.15)$$

since $\det g = 1 + (f_{y_1})^2 + (f_{y_2})^2$, and so

$$0 < \lambda \leq 1, \Lambda \geq 1 \quad \forall (x, y) \in Y. \quad (2.16)$$

Note that \mathcal{A} is also a SPD matrix.

2.2.7 2D periodic domain

To get a problem for describing the abnormal cell dynamics in the colon epithelium, that has scales as those depicted in Figure 6, we represent the colon as rectangle $\Omega \subset \mathbb{R}^2$ with a periodically repeated planified crypt structure Ω_c^ε below, where Ω_c^ε is a square domain (that can be thought as shifted Y , see next paragraph) representing a single crypt with side size ε and center c

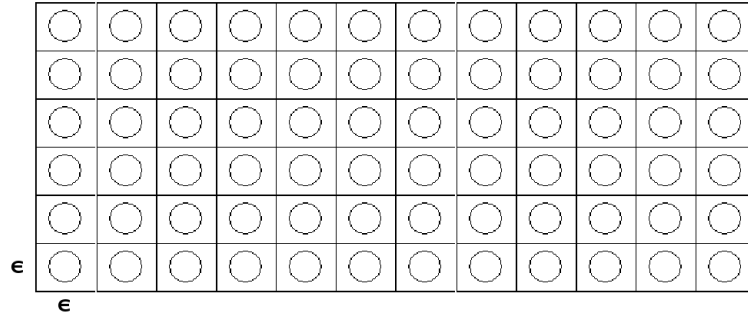


Figure 9 – 2D domain

Source: produced by the author.

We can do it easily defining the problem (2.5) in $\Gamma \times (0, T]$, where Γ is a surface obtained by a graph of function as before with $\varphi(y_1, y_2) = (y_1, y_2, f(y_1, y_2))$ parameterized in Ω_c^ε and distributing the problem periodically in Ω .

2.2.8 Periodic distribution

In what follows $Y = [0, 1]^2$. Let Γ be a surface defined previously and consider a linear transformation T_c that takes Ω_c^ε to Y given by $T_c(x_1, x_2) = \left(\frac{1}{2}, \frac{1}{2}\right) + \left(\frac{x_1 - c_1}{\varepsilon}, \frac{x_2 - c_2}{\varepsilon}\right) = (y_1, y_2)$, where $c = (c_1, c_2)$ is the center of Ω_c^ε . The domain Y will be used as a domain of reference (this is because we refer Γ as a reference crypt). In Y , the

function $\bar{\beta}$ (local coordinates) is defined as

$$\bar{\beta}(y_1, y_2) = \begin{cases} \tau \left(1 - \frac{f(y_1, y_2)}{2h/3}\right)^2 & \text{if } f(y_1, y_2) \leq \frac{2h}{3} \\ 0 & \text{otherwise.} \end{cases} \quad (2.17)$$

In Ω_c^ε the function $\bar{\beta}^\varepsilon$ is defined as

$$\bar{\beta}^\varepsilon(x_1, x_2) = \begin{cases} \tau \left(1 - \frac{f^\varepsilon(x_1, x_2)}{2h_\varepsilon/3}\right)^2 & \text{if } f^\varepsilon(x_1, x_2) \leq \frac{2h_\varepsilon}{3} \\ 0 & \text{otherwise,} \end{cases} \quad (2.18)$$

where $h, h_\varepsilon = \varepsilon h$ are the crypt heights (reference and micro levels), respectively. Using the linear transformation T_c and taking $f^\varepsilon(x_1, x_2) = h_\varepsilon \left(1 - e^{-\left(\frac{R^\varepsilon(x_1, x_2)}{\sigma_\varepsilon}\right)^2}\right)$, where $R^\varepsilon(x_1, x_2) = (x_1 - c_1)^2 + (x_2 - c_2)^2$ (similarly to $f(y_1, y_2)$, with $\sigma = \sigma_\varepsilon/\varepsilon$) we can check easily that holds

$$\begin{aligned} \bar{\beta}^\varepsilon(x_1, x_2) &= \tau \left(1 - \frac{f^\varepsilon(x_1, x_2)}{2h_\varepsilon/3}\right)^2 \\ &= \tau \left(1 - \frac{f(y_1, y_2)}{2h/3}\right)^2 \\ &= \bar{\beta}(y_1, y_2), \end{aligned}$$

with the suitable change of coordinates. Look that the same holds to $\bar{\alpha}^\varepsilon$, where

$$\bar{\alpha}^\varepsilon(x_1, x_2) = \begin{cases} -\tau \left(1 - \frac{f^\varepsilon(x_1, x_2)}{2h_\varepsilon/3}\right)^2 & \text{if } f^\varepsilon(x_1, x_2) \leq \frac{2h_\varepsilon}{3} \\ \tau \left(1 - \frac{f^\varepsilon(x_1, x_2)}{2h_\varepsilon/3}\right)^2 & \text{otherwise.} \end{cases} \quad (2.19)$$

Now, let g be the metric of Γ induced by \mathbb{R}^3 (similarly to g^ε). We can check that

$$\frac{\partial f^\varepsilon(x_1, x_2)}{\partial x_1} = \frac{4(x_1 - c_1)(f^\varepsilon(x_1, x_2) - h_\varepsilon)R^\varepsilon(x_1, x_2)}{\sigma_\varepsilon^2}.$$

That leads us to

$$\begin{aligned} g_{1,1}^\varepsilon(x_1, x_2) &= 1 + \left(\frac{\partial f^\varepsilon(x_1, x_2)}{\partial x_1}\right)^2 \\ &= 1 + \left(\frac{4(x_1 - c_1)(f^\varepsilon(x_1, x_2) - h_\varepsilon)R^\varepsilon(x_1, x_2)}{\sigma_\varepsilon^2}\right)^2 \\ &= 1 + \left(\frac{4(y_1 - \frac{1}{2})(f(y_1, y_2) - h)R(y_1, y_2)}{\sigma^2}\right)^2 \\ &= g_{1,1}(y_1, y_2). \end{aligned}$$

since $f^\varepsilon(x_1, x_2) = f(y_1, y_2)\varepsilon$, $R^\varepsilon(x_1, x_2) = R(y_1, y_2)\varepsilon^2$, $\sigma_\varepsilon = \sigma\varepsilon$. From this, we conclude that $\mathcal{A}^\varepsilon(x_1, x_2) = \mathcal{A}(y_1, y_2)$ and $|g|^\varepsilon(x_1, x_2) = |g|(y_1, y_2)$ with the suitable change of coordinates. Now, we are able to distribute Ω_c^ε periodically in Ω using the definitions

$$\mathcal{A}^\varepsilon(x_1, x_2) = \mathcal{A}(y_1, y_2), \quad \bar{\beta}^\varepsilon(x_1, x_2) = \bar{\beta}(y_1, y_2), \quad \bar{\alpha}^\varepsilon(x_1, x_2) = \bar{\alpha}(y_1, y_2), \quad (2.20)$$

where $(y_1, y_2) = \left(\frac{1}{2}, \frac{1}{2}\right) + \left(\frac{x_1 - c_1}{\varepsilon}, \frac{x_2 - c_2}{\varepsilon}\right)$.

2.3 Multiscale modeling

It is clear that cell interactions occur in a scale smaller than the observed one, and so we can model this problem using two scales: the macroscale describes the region (measurable in decimeters) of the colon where the evolution of ACF (Aberrant Crypt Foci) is taking place, whilst the microscale describes the region (measurable in micrometers) occupied by a single crypt. Pressure and density are computed at the macroscale level with the coefficients responsible for diffusion and proliferation defined at the microscale.

The multiscale problem is defined as

$$\left\{ \begin{array}{ll} |g|^\varepsilon \frac{\partial \bar{C}^\varepsilon}{\partial t} & = \nabla \cdot (\mathcal{A}^\varepsilon \nabla \bar{p}^\varepsilon \bar{C}^\varepsilon) + \nabla \cdot (\bar{D}^\varepsilon \mathcal{A}^\varepsilon \nabla \bar{C}^\varepsilon) + |g|^\varepsilon \bar{\alpha}^\varepsilon \bar{C}^\varepsilon & \text{in } \Omega \times (0, T] \\ -\nabla \cdot (\mathcal{A}^\varepsilon \nabla \bar{p}^\varepsilon) & = |g|^\varepsilon \bar{\beta}^\varepsilon \bar{C}^\varepsilon & \text{in } \Omega \times (0, T] \\ \bar{C}^\varepsilon = \bar{p}^\varepsilon & = 0 & \text{on } \partial\Omega \times (0, T] \\ \bar{C}^\varepsilon(\cdot, 0) & = \bar{C}_0^\varepsilon & \end{array} \right. \quad (2.21)$$

where $|g|^\varepsilon = \sqrt{\det g^\varepsilon}$, $\mathcal{A}^\varepsilon = (g^\varepsilon)^{-1} \sqrt{\det g^\varepsilon}$, $\bar{\beta}^\varepsilon$ and $\bar{\alpha}^\varepsilon$ are defined in Ω by periodicity. Then the unknown functions $(\bar{C}^\varepsilon, \bar{p}^\varepsilon)$ are defined in $\Omega \times (0, T]$. Note that \mathcal{A}^ε , g^ε , $\bar{\alpha}^\varepsilon$ and $\bar{\beta}^\varepsilon$ depend only of the microscale, that is

$$f^\varepsilon(x_1, x_2) = \begin{cases} f\left(\frac{x_1}{\varepsilon}, \frac{x_2}{\varepsilon}\right) & \text{if } \frac{x}{\varepsilon} \text{ is in } Y \\ \text{by periodicity} & \text{elsewhere.} \end{cases} \quad (2.22)$$

By periodicity we mean that if $(\frac{x_1}{\varepsilon}, \frac{x_2}{\varepsilon}) \notin Y$ then $f^\varepsilon(x_1, x_2) = f(y_1, y_2)$ where (y_1, y_2) is the unique point such that $(y_1, y_2) = (\frac{x_1}{\varepsilon}, \frac{x_2}{\varepsilon}) + \varepsilon k$ for some $k \in \mathbb{Z}^2$.

Note that exists a unique solution for the homogenized system, the proof can be found in ([FIGUEIREDO et al., 2016](#)).

3 Multiscale problems and homogenization

Consider a domain Ω where the quantity u , that can be a cell-cell pressure in our case, satisfies a diffusion problem with diffusion tensor $\mathcal{K} = \mathcal{K}(x)$. For simplicity, we assume that the domain is isotropic, which means that \mathcal{K} is a scalar. Suppose that f represents a source term for u and u is null on the surface $\partial\Omega$. Then $u = u(x)$ at the point $x \in \Omega$ satisfies the following boundary value problem with homogeneous Dirichlet conditions

$$\begin{cases} -\nabla \cdot (\mathcal{K} \nabla u(x)) = f, & \text{in } \Omega, \\ u = 0, & \text{on } \partial\Omega. \end{cases} \quad (3.1)$$

This is a classic elliptic boundary value problem and it is well known that if f is sufficiently smooth, it admits a unique solution u which is twice differentiable and solves system (3.1) at any point $x \in \Omega$. If now we consider a heterogeneous or composite material Ω , then \mathcal{K} takes different values in each component of the composite material. Hence, \mathcal{K} is now a function, which is discontinuous in Ω , since it jumps over the surfaces that separate the components. Suppose that the heterogeneities are very small with respect to the size of Ω and that they are periodically distributed. This is a realistic assumption for a large class of applications that can be modeled with a domain that is periodically distributed.

The periodic domain is supposed to be characterized by a dimension ε (CIORANESCU; DONATO, 1999; MURAT; TARTAR, 1997). Then the coefficient \mathcal{K} depends on ε and the problem (3.1) can be written as

$$\begin{cases} \text{Find } u^\varepsilon \in H_0^1(\Omega) \text{ such that} \\ \sum_{i=1}^n \int_{\Omega} \mathcal{K}^\varepsilon(x) \frac{\partial u^\varepsilon}{\partial x_i} \frac{\partial v}{\partial x_i} dx = \int_{\Omega} f v dx, \quad \forall v \in H_0^1(\Omega) \end{cases} \quad (3.2)$$

A natural way to introduce the periodicity of \mathcal{K}^ε in (3.2) is to suppose that it has the form

$$\mathcal{K}^\varepsilon = \mathcal{K}\left(\frac{x}{\varepsilon}\right), \quad (3.3)$$

where $(\mathcal{K}_{i,j})_{i,j=1,\dots,n}$ is a given periodic matrix function of period Y . This means that we are given a reference period Y , in which the reference heterogeneities are periodically distributed. Observe that two scales characterize the model problem (3.2), the macroscopic scale x and the microscopic one $\frac{x}{\varepsilon}$, describing the micro-oscillations in Y . Observe that the pointwise knowledge of the characteristic of the material does not provide in a simple way any information on its global behavior and that making the heterogeneities smaller and smaller means that we “homogenize” the mixture (from the mathematical point of view this means that ε tends to zero).

Many natural questions arise:

- Does the temperature u^ε converge to some limit function u^0 ?
- Does u^0 solve some limit boundary value problem?
- is u^0 a good approximation of u^ε ? Which is the rate of convergence?

We are going to answer some of these questions in the next sections. For more details see (CIORANESCU; DONATO, 1999).

3.1 Introduction to homogenization

The aim of this Chapter is to present the key issues of the mathematical theory of homogenization applied to our model. Generally speaking, in a composite material the heterogeneities are small compared to its global dimension. From the macroscopic point of view, the composite looks like a “homogeneous” material. The aim of “homogenization” is precisely to give the macroscopic properties of the composite by taking into account the properties of the microscopic composite.

Here we will follow very closely the book (CIORANESCU; DONATO, 1999). The purpose of homogenization theory is to study the limit of u^ε as $\varepsilon \rightarrow 0$. In particular it is desirable to identify the equation satisfied by u^ε in the limit. In next sections we will discuss that, under appropriate assumptions on $\mathcal{K}(\frac{x}{\varepsilon})$, $f(x)$, and Ω , the homogenized equation is

$$\begin{cases} -\nabla \cdot (\mathcal{K}^0 \nabla u^0) = f & \text{in } \Omega, \\ u^0 = 0 & \text{on } \partial\Omega \end{cases} \quad (3.4)$$

and \mathcal{K}^0 is called the homogenized tensor (revisit the well-known theory (CIORANESCU; DONATO, 1999)).

3.2 Homogenization of elliptic equations: some results

In this section we present some important results that will be used in this work. Consider the elliptic problem

$$\begin{cases} -\nabla \cdot (\mathcal{K}^\varepsilon \nabla u^\varepsilon) = f & \text{in } \Omega, \\ u^\varepsilon = 0 & \text{on } \partial\Omega. \end{cases} \quad (3.5)$$

The following classic result is valid (CIORANESCU; DONATO, 1999)

Theorem 1. Let $f \in H^{-1}(\Omega)$ a function in the dual space of $H_0^1(\Omega)$ and u^ε be solution of (3.5) where \mathcal{K}^ε is a Y -periodic matrix that satisfies $\mathcal{K}^\varepsilon(x) = \mathcal{K}(\frac{x}{\varepsilon})$ and the differential operator of (3.5) is coercive. Then

$$\begin{cases} i) & u^\varepsilon \rightharpoonup u^0 \text{ weakly in } H_0^1(\Omega) \\ ii) & \mathcal{K}^\varepsilon \nabla u^\varepsilon \rightharpoonup \mathcal{K}^0 \nabla u^0 \text{ weakly in } L^2(\Omega) \end{cases} \quad (3.6)$$

where u^0 is the unique solution in $H_0^1(\Omega)$ of the homogenized problem (3.4). The matrix \mathcal{K}^0 is constant and coercive.

Corollary 1. If \mathcal{K}^ε is symmetric then \mathcal{K}^0 is symmetric.

Besides that, the classical homogenization theory (JIKOV et al., 1994) provide us: $\exists C > 0, \forall \varepsilon > 0$ such that

$$\|u^\varepsilon - u^0\|_{L^2(\Omega)} \leq C\varepsilon. \quad (3.7)$$

As mentioned before, we consider multiscale problems with two scales: the variable x describe the ‘‘macroscopic’’ scale, while x/ε describes the ‘‘microscopic’’ one. Indeed, if $x \in \Omega$, by the definition of Y , there exists $k \in \mathbb{Z}^n$ such that $x/\varepsilon = (y + k_l)$ with $y \in Y$ and where $k_l = (k_1 l_1, \dots, k_n l_n)$. Here, x gives the position of a point in the domain Ω whereas y gives its position in the reference cell Y .

Studying the limit function u^0 suggests to write down u^ε using a asymptotic expansion of the form

$$u^\varepsilon(x) = u^0(x, \frac{x}{\varepsilon}) + \varepsilon u^1(x, \frac{x}{\varepsilon}) + \varepsilon^2 u^2(x, \frac{x}{\varepsilon}) + \dots \quad (3.8)$$

with $u^j(x, y)$ for $j = 1, 2, \dots$, such that

$$\begin{cases} u^j(x, y) & \text{is defined for } x \in \Omega \text{ and } y \in Y \\ u^j(x, \cdot) & \text{is } Y\text{-periodic} \end{cases} \quad (3.9)$$

where $u(x, \cdot)$ Y -periodic means that function $u = u(x, y)$ is periodic with respect the second variable y and has Y as the periodic domain. Let $\psi(x, y)$ be a function on the two x, y variables in \mathbb{R}^n , we denote by $\psi^\varepsilon(x)$ the associated multiscale function such that $\psi^\varepsilon(x) = \psi(x, \frac{x}{\varepsilon})$. Its derivatives satisfies

$$\frac{\partial \psi^\varepsilon}{\partial x_i}(x) = \frac{1}{\varepsilon} \frac{\partial \psi}{\partial y_i}(x, \frac{x}{\varepsilon}) + \frac{\partial \psi}{\partial x_i}(x, \frac{x}{\varepsilon}). \quad (3.10)$$

Consequently, defining the operator $K_\varepsilon = - \sum_{i,j=1}^n \frac{\partial}{\partial x_i} (\mathcal{K}_{i,j}^\varepsilon \frac{\partial}{\partial x_j})$, one can write $K_\varepsilon \psi^\varepsilon$ as follows:

$$K_\varepsilon \psi^\varepsilon = ((\varepsilon^{-2} K_0 + \varepsilon^{-1} K_1 + K_2) \psi) (x, \frac{x}{\varepsilon}) \quad (3.11)$$

where

$$\begin{cases} K_0 = - \sum_{i,j=1}^n \frac{\partial}{\partial y_i} (\mathcal{K}_{i,j}(y) \frac{\partial}{\partial y_j}) \\ K_1 = - \sum_{i,j=1}^n \frac{\partial}{\partial x_i} (\mathcal{K}_{i,j}(y) \frac{\partial}{\partial y_j}) - \sum_{i,j=1}^n \frac{\partial}{\partial y_i} (\mathcal{K}_{i,j}(y) \frac{\partial}{\partial x_j}) \\ K_2 = - \sum_{i,j=1}^n \frac{\partial}{\partial x_i} (\mathcal{K}_{i,j}(y) \frac{\partial}{\partial x_j}). \end{cases} \quad (3.12)$$

Equalizing the ε power terms, we have to solve the following infinite system of equations:

$$\begin{cases} K_0 u^0 = 0 \text{ in } Y \\ u^0 \text{ } Y\text{-periodic,} \end{cases} \quad (3.13)$$

$$\begin{cases} K_0 u^1 = -K_1 u^0 \text{ in } Y \\ u^1 \text{ } Y\text{-periodic,} \end{cases} \quad (3.14)$$

$$\begin{cases} K_0 u^2 = f - K_1 u^1 - K_2 u^0 \text{ in } Y \\ u^2 \text{ } Y\text{-periodic,} \end{cases} \quad (3.15)$$

and for $s \geq 1$

$$\begin{cases} K_0 u^{s+2} = -K_1 u^{s+1} - K_2 u^s \text{ in } Y \\ u^{s+2} \text{ } Y\text{-periodic.} \end{cases} \quad (3.16)$$

with $u^j \in H^2(\Omega \times Y)$.

Let us now solve successively systems (3.13)-(3.15). Let $\mathcal{W}_{per(Y)}$ the quotient space associated to the relation $u \sim v$, see B.3.

We consider the variational formulation of (3.13) as follows

$$\begin{cases} \text{Find } \dot{u}_0 \in \mathcal{W}_{per}(Y) \text{ such that} \\ \mathcal{K}_Y(\dot{u}_0, \dot{v}) = 0, \quad \forall \dot{v} \in \mathcal{W}_{per}(Y) \end{cases} \quad (3.17)$$

where $\forall \dot{u}, \dot{v} \in \mathcal{W}_{per}(Y) \forall u \in \dot{u}, v \in \dot{v}$ and $\mathcal{K}_Y(\dot{u}, \dot{v}) = \int_Y \mathcal{K} \nabla u \nabla v dy$. For the Lax-Milgram Theorem (see appendix) $\dot{u} = \dot{0}$ is the unique solution of (3.17). This implies that the solution u^0 of (3.17) is independent of y , so that

$$u^0(x, y) = u^0(x),$$

then $u^0 \in H^2(\Omega)$.

Consider now equation (3.14), since $u^0(x)$ not depends on y , (3.14) can be written as

$$\begin{cases} K_0 u^1 = \sum_{i,j=1}^n \frac{\partial \mathcal{K}_{i,j}}{\partial y_i} \frac{\partial u^0}{\partial x_j} & \text{in } Y \\ u^1 & Y - \text{periodic.} \end{cases} \quad (3.18)$$

Its variational formulation is

$$\begin{cases} \text{Find } \dot{u}_1 \in \mathcal{W}_{per}(Y) \text{ such that} \\ \mathcal{K}_Y(\dot{u}_1, \dot{v}) = \langle F, \dot{v} \rangle_{(\mathcal{W}_{per})', \mathcal{W}_{per}} \\ \forall \dot{v} \in \mathcal{W}_{per}(Y), \end{cases} \quad (3.19)$$

where F is defined by

$$\langle F, \dot{\psi} \rangle_{(\mathcal{W}_{per})', \mathcal{W}_{per}} = \sum_{i,j=1}^n \frac{\partial u^0}{\partial x_j} \int_Y \mathcal{K}_{i,j} \frac{\partial \dot{\psi}}{\partial y_i} dy. \quad \forall \dot{\psi} \in \dot{\psi}, \dot{\psi} \in \mathcal{W}_{per}(Y). \quad (3.20)$$

Observe that if $\psi_1, \psi_2 \in \dot{\psi}$ then

$$\frac{\partial \psi_1}{\partial y_i} = \frac{\partial \psi_2}{\partial y_i} \quad (3.21)$$

and so

$$\langle F, \psi_1 \rangle_{H^1_{per}, H^1_{per}} = \langle F, \psi_2 \rangle_{H^1_{per}, H^1_{per}}. \quad (3.22)$$

This defines F as an element of $\mathcal{W}'_{per}(Y)$.

The linearity of K_0 together with the fact that $\partial u^0 / \partial x_j$ is independent of y , suggests to write \dot{u}_1 solution of (3.19) in the following form:

$$\dot{u}_1(x, y) = - \sum_{j=1}^n \dot{\chi}_j(y) \frac{\partial \dot{u}_0}{\partial x_j}(x), \quad \text{in } \mathcal{W}_{per}(Y) \quad (3.23)$$

where $\dot{\chi}$ satisfies

$$\begin{cases} K_0 \dot{\chi}_j = \sum_{i=1}^n \frac{\partial \mathcal{K}_{i,j}}{\partial y_i} & \text{in } Y \\ \dot{\chi}_j & Y - \text{periodic,} \end{cases} \quad (3.24)$$

for $j = 1, 2, \dots, n$. It is easy to see that from Lax-Milgram theorem there is a unique solution $\dot{\chi} \in \mathcal{W}_{per}(Y)$ of this problem. Moreover, we can choose a representative element of $\dot{\chi}_j$. Hence, there is a unique $\chi_j \in \dot{\chi}_j$, such that

$$\begin{cases} \mathcal{K}_Y(\chi_j, \psi) = \sum_i^n \int_Y \mathcal{K}_{i,j}(y) \frac{\partial \psi}{\partial y_i} dy \\ \forall \psi \in W_{per,0}(Y), \end{cases} \quad (3.25)$$

where

$$W_{per,0}(Y) = \{v \in H^1_{per}(Y); \int_Y v dy = 0\}. \quad (3.26)$$

On the other hand, from (3.23) we see that any solution $u^1(x, y) \in \dot{u}_1$ of (3.14) has the form

$$u^1(x, y) = - \sum_{j=1}^n \chi_j(y) \frac{\partial u^0}{\partial x_j} + \tilde{u}_1(x), \quad (3.27)$$

where \tilde{u}_1 is independent of y , i.e.

$$\tilde{u}_1(x) \in \dot{0} \text{ in } \mathcal{W}_{per}(Y). \quad (3.28)$$

Now we use (3.15) to obtain the form of $u^2(x, y)$. Since

$$f - K_1 u^1 - K_2 u^0 = f + \sum_{i,j=1}^n \frac{\partial}{\partial y_i} (\mathcal{K}_{i,j}(y) \frac{\partial u^1}{\partial x_j}) + \sum_{i,j=1}^n \frac{\partial}{\partial x_i} (\mathcal{K}_{i,j}(y) (\frac{\partial u^1}{\partial y_j} + \frac{\partial u^0}{\partial x_j})). \quad (3.29)$$

We have that, the variational formulation of (3.15) is

$$\begin{cases} \text{Find } \dot{u}_2 \in \mathcal{W}_{per}(Y) \text{ such that} \\ \mathcal{K}_Y(\dot{u}_2, \dot{v}) = \langle F_1, \dot{v} \rangle_{(\mathcal{W}_{per})', (\mathcal{W}_{per})} \\ \forall \dot{v} \in \mathcal{W}_{per}(Y), \end{cases} \quad (3.30)$$

where F_1 is defined by

$$\langle F_1, \dot{\psi} \rangle_{(\mathcal{W}_{per})', (\mathcal{W}_{per})} = \int_Y f \psi \, dy - \sum_{i,j=1}^n \int_Y \mathcal{K}_{i,j}(y) \frac{\partial u^1}{\partial x_j} \frac{\partial \psi}{\partial y_i} \quad (3.31)$$

$$+ \sum_{i,j=1}^n \int_Y \frac{\partial}{\partial x_i} (\mathcal{K}_{i,j}(y) (\frac{\partial u^1}{\partial y_j} + \frac{\partial u^0}{\partial x_j})) \psi \, dy, \quad (3.32)$$

$\forall \psi \in \dot{\psi}, \dot{\psi} \in \mathcal{W}_{per}(Y)$.

We use now the following Lemma (PERSSON et al., 1993) to prove the existence of solution of (3.15).

Lemma 1. *Let $\zeta(y) \in L^2(\Omega)$ e Y -periodic. For the boundary value problem*

$$K_0 \psi = \zeta(y) \text{ on } Y, \quad (3.33)$$

where $\psi(y)$ is Y -periodic. There exists a solution ψ if and only if $\langle \zeta \rangle = 0$, where $\langle \cdot \rangle$ denote the average over Y .

Using this result, (3.15) has a solution if $\langle F_1, \dot{0} \rangle = 0$. Note that (3.33) guarantee also that $\langle F_1, \dot{\psi} \rangle$ is unique. Now (3.15) can be written as

$$- \sum_{i,j=1}^n \int_Y \frac{\partial}{\partial x_i} (\mathcal{K}_{i,j}(y) (\frac{\partial u^1}{\partial y_j} + \frac{\partial u^0}{\partial x_j})) \, dy = \int_Y f \, dy. \quad (3.34)$$

Replacing (3.34), and since $f = f(x)$, we find that u^0 has to satisfy

$$- \sum_{i,j=1}^n \int_Y \frac{\partial}{\partial x_i} (\mathcal{K}_{i,j}(y) (- \sum_{k=1}^n \frac{\partial \chi_k}{\partial y_j} \frac{\partial u^0}{\partial x_k} + \frac{\partial u^0}{\partial x_j})) \, dy = |Y|f, \quad (3.35)$$

or equivalently

$$- \sum_{i,k=1}^n \left(\int_Y (\mathcal{K}_{i,k}(y) - \sum_{j=1}^n \mathcal{K}_{i,j}(y) \frac{\partial \chi_k}{\partial y_j}) dy \right) \frac{\partial^2 u^0}{\partial x_i \partial x_k} = |Y|f. \quad (3.36)$$

Consequently, (3.36) is nothing else than

$$- \sum_{i,j=1}^n \frac{\partial}{\partial x_i} \left(\mathcal{K}_{i,k}^0 \frac{\partial u^0}{\partial x_k} \right) = f \text{ in } \Omega, \quad (3.37)$$

where $u^0 \in H^2$ and

$$\mathcal{K}_{i,k}^0 = \frac{1}{|Y|} \int_Y \left(\mathcal{K}_{i,k} - \sum_{j=1}^n \mathcal{K}_{i,j} \frac{\partial \chi_k}{\partial y_j} \right) dy, \forall i, k = 1, \dots, n. \quad (3.38)$$

The existence and uniqueness of $u^0 \in H_0^1(\Omega)$ solution of variational form of (3.37) in the weak form follows from Lax-Milgram theorem.

3.3 Homogenization of parabolic equations: some results (PERSOSON et al., 1993)

In this section we consider the following sequence of parabolic problems:

$$\begin{cases} \rho^\varepsilon \frac{\partial u^\varepsilon}{\partial t} + K_\varepsilon u^\varepsilon = f^\varepsilon, u^\varepsilon(0) = g, \\ u^\varepsilon \in L^2(0, T; H_0^1(\Omega)), \end{cases} \quad (3.39)$$

where Ω is an open bounded subset of \mathbb{R}^n and where class $\{K_\varepsilon\}$ of operators has the form

$$K_\varepsilon = - \sum_{i,j=1}^n \frac{\partial}{\partial x_i} \left(\mathcal{K}_{i,j}^\varepsilon(x) \frac{\partial}{\partial x_j} \right). \quad (3.40)$$

We assume that the functions $\mathcal{K}^\varepsilon(x) = \mathcal{K}_{i,j}(x/\varepsilon)$ are measurable and satisfy the coercivity and boundedness assumptions. Further, $\rho^\varepsilon(x) = \rho(x/\varepsilon)$ is assumed to be positive and to belong to $L^\infty(\Omega)$ and f^ε are assumed to belong to $L^2(0, T; L^2(\Omega))$, $T > 0$, and g_0 is assumed to belong to $L^2(\Omega)$. The main result is that the sequence u^ε of solutions of (3.39) converges weakly in $L^2(0, T; H_0^1(\Omega))$ to the solution u^0 of the following problem, homogenization problem associated to (3.39)

$$\begin{cases} \langle \rho \rangle \frac{\partial u^0}{\partial t} + K u^0 = f, u^0(0) = g, \\ u \in L^2(0, T; H_0^1(\Omega)), \end{cases} \quad (3.41)$$

as ε tends to zero, where $\langle \cdot \rangle$ is the average over Y and the operator K is of the form

$$K = - \sum_{i,j=1}^n \frac{\partial}{\partial x_i} \left(\mathcal{K}_{i,j}^0 \frac{\partial}{\partial x_j} \right). \quad (3.42)$$

The coefficients $\mathcal{K}_{i,j}^0$ in (3.42) are defined as (3.38).

The parabolic differential operators P^ε and P are defined by

$$P_\varepsilon = \left(\rho^\varepsilon \frac{\partial}{\partial t} + K_\varepsilon \right) \quad (3.43)$$

and

$$P = \left(\langle \rho \rangle \frac{\partial}{\partial t} + K \right). \quad (3.44)$$

Consider the problems (3.41) and (3.39). We say that the sequence $\{P_\varepsilon\}$ G-converges to P as $\varepsilon \rightarrow 0$ if

$$u^\varepsilon \rightarrow u^0 \text{ in } L^2(0, T; H_0^1(\Omega)) \text{ weakly,} \quad (3.45)$$

and

$$\mathcal{K}_{i,j}^\varepsilon \frac{\partial u^\varepsilon}{\partial x_j} \rightarrow \mathcal{K}_{i,j}^0 \frac{\partial u^0}{\partial x_j} \text{ in } L^2(0, T; (L^2(\Omega))^n) \text{ weakly,} \quad (3.46)$$

whenever

$$f^\varepsilon \rightarrow f \text{ in } L^2(0, T; L^2(\Omega)) \text{ weakly.} \quad (3.47)$$

Theorem 2. *Consider the problems (3.41) and (3.39). If $\mathcal{K}_{i,j}^\varepsilon$ is Y -periodic and symmetric, if ρ^ε is Y -periodic and uniformly bounded and if $f^\varepsilon \rightarrow f$ in $L^2(0, T; L^2(\Omega))$ weakly as $\varepsilon \rightarrow 0$, then, P^ε G-converges to P .*

For more details see (PERSSON et al., 1993).

3.4 Homogenization of our multiscale colonic cell problem (2.21)

The main benefit of the homogenization is that it permits to describe, with a simpler model, a very complex, periodic, and multiscale problem, providing numerical solutions which can be easily computed. We describe in the following the homogenization for the elliptic and parabolic equations (2.21). We use in the next sections the notation $C^\varepsilon, p^\varepsilon$ instead of $\bar{C}^\varepsilon, \bar{p}^\varepsilon$.

3.4.1 Elliptic equation

Firstly, let us begin by homogenizing the elliptic equation using similar steps of that discussed in Section 3.2. In what follows, we consider the Einstein notation. The elliptic equation is

$$-\frac{\partial}{\partial x_i} \left(\mathcal{A}_{ij}^\varepsilon \frac{\partial p^\varepsilon}{\partial x_j} \right) = |g|^\varepsilon \beta^\varepsilon C^\varepsilon \equiv f^\varepsilon. \quad (3.48)$$

and where $f(x, y) = |g(y)|\beta(y)C(x, y)$ with $f^\varepsilon(x) = f(x, \frac{x}{\varepsilon})$. We suppose that exists an asymptotic expansion for p^ε and f^ε as function of ε . Then, $p^\varepsilon(x) = p^0(x) + \varepsilon p^1(x, y) +$

$\varepsilon^2 p^2(x, y) + \dots$ with each p^i and its derivatives Y -periodic with respect to y and $f^\varepsilon = f^0 + \varepsilon f^1 + \varepsilon^2 f^2 + \dots$. Therefore we have

$$\frac{\partial p^\varepsilon}{\partial x_i} = \left(\frac{\partial p^0}{\partial x_i} + \frac{\partial p^1}{\partial y_i} \right) + \varepsilon \left(\frac{\partial p^1}{\partial x_i} + \frac{\partial p^2}{\partial y_i} \right) + \varepsilon^2 \left(\frac{\partial p^2}{\partial x_i} + \frac{\partial p^3}{\partial y_i} \right) \dots \quad (3.49)$$

and then let $h_i^\varepsilon := \mathcal{A}_{ij}^\varepsilon \frac{\partial p^\varepsilon}{\partial x_j}$. From (3.49)

$$h_i^\varepsilon = h_i^0(x, y) + \varepsilon h_i^1(x, y) + \varepsilon^2 \dots = \mathcal{A}_{ij}(y) \frac{\partial p^\varepsilon}{\partial x_j}, \quad (3.50)$$

where

$$\begin{cases} h_i^0(x, y) = \mathcal{A}_{i,j}(y) \left(\frac{\partial p^0}{\partial x_j} + \frac{\partial p^1}{\partial y_j} \right) \\ h_i^1(x, y) = \mathcal{A}_{i,j}(y) \left(\frac{\partial p^1}{\partial x_j} + \frac{\partial p^2}{\partial y_j} \right) \\ h_i^l(x, y) = \mathcal{A}_{i,j}(y) \left(\frac{\partial p^l}{\partial x_j} + \frac{\partial p^{l+1}}{\partial y_j} \right) \end{cases} . \quad (3.51)$$

We have in particular that each $h_i^l(x, y)$ is Y -periodic with respect y . Since in general $\frac{\partial}{\partial x_i} \psi(x, \frac{x}{\varepsilon}) = \frac{\partial \psi}{\partial x_i} + \frac{1}{\varepsilon} \frac{\partial \psi}{\partial y_j}$, we can rewrite equation (3.48) in the form

$$\left(-\frac{\partial}{\partial x_i} - \frac{1}{\varepsilon} \frac{\partial}{\partial y_i} \right) (h_i^0 + \varepsilon h_i^1 + \dots) = f^\varepsilon(x). \quad (3.52)$$

Note that since $|g|^\varepsilon \beta^\varepsilon C^\varepsilon$ has not ε powers with negative exponents we have equalizing the ε powers in (3.49). Which allow us to get the following powered ε equations:

- The ε^{-1} equation:

$$-\frac{\partial h_i^0}{\partial y_i}(x, y) = 0 \iff \frac{\partial}{\partial y_i} \left(\mathcal{A}_{i,j}(y) \left(\frac{\partial p^0}{\partial x_j} + \frac{\partial p^1}{\partial y_j} \right) \right) = 0. \quad (3.53)$$

- The ε^0 equation:

$$-\left(\frac{\partial h_i^0}{\partial x_i} + \frac{\partial h_i^1}{\partial y_i} \right) (x, y) = f^0(x, y) \quad (3.54)$$

where $f^0(x, y) = |g(y)|\beta(y)C^0(x)$.

By applying the operator $\langle \cdot \rangle$ to (3.54), we have $\forall x \in \Omega$

$$-\left\langle \frac{\partial h_i^0}{\partial x_i} \right\rangle - \left\langle \frac{\partial h_i^1}{\partial y_i} \right\rangle = \langle f^0 \rangle. \quad (3.55)$$

On the other hand, by using the divergence theorem we have

$$-\left\langle \frac{\partial h_i^1}{\partial y_i}(x) \right\rangle = -\frac{1}{|Y|} \int_Y \frac{\partial h_i^1}{\partial y_i}(x, y) dy = -\frac{1}{|Y|} \int_{\partial Y} \eta_i h_i^1(x, s) ds \quad (3.56)$$

where $\eta = \eta_i$ is i -th component of the the outer unit normal on the boundary ∂Y of Y . But since $h_i^1(x, y)$ is Y -periodic in y , then the integral on two opposite faces of ∂Y takes opposite values because $h(x, y)$ (resp. $\eta(y)$) takes the same (resp. opposite) values in homologous points. Thus using (3.56) we conclude that $-\langle \frac{\partial h_i^1}{\partial y_i}(x) \rangle = 0$ and using (3.55) we get

$$-\langle \frac{\partial h_i^0}{\partial x_i} \rangle = \langle f^0 \rangle. \quad (3.57)$$

The next step is to obtain a relation between $\langle h^0 \rangle$ and p^0 . We write the local equation (3.53) (for a fixed x) in the form

$$-\frac{\partial}{\partial y_i} (\mathcal{A}_{ij}(y) \frac{\partial p^1}{\partial y_j}(x, y)) = \frac{\partial p^0}{\partial x_j}(x) \frac{\partial \mathcal{A}_{ij}}{\partial y_i}(y) \quad (3.58)$$

and we consider it as an equation in y with the unknown $p^1(x, y)$. Here x is just a parameter and the equation may be regarded as a problem depending on the variable y only. Therefore it suffices to consider the *cell problem*

$$-\frac{\partial}{\partial y_i} (\mathcal{A}_{ij}(y) \frac{\partial \chi_k}{\partial y_j}(y)) = -\frac{\partial \mathcal{A}_{ik}}{\partial y_i}(y) \quad (3.59)$$

Now, assuming that a solution $\chi_k(y)$ of (3.59) is given, for $k = 1, 2, \dots, n$. By using the linearity, we conclude that the function

$$p^1(x, y) = -\sum_k \frac{\partial p^0}{\partial x_k}(x) \chi_k(y) + c(x).$$

is the weak solution of (3.58). Thus we have

$$h_i^0(x, y) = \mathcal{A}_{ij}(y) \left(\frac{\partial p^0}{\partial x_j}(x) + \frac{\partial p^1}{\partial y_j}(x, y) \right) = \mathcal{A}_{ij}(y) \left(\frac{\partial p^0}{\partial x_j} + \sum_k \frac{\partial p^0}{\partial x_k} \frac{\partial \chi_k}{\partial y_j}(x, y) \right) \quad (3.60)$$

$$= \sum_k (\mathcal{A}_{ik}(y) - \sum_j \mathcal{A}_{ij} \frac{\partial \chi_k}{\partial y_j}(y)) \frac{\partial p^0}{\partial x_k}(x) \quad (3.61)$$

and by (3.57) we obtain the homogenized equation associated to (3.48)

$$-\frac{\partial}{\partial x_i} (\mathcal{A}_{ik}^0 \frac{\partial p^0}{\partial x_k}(x)) = \langle f^0 \rangle, \quad (3.62)$$

where

$$\mathcal{A}_{ik}^0 := \langle \mathcal{A}_{ik} - \sum_j \mathcal{A}_{ij} \frac{\partial \chi_k}{\partial y_j} \rangle \quad (3.63)$$

are the homogenized coefficients.

3.4.2 Parabolic equation

In what follows we suppose that the diffusion matrix D^ε is not singular and constant. A similar analysis can be obtained when $D = D(y)$ varies only at the microscale.

$$|g|^\varepsilon \frac{\partial C^\varepsilon}{\partial t} - D^\varepsilon \frac{\partial}{\partial x_i} \left(\mathcal{A}_{ij}^\varepsilon \frac{\partial C^\varepsilon}{\partial x_j} \right) - \mathcal{A}_{ij}^\varepsilon \frac{\partial C^\varepsilon}{\partial x_i} \frac{\partial p^\varepsilon}{\partial x_j} - C^\varepsilon |g|^\varepsilon (\alpha^\varepsilon - \beta^\varepsilon C^\varepsilon) = 0 \quad (3.64)$$

Defining $h_i^\varepsilon = \mathcal{A}_{ij}^\varepsilon \frac{\partial C^\varepsilon}{\partial x_j}$, we consider the expansions $h_i^\varepsilon = h_i^0(x, y, t) + \varepsilon h_i^1(x, y, t) + \varepsilon^2 \dots$ and $C^\varepsilon(x, t) = C^0(x, t) + \sum_i^\infty \varepsilon^i C^i(x, y, t)$. Note that h_i^k with $k = 0, 1, 2, \dots$ have a similar definition of those defined in (3.51) with p replaced by C .

Since $p^0 = p^0(x, t)$ and $C^0 = C^0(x, t)$ the expression $\mathcal{A}_{ij}^\varepsilon \frac{\partial C^\varepsilon}{\partial x_i} \frac{\partial p^\varepsilon}{\partial x_j}$ has not ε^{-2} terms. Using an similar analysis of that implemented in the previous section, the ε^{-1} equation is associated

$$-D \frac{\partial}{\partial y_i} \left(\mathcal{A}_{ij}(y) \left(\frac{\partial C^0}{\partial x_j}(x, t) + \frac{\partial C^1}{\partial y_j}(x, y, t) \right) \right) = 0. \quad (3.65)$$

Note that since D is a non singular matrix independent on x the equation (3.65) yields to

$$\frac{\partial}{\partial y_i} \left(\mathcal{A}_{ij}(y) \left(\frac{\partial C^0}{\partial x_j}(x, t) + \frac{\partial C^1}{\partial y_j}(x, y, t) \right) \right) = 0. \quad (3.66)$$

Using the Y -periodicity of \mathcal{A} and its symmetry, we have that the ε^0 equation is

$$|g(y)| \frac{\partial C^0}{\partial t} - D \left(\frac{\partial h_i^0}{\partial x_i} + \frac{\partial h_i^1}{\partial y_i} \right) - \mathcal{A}_{ij} \left(\frac{\partial p^0}{\partial x_i} + \frac{\partial p^1}{\partial y_i} \right) \left(\frac{\partial C^0}{\partial x_j} + \frac{\partial C^1}{\partial y_j} \right) - C^0 |g(y)| (\alpha(y) - \beta(y) C^0) = 0. \quad (3.67)$$

As before by applying the mean operator $\langle \cdot \rangle$ to the Y -periodic function $\frac{\partial h_i^1(x, y)}{\partial y_i}$ we have

$$\left\langle \frac{\partial h_i^1}{\partial y_i} \right\rangle = 0$$

and then applying the mean operator to (3.67) we obtain for each $x \in \Omega$

$$\langle |g| \rangle \frac{\partial C^0}{\partial t} - D \left(\left\langle \frac{\partial h_i^0}{\partial x_i} \right\rangle \right) - \left\langle \mathcal{A}_{ij} \left(\frac{\partial p^0}{\partial x_i} + \frac{\partial p^1}{\partial y_i} \right) \left(\frac{\partial C^0}{\partial x_j} + \frac{\partial C^1}{\partial y_j} \right) \right\rangle - C^0 \langle |g| (\alpha - \beta C^0) \rangle = 0. \quad (3.68)$$

As in the previous section, using the ε^{-1} equation (3.66) we get

$$C^1(x, y, t) = - \sum_k \frac{\partial C^0}{\partial x_k} \chi_k(y) + c_1(x, t).$$

where χ_k is the same solutions of (3.59) obtained before. Substituting $C^1(x, y)$ into h_i^0

$$h_i^0 = \mathcal{A}_{ij} \left(\frac{\partial C^0}{\partial x_j} + \frac{\partial C^1}{\partial y_j} \right) = \mathcal{A}_{ij}(y) \left(\frac{\partial C^0}{\partial x_j} - \frac{\partial C^0}{\partial x_k} \frac{\partial \chi_k}{\partial y_j}(y) \right) \quad (3.69)$$

$$= \left(\mathcal{A}_{ik}(y) - \sum_j \mathcal{A}_{ij} \frac{\partial \chi_k}{\partial y_j}(y) \right) \frac{\partial C^0}{\partial x_k}(x, t) \quad (3.70)$$

and then applying the mean operator $\langle \cdot \rangle$ to h_i^0 we have

$$\langle h_i^0 \rangle = \mathcal{A}_{ik}^0 \frac{\partial C^0}{\partial x_k} \quad (3.71)$$

where \mathcal{A}_{ik}^0 is defined in (3.63). We observe that since $h_i^0 = \mathcal{A}_{ij} \left(\frac{\partial C^0}{\partial x_j} + \frac{\partial C^1}{\partial y_j} \right)$

$$\mathcal{A}_{ij} \left(\frac{\partial p^0}{\partial x_i} + \frac{\partial p^1}{\partial y_i} \right) \left(\frac{\partial C^0}{\partial x_j} + \frac{\partial C^1}{\partial y_j} \right) = h_i^0 \left(\frac{\partial p^0}{\partial x_i} + \frac{\partial p^1}{\partial y_i} \right) = h_i^0 \left(\frac{\partial p^0}{\partial x_i} \right) + h_i^0 \left(\frac{\partial p^1}{\partial y_i} \right) \quad (3.72)$$

and then by applying the average operator $\langle \cdot \rangle$,

$$\langle \mathcal{A}_{ij} \left(\frac{\partial p^0}{\partial x_i} + \frac{\partial p^1}{\partial y_i} \right) \left(\frac{\partial C^0}{\partial x_j} + \frac{\partial C^1}{\partial y_j} \right) \rangle = \langle h_i^0 \rangle \frac{\partial p^0}{\partial x_i} + \langle h_i^0 \frac{\partial p^1}{\partial y_i} \rangle = \mathcal{A}_{ik}^0 \frac{\partial p^0}{\partial x_i} \frac{\partial C^0}{\partial x_k} \quad (3.73)$$

where we used the relation (3.71) and that $\langle h_i^0 \frac{\partial p^1}{\partial y_i} \rangle = 0$. This is true since using the divergence theorem and (3.66) we obtain

$$\langle h_i^0 \frac{\partial p^1}{\partial y_i} \rangle = -\frac{1}{|Y|} \int_Y \frac{\partial}{\partial y_i} \left(\mathcal{A}_{ij} \left(\frac{\partial C^0}{\partial x_j} + \frac{\partial C^1}{\partial y_j} \right) \right) p^1(x, y) dy = 0. \quad (3.74)$$

Therefore using (3.73), (3.68), (3.57) and (3.62) the homogenization of (2.21) is

$$\begin{cases} \langle |g| \rangle \frac{\partial C^0}{\partial t} &= D \nabla \cdot (\mathcal{A}^0 \nabla C^0) + \nabla p^0 \cdot \mathcal{A}^0 \nabla C^0 + C^0 \langle |g| (\alpha - \beta C^0) \rangle \\ -\nabla \cdot (\mathcal{A}^0 \nabla p^0) &= \langle |g| \beta \rangle C^0. \end{cases} \quad (3.75)$$

We can obtain this homogenized system starting also with the parabolic equation without developing in series its derivatives as done in (3.64). Consider

$$|g|^\varepsilon(x) \frac{\partial C^\varepsilon}{\partial t} - D \frac{\partial}{\partial x_i} \left(\mathcal{A}_{ij}^\varepsilon \frac{\partial C^\varepsilon}{\partial x_j} \right) - \frac{\partial}{\partial x_i} \left(\mathcal{A}_{ij}^\varepsilon \frac{\partial p^\varepsilon}{\partial x_j} C^\varepsilon \right) - C^\varepsilon |g|^\varepsilon \alpha^\varepsilon = 0, \quad (3.76)$$

since $\frac{\partial}{\partial x} \psi(x, \frac{x}{\varepsilon}) = \frac{\partial \psi}{\partial x}(x, y) + \frac{1}{\varepsilon} \frac{\partial}{\partial y} \psi(x, y)$ we obtain

$$\begin{aligned} \frac{\partial}{\partial x_i} \left(\mathcal{A}_{ij}^\varepsilon \frac{\partial p^\varepsilon}{\partial x_j} C^\varepsilon \right) &= \frac{\partial}{\partial x_i} \left(\mathcal{A}_{ij}(y) \left(\left(\frac{\partial p^0}{\partial x_j} + \frac{\partial p^1}{\partial y_j} \right) + \varepsilon \left(\frac{\partial p^1}{\partial x_j} + \frac{\partial p^2}{\partial y_j} \right) + \varepsilon^2 \dots \right) \left(\sum_{i=0} \varepsilon^i C^i \right) \right) \\ &+ \frac{1}{\varepsilon} \frac{\partial}{\partial y_i} \left(\mathcal{A}_{ij}(y) \left(\left(\frac{\partial p^0}{\partial x_j} + \frac{\partial p^1}{\partial y_j} \right) + \varepsilon \left(\frac{\partial p^1}{\partial x_j} + \frac{\partial p^2}{\partial y_j} \right) + \varepsilon^2 \dots \right) \left(\sum_{i=0} \varepsilon^i C^i \right) \right). \end{aligned}$$

Then the ε^{-1} equation becomes

$$-D \frac{\partial}{\partial y_i} (\mathcal{A}_{ij}(y) (\frac{\partial C^0}{\partial x_j} + \frac{\partial C^1}{\partial y_j})) - \frac{\partial}{\partial y_i} (\mathcal{A}_{ij} (\frac{\partial p^0}{\partial x_j} + \frac{\partial p^1}{\partial y_j}) C^0) = 0,$$

but from (3.53) we get

$$-D \frac{\partial}{\partial y_i} (\mathcal{A}_{ij}(y) (\frac{\partial C^0}{\partial x_j} + \frac{\partial C^1}{\partial y_j})) = 0. \quad (3.77)$$

Look that this is the same ε^{-1} equation obtained before in (3.65). The ε^0 equation is

$$\begin{aligned} & |g(y)| \frac{\partial C^0}{\partial t} - D (\frac{\partial h_i^0}{\partial x_i} + \frac{\partial h_i^1}{\partial y_i}) - \frac{\partial}{\partial x_i} (\mathcal{A}_{ij} (\frac{\partial p^0}{\partial x_j} + \frac{\partial p^1}{\partial y_j}) C^0) \\ & - \frac{\partial}{\partial y_i} (\mathcal{A}_{ij} ((\frac{\partial p^1}{\partial x_j} + \frac{\partial p^2}{\partial y_j}) C^0 + (\frac{\partial p^0}{\partial x_j} + \frac{\partial p^1}{\partial y_j}) C^1)) - C^0 |g(y)| \alpha(y) \\ & = 0. \end{aligned}$$

Look that for the Y -periodicity

$$\int_Y \frac{\partial}{\partial y_i} (\mathcal{A}_{ij} ((\frac{\partial p^1}{\partial x_j} + \frac{\partial p^2}{\partial y_j}) C^0 + (\frac{\partial p^0}{\partial x_j} + \frac{\partial p^1}{\partial y_j}) C^1)) dy = 0$$

and then applying the average operator and using the equation (3.77) we get a similar expression to $C^1(x, y, t) = -\sum_k \frac{\partial C^0}{\partial x_k} \chi_k + c_1(x, t)$. Now, using also $p^1(x, y, t) = -\sum_k \frac{\partial p^0}{\partial x_k} \chi_k + c_2(x, t)$ we obtain the following homogenized system

$$\begin{cases} \langle |g| \rangle \frac{\partial C^0}{\partial t} - D \nabla \cdot (\mathcal{A}^0 \nabla C^0) - \nabla \cdot (\mathcal{A}^0 \nabla p^0 C^0) - C^0 \langle |g| \alpha \rangle = 0 \\ -\nabla \cdot (\mathcal{A}^0 \nabla p^0) = \langle |g| \beta \rangle C^0 \end{cases} \quad (3.78)$$

which is equivalent to (3.75).

4 Heterogeneous Multiscale Method(HMM)

The main purpose of this Chapter together with Chapter 3 is to provide an approximation of the original multiscale problem. In Chapter 3 we saw that the homogenization provide us a strategy to represent at the macro level the behavior of a multiscale problem making the heterogeneities smaller and smaller. The HMM method is a framework to design multiscale methods for a wide variety of applications. The aim of HMM is to study the macroscopic behavior of a problem for which the macroscale model is only partially known whereas the microscale model is completely known. The first natural idea could be to solve the microscale problem in the whole domain, but this will require a huge computational effort since the mesh needs elements with dimension smaller than ε . HMM uses instead a efficient numerical method at the macroscale, as if the macroscale model is completely known, and then solves numerically some microproblems in the regions where the macroscale information is missed.

After a brief description of the HMM method in Section 4.1, we discuss the HMM-FEM method to solve a generic elliptic Laplace equation in Section 4.2. Here we also present some known convergence results of this method to approximate the homogenized solution of parabolic or elliptic multiscale equations. This result is used also to give estimates of the approximation error between HMM-FEM solution and the theoretical multiscale solution of parabolic and elliptic equations. Then in Section 4.3 we describe our HMM-FEM method to solve the coupled elliptic-parabolic multiscale equations in 2.21. We plot at the end of this Section one test results of the implemented HMM-FEM. During the implementation of HMM-FEM we can compute, as described in Subsection 4.3.1 an approximation of the homogenized tensor \mathcal{A}^0 . This is useful to approximate \mathcal{A}^0 that is computationally complex to be obtained and thus we can solve the homogenized problem 3.78 with a such approximated homogenized tensor by a simple FEM method based on Backward Euler in time and piecewise linear finite element basis on space. Thus in Section 4.4 we measure the error in L_2 and H_1 norm between the HMM-FEM numerical solution and the homogenized numerical solution. We compare then such results with the expected norm presented in Section 4.2.

4.1 The HMM framework

We consider a microscale model, written as

$$f(u, b) = 0 \tag{4.1}$$

where u is the state variable and b is the set of auxiliary conditions, such as initial and boundary conditions for the problem. We are not interested in the microscopic details of u , but rather the macroscopic state of the system which we denote by U , where U satisfies some abstract macroscopic equation:

$$F(U, D) = 0. \quad (4.2)$$

where D is the missing macroscale data. The goal of HMM is to compute U using the abstract form of F and the microscale model (4.1). A such unknown U is obtained with the HMM method in two steps:

- Selection of a macroscopic solver even though the macroscopic model is not completely available.
- Estimation of the missing macroscale data D using the microscale model.

In the following section we discuss a particular HMM based on finite elements method for solving an elliptic equation. Later we present a HMM-FEM method for solving our multiscale elliptic-parabolic problem.

4.2 Review of HMM-FEM method

Consider

$$-\nabla(\mathcal{A}^\varepsilon(x)\nabla u^\varepsilon(x)) = f(x), \quad x \in \Omega \subset \mathbb{R}^2. \quad (4.3)$$

Here ε is a small parameter that represents explicitly the multiscale nature of the matrix $\mathcal{A}^\varepsilon(x)$. The HMM-FEM method (ENGQUIST et al., 2007) permits to solve multiscale PDE problems at the macroscale level avoiding the theoretical problems of the homogenization. In this section we present the HMM-FEM that is a HMM method based on finite elements, We discuss its deduction and numerical implementation.

4.2.1 The macro solver and the needed data

We use a finite element approach to solve at macroscale the multiscale problem (4.3). We denote by X_H the macroscopic finite element space which can be standard piecewise linear functions over some triangularization \mathcal{T}_H where H denotes the element size. The data needed is the stiffness matrix on $\mathcal{T}_H : S = (S_{ij})$, where

$$S_{ij} = \int_{\Omega} \nabla \phi_i(x)^T \mathcal{A}_H(x) \nabla \phi_j \, dx. \quad (4.4)$$

Here $\mathcal{A}_H(x)$ is the missing effective conductivity tensor at scale H that describes the behavior of the multiscale tensor $\mathcal{A}^\varepsilon(x)$ at the macroscale level and $\{\phi_i(x)\}$ are the

basis functions for X_H . We can evaluate S_{ij} simply by numerical quadrature: let $f_{ij} = \nabla\phi_i(x)^T \mathcal{A}_H(x) \nabla\phi_j(x)$, then

$$S_{ij} = \int_{\Omega} f_{ij}(x) dx = \sum_{K \in \mathcal{T}_H} \int_K f_{ij}(x) dx \simeq \sum_{K \in \mathcal{T}_H} |K| \sum_{l=1}^{\mathcal{L}} \omega_l f_{ij}(x_l), \quad (4.5)$$

where $\{x_l\}_{l=1, \dots, \mathcal{L}}$ and $\{\omega_l\}_{l=1, \dots, \mathcal{L}}$ are, respectively, the quadrature points and weights of the integration quadrature formula used to approximate the integral in the macro element K . Here $|K|$ is the volume of element K . In this analysis we use quadrilateral or triangle elements with, respectively, $\mathcal{L} = 4$ and $\mathcal{L} = 3$ quadrature points. We suppose also to use the same quadrature formula for each element K . Our problem reduces to approximate the values $\{\mathcal{A}_H(x_l)\}$, that can be done by solving locally the original microscale problem around each quadrature point x_l .

Let $I_{\delta}(x_l)$, also denoted by I_{δ_l} , the cube of edge δ and barycenter x_l , and consider a microfunction ϕ^{ε} such that

$$-\nabla \cdot (\mathcal{A}^{\varepsilon}(x) \nabla \phi^{\varepsilon}(x)) = 0, \quad x \in I_{\delta_l}. \quad (4.6)$$

The local microscale problem (4.6) is constrained by the local macroscopic state through the generic constraint:

$$\frac{1}{|I_{\delta_l}|} \int_{I_{\delta}(x_l)} \nabla \phi^{\varepsilon} dx = G \quad (4.7)$$

for some fixed constant vector G (ENGQUIST et al., 2007). In section 4.3 we will present a specific constraint in our multiscale problem to define the associated microscale problems. Two natural boundary conditions for the microscale problem are the periodic boundary condition and the Dirichlet boundary condition which the above condition is satisfied.

- Dirichlet: In this case, Dirichlet boundary condition is used for problem (4.6):

$$\phi^{\varepsilon}(x) = Gx, \quad \text{on } \partial I_{\delta}. \quad (4.8)$$

- Periodic: The problem (4.6) is subjected to:

$$\phi^{\varepsilon}(x) - Gx \text{ is periodic with period } I_{\delta}. \quad (4.9)$$

Thus in this case we can define the effective conductivity tensor at x_l by the relation

$$\langle \mathcal{A}^{\varepsilon} \nabla \phi^{\varepsilon} \rangle_{I_{\delta}} = \mathcal{A}_H(x_l) \langle \nabla \phi^{\varepsilon} \rangle_{I_{\delta}}, \quad (4.10)$$

where $\langle v \rangle_{I_{\delta}} = \frac{1}{|I_{\delta}|} \int_{I_{\delta}} v(x) dx$. The main objective of the HMM-FEM is to link efficiently the microscale behavior of ϕ^{ε} with $\mathcal{A}_H(x_l)$, under the assumption that $\mathcal{A}_H(x)$ is practically constant around x_l for a small δ , and that the average gradient of ϕ^{ε} is fixed independently of the element and of the quadrature point considered.

In summary, the overall algorithm in $\Omega \subset \mathbb{R}^2$ consists in the following steps:

- Determine for $\phi_1^\varepsilon, \phi_2^\varepsilon$ by using the constraint $\langle \nabla \phi_i^\varepsilon \rangle_{I_\delta} = \mathbf{e}_i$.
- Obtain the approximate values of $\mathcal{A}_H(x_l)$ by using (4.10).
- Assemble the effective stiffness matrix A (4.5).
- Solve the macroscale finite element equation using the effective stiffness matrix A (4.5).

This overall procedure is called herein HMM-FEM method (ENGQUIST et al., 2007), that stays for Finite Element Heterogeneous Multiscale Method. The homogenization theory allows us to define the effective (homogenized) conductivity tensor, by considering the infinite volume limit ($\varepsilon \rightarrow 0$) of the solution of the microscale problem subject to the constraint that average gradient remains fixed. When the microstructure is periodic, the infinite volume problem reduces to a periodic problem.

Since the homogenization is another technique to describe the multiscale problem averaging the micro-behavior at the macro scale level, it is natural to consider the HMM-FEM solution as a approximation of the homogenized problem. In (ABDULLE, 2009), HMM-FEM is used to solve an elliptic equation as (4.3). They choose piecewise linear macro and micro FE spaces and periodic coupling to provide the following a prior convergence rates ($\delta = \varepsilon$)

$$\|u^0 - u^{HMM}\|_{H^1(\Omega)} \leq C(H + (\frac{h}{\varepsilon})^2), \|u^0 - u^{HMM}\|_{L^2(\Omega)} \leq C(H^2 + (\frac{h}{\varepsilon})^2). \quad (4.11)$$

For the following parabolic equation

$$\begin{cases} \partial_t u^\varepsilon(x, t) = \nabla(\mathcal{A}^\varepsilon(x, \nabla u^\varepsilon(x, t))) + f(x) & \text{in } \Omega \times (0, T) \\ u^\varepsilon(x, t) = 0 & \text{on } \partial\Omega \times (0, T) \\ u^\varepsilon(x, 0) = g(x) & \text{in } \Omega, \end{cases} \quad (4.12)$$

under some refinements strategies, one can get the following error estimates

$$\max_{1 \leq n \leq N} \|u^0(\cdot, t_n) - u^{HMM}(t_n)\|_{L^2(\Omega)} \leq C(\Delta t + H^2 + (\frac{h}{\varepsilon})), \quad (4.13)$$

$$\left(\sum_{n=1}^N \Delta t \|\nabla u^0(\cdot, t_n) - \nabla u^{HMM}(t_n)\|_{L^2(\Omega)}^2 \right)^{1/2} \leq C(\Delta t + H + (\frac{h}{\varepsilon})). \quad (4.14)$$

For more details see (ABDULLE; HUBER, 2014).

4.3 HMM-FEM applied to our problem

Let consider our differential problem defined in single crypt $\Gamma \subset \mathbb{R}^3$

$$\begin{cases} \frac{\partial C}{\partial t} - \nabla_\Gamma \cdot (\nabla_\Gamma p C) - \nabla_\Gamma \cdot (D \nabla_\Gamma C) - \alpha C = 0 \\ -\Delta_\Gamma p = \beta C \end{cases} \quad (4.15)$$

in $\Gamma \times (0, T]$, with the parametrization $\varphi : Y \rightarrow \Gamma$, as described in Chapter 2. We can rewrite the system (4.15) in local coordinates $(y_1, y_2) \in Y$ as follows

$$\begin{cases} |g| \frac{\partial C}{\partial t} &= \nabla \cdot (\mathcal{A} \nabla p C) + \nabla \cdot (D \mathcal{A} \nabla C) + |g| \alpha C \\ -\nabla \cdot (\mathcal{A} \nabla p) &= |g| \beta C. \end{cases} \quad (4.16)$$

If we accept this choice of variables in Y , we should change (x, y) with (y_1, y_2) also in 2.2.5. The variational problem associated with (4.16) is the following: Find $C, p \in H_0^1(\Omega)$ such that

$$\begin{cases} \int_Y |g| \frac{\partial C}{\partial t} v \, dy &= - \int_Y C (\nabla p)^T \mathcal{A} \nabla v \, dy - D \int_Y (\nabla C)^T \mathcal{A} \nabla v \, dy + \int_Y |g| \alpha C v \, dy \\ \int_Y (\nabla p)^T \mathcal{A} \nabla v \, dy &= \int_Y |g| \beta C v \, dy, \end{cases} \quad (4.17)$$

where $v \in H_0^1(\Omega)$, $\mathcal{A} = (g)^{-1} \sqrt{\det(g)}$ and $|g| = \sqrt{\det(g)}$ as described in 2.2.5. Note that we are using the column notation for the vectors, for instance $\nabla v = \left(\frac{\partial v}{\partial x}, \frac{\partial v}{\partial y} \right)$.

Let ε be the microscale dimension of the crypt in colon. The two dimensional multiscale problem (4.17) is modeled in a rectangular domain Ω formed by a periodic distribution of planified crypts Γ as shown in the figure 9. In order to define a problem in Ω we consider the multiscale periodic coefficients $\mathcal{A}^\varepsilon, \alpha^\varepsilon, \beta^\varepsilon$ defined in Ω in the following way: $\forall x \in \Omega$

$$\mathcal{A}^\varepsilon(x) = \mathcal{A}\left(\frac{x}{\varepsilon}\right) \text{ with } \mathcal{A}(y) = \begin{cases} \mathcal{A} \text{ if } y \in Y \\ \text{by periodicity elsewhere.} \end{cases}$$

Similar definitions are valid for α^ε and β^ε . Then we can rewrite the variational problem (4.17) in Ω as follows

$$\begin{cases} \int_\Omega |g^\varepsilon| \frac{\partial C^\varepsilon}{\partial t} v \, dx &= - \int_\Omega C^\varepsilon (\nabla p^\varepsilon)^T \mathcal{A}^\varepsilon (\nabla v) \, dx - D \int_\Omega (\nabla C^\varepsilon)^T \mathcal{A}^\varepsilon \nabla v \, dx \\ &+ \int_\Omega |g^\varepsilon| \alpha^\varepsilon C^\varepsilon v \, dx \\ \int_\Omega (\nabla p^\varepsilon)^T \mathcal{A}^\varepsilon \nabla v \, dx &= \int_\Omega |g^\varepsilon| \beta^\varepsilon C^\varepsilon v \, dx. \end{cases} \quad (4.18)$$

In the following, we analyze separately the above equations. First, we consider the parabolic equation (4.18)₁. The finite element discretization used is standard. Let \mathcal{T}_H be a partition of Ω in simplicial or quadrilateral elements K . For this partition we define the finite dimensional subspace $V^p = V^p(\Omega, \mathcal{T}_H)$ of $H_0^1(\Omega)$ by

$$V^p(\Omega, \mathcal{T}_H) = \{v^H \in H_0^1(\Omega) : u^H|_K \in \mathcal{R}^p(K), \forall K \in \mathcal{T}_H\},$$

where $\mathcal{R}^p(K)$ is the space of polynomials defined in K with largest degree p . The solution of the discretized problem reads: Find $C^H(t) \in V^p(\Omega, \mathcal{T}_H)$ such that

$$\int_{\Omega} |g^\varepsilon| \frac{\partial C^H}{\partial t} v^H dx + B^\varepsilon(C^H(t), v^H) = 0 \quad \forall v^H \in V^p(\Omega^\varepsilon, \mathcal{T}_H), \quad (4.19)$$

where

$$B^\varepsilon(C^H, v^H) = \int_{\Omega} C^H (\nabla p^\varepsilon)^T \mathcal{A}^\varepsilon \nabla v^H + D(\nabla C^H)^T \mathcal{A}^\varepsilon (\nabla v^H) - |g^\varepsilon| \alpha^\varepsilon C^H v^H dx. \quad (4.20)$$

We proceed with our HMM-FEM method by rewriting the bilinear term (4.20), such that it will depend on some microfunctions v^h whose averaging resemble the v^H macroscale functions in V^p . For $v^H, w^H \in V^p(\Omega, \mathcal{T}_H)$ we define

$$\hat{B}(v^H, w^H) = \hat{B}_1(v^H, w^H) + \hat{B}_2(v^H, w^H) + \hat{B}_3(v^H, w^H) \quad (4.21)$$

where

$$\hat{B}_1(v^H, w^H) = \sum_{K \in \mathcal{T}_H} \sum_{l=1}^{\mathcal{L}} \frac{\omega_{K_l}}{|K_{\delta_{K_l}}|} \int_{K_{\delta_l}} (v_{K_l}^h \nabla p^\varepsilon)^T \mathcal{A}^\varepsilon \nabla w_{K_l}^h dx \quad (4.22)$$

$$\hat{B}_2(v^H, w^H) = \sum_{K \in \mathcal{T}_H} \sum_{l=1}^{\mathcal{L}} \frac{\omega_{K_l}}{|K_{\delta_{K_l}}|} \int_{K_{\delta_l}} D(\nabla v_{K_l}^h)^T \mathcal{A}^\varepsilon \nabla w_{K_l}^h dx \quad (4.23)$$

$$\hat{B}_3(v^H, w^H) = - \sum_{K \in \mathcal{T}_H} \sum_{l=1}^{\mathcal{L}} \frac{\omega_{K_l}}{|K_{\delta_{K_l}}|} \int_{K_{\delta_l}} |g^\varepsilon| \alpha^\varepsilon v_{K_l}^h w_{K_l}^h dx, \quad (4.24)$$

where $v_{K_l}^h, w_{K_l}^h$ are appropriated microfunctions defined on sampling domains K_{δ_l} (written as K_l) and the factor $|K_{\delta_l}|$ gives the appropriated weight for the contribution of the integral defined on K_{δ_l} instead of K . Note that $\hat{B}(v^H, w^H)$ is an approximation to $B^\varepsilon(v^H, w^H)$, this is because we used a quadrature formula with weight w_{K_l} associated to the quadrature points x_l in the macroelement K to approximate the integral in K . Then we find appropriate microfunctions $v_{K_l}^h, w_{K_l}^h$ defined only in the sampling domains I_{δ_l} (that resemble the macrofunctions v^H, w^H in I_{δ_l}) that verifies $\hat{B}_K = \hat{B}_{1,K} + \hat{B}_{2,K} + \hat{B}_{3,K}$. Sometimes we write K_l and I_l instead of K_{δ_l} and I_{δ_l} .

For each macroelement K we compute the sum contribution in (4.22)-(4.24) by computing the microfunctions $v_{K_l}^h, w_{K_l}^h$ obtained by solving microfunctions on sampling domains $K_{\delta_l}, l = 1, \dots, \mathcal{L}$. The microproblems read as follows: find $v_{K_l}^h$ such that $(v_{K_l}^h - v_{lin,K_l}^H) \in S_{per}^1(K_{\delta_l}, \mathcal{T}_h)$ and

$$\int_{I_l} v_l^h (\nabla_p^\varepsilon)^T \mathcal{A}^\varepsilon \nabla z^h dx + \int_{I_l} D(\nabla v_l^h)^T \mathcal{A}^\varepsilon \nabla z^h dx - \int_{I_l} |g^\varepsilon| \alpha^\varepsilon v_l^h z^h dx = 0 \quad \forall z^h \in S^q(K_{\delta_l}, \mathcal{T}_h), \quad (4.25)$$

where

$$v_{lin,K_l}^H(x) = v^H(x_{K_{\delta_l}}) + (x - x_{K_{\delta_l}}) \nabla v^H(x_{K_{\delta_l}})$$

is a linearization in I_{δ_l} of the macrofunction v^H at the integration quadrature point $x_{K_{\delta_l}}$ and

$$S^1(K_{\delta_l}, \mathcal{T}_h) = \{z^h \in H^1(K_{\delta_l}); z^h|_T \in \mathcal{R}^q(T), T \in \mathcal{T}_h, \int_{K_{\delta_l}} z^h(x) dx = 0\}. \quad (4.26)$$

$$S_{per}^1(K_{\delta_l}, \mathcal{T}_h) = \{v \in S^1(K_{\delta_l}, \mathcal{T}_h); v \text{ periodic in } K_{\delta_l}\}. \quad (4.27)$$

In what follows we denote by

- $\{\varphi_m^H\}_{m=1}^{M_{mac}}$ the basis of the macro FE space $V^1(\Omega, \mathcal{T}_H)$, where M_{mac} is the number of discretization points in the macrodomain Ω .
- $\{\phi_{m,K_l}^h\}_{m=1}^{M_{mic}}$ the basis of micro FE space $S^1(K_{\delta_l}, \mathcal{T}_h)$, where M_{mic} is the number of discretization points in K_{δ_l} .

Following a standard assembly process for the macro form (4.21) we compute the contribution \hat{B}_K in \hat{B} associated to the macroelement K by the contribution of the microfunctions. We use the macro basis functions with non-zero support in K denoted by $\varphi_i^H, i = 1, \dots, \mu_K$, and determine \hat{B}_K based on contribution computed in sampling domains as follows:

$$\hat{B}_K = \hat{B}_K(\varphi_i^H, \varphi_j^H)_{i,j=1}^{\mu_K} = \sum_{m=1}^3 \hat{B}_{m,K}(\varphi_i^H, \varphi_j^H)_{i,j=1}^{\mu_K} \quad (4.28)$$

$$= \sum_{l=1}^{\mathcal{L}} \frac{\omega_{K_l}}{|K_{\delta_l}|} \left(\int_{K_l} \varphi_{K_l,i}^h \nabla p \mathcal{A} \nabla \varphi_{K_l,j}^h + \nabla \varphi_{K_l,i}^h \mathcal{A} \nabla \varphi_{K_l,j}^h - |g| \alpha \varphi_{K_l,i}^h \varphi_{K_l,j}^h \right)_{i,j=1}^{\mu_K} \quad (4.29)$$

$$= \sum_{l=1}^{\mathcal{L}} \frac{\omega_{K_l}}{|K_{\delta_l}|} (A_{K_l}^T (B_{1mic,K_l} + B_{2mic,K_l} + B_{3mic,K_l}) A_{K_l}). \quad (4.30)$$

Then, for each sampling domain $K_{\delta_l} \subset K$ and considering the associated linearized macro basis function $\varphi_{lin,K_l,i}^H$ we write instead of (4.25) the minimization problem (ABDULLE; NONNENMACHER, 2009)

$$\varphi_{K_l,i}^h = \arg \min \int_{I_{\delta_l}} \nabla w^h (\nabla p^\varepsilon)^T \mathcal{A}^\varepsilon(x) \nabla w^h + D(\nabla w^h)^T \mathcal{A}^\varepsilon(x) (\nabla w^h)^T - |g^\varepsilon| \alpha^\varepsilon w^h w^h dx \quad (4.31)$$

over all function $w^h \in S^1(K_{\delta_l}, \mathcal{T}_h)$ such that $w^h - \varphi_{lin,K_l,i}^H \in S_{per}^1$, where $\varphi_{lin,K_l,i}^H(x) = \varphi_i^H(x_{\delta_l}) + (x - x_{\delta_l}) \cdot \nabla \varphi_i^H(x_{\delta_l})$.

To compute (4.31) we expand $\varphi_{lin,K_l,i}^H$ in the basis of $S^1(K_{\delta_l}, \mathcal{T}_h)$

$$\varphi_{lin,K_{\delta_l},i}^H = \sum_{m=1}^{M_{mic}} \beta_{i,m} \phi_{K_{\delta_l},m}^h \quad (4.32)$$

and the above minimization problem leads, by introducing Lagrange multipliers λ , to a saddle point problem given in linear form by

$$(B_{1mic,K_l} + B_{2mic,K_l} + B_{3mic,K_l}) \alpha_{K_{\delta_l},i} + M^T \lambda = 0, \quad (4.33)$$

$$M(\alpha_{K_{\delta_l},i} - \beta_{K_{\delta_l},i}) = 0, \quad (4.34)$$

where $\beta_{K_{\delta_l},i} = \{\beta_{i,m}\}_{m=1}^{M_{mic}}$ and $\alpha_{i,K_{\delta_l}} = \{\eta_{i,m}\}_{m=1}^{M_{mic}}$ are associated to the solution and M is the matrix of the constraints detailed below. We then have

$$\varphi_{K_{\delta_l},i}^h = \sum_{m=1}^{M_{mic}} \alpha_m \phi_{K_{\delta_l},m}^h. \quad (4.35)$$

The matrix $(B_{1mic,K_l} + B_{2mic,K_l} + B_{3mic,K_l})$ has coefficients

$$\begin{aligned} (B_{1mic,K_l} + B_{2mic,K_l} + B_{3mic,K_l})_{mn} &= \int_{K_{\delta_l}} \phi_{K_{\delta_l},m}^h (\nabla p^\varepsilon)^T \mathcal{A}^\varepsilon \nabla \phi_{K_{\delta_l},n}^h \\ &+ (\nabla \phi_{K_{\delta_l},m}^h)^T \mathcal{A}^\varepsilon \nabla \phi_{K_{\delta_l},n}^h \\ &- \alpha^\varepsilon |g^\varepsilon| \phi_{K_{\delta_l},m}^h \phi_{K_{\delta_l},n}^h. \end{aligned}$$

In order to write M we observe that if $(\varphi^h - \varphi_{lin}^H) \in S_{per}^1(K_\delta, \mathcal{T}_h)$ we have

1. $\int_{K_\delta} (\varphi^h - \varphi_{lin}^H) dx = 0$,
2. $(\varphi^h - \varphi_{lin}^H)(p) = (\varphi^h - \varphi_{lin}^H)(p')$, for all L couples (p, p') of boundary nodes on opposite edges avoiding redundant couples at the corner.

In this situation, the matrix M has the form

$$M = \begin{pmatrix} b_1 & \dots & b_{M_{mic}} \\ & & \tilde{M} \end{pmatrix}, \quad (4.36)$$

where the first row corresponds to the condition 1 and the $L \times M_{mic}$ matrix \tilde{M} corresponds to the condition 2.

The problem (4.33),(4.34) is solved for each function $\varphi_{lin,i,K_{\delta_l}}^H, i = 1, \dots, \mu_K$. This is done for each quadrature node of the macroelement and we obtain

$$\hat{B}_K = \sum_{l=1}^{\mathcal{L}} \frac{\omega_{K_l}}{|K_{\delta_l}|} (\mathcal{A}_{K_l}^T (B_{1mic,K_l} + B_{2mic,K_l} + B_{3mic,K_l}) \mathcal{A}_{K_l}). \quad (4.37)$$

with $\mathcal{A}_{K_l} = (\alpha_{l,1}, \dots, \alpha_{l,\mu_K})^T$. Using the simple backward Euler method in time we have the following weak form of the parabolic multiscale equation

$$\int_{\Omega} |g^\varepsilon| C^H(t_n) v^H dx + \Delta t \hat{B}(C^H(t_n), p^H, v^H) = \int_{\Omega} C^H(t_{n-1}) v^H |g^\varepsilon| dx. \quad (4.38)$$

The mass matrix is given by

$$\bar{M}_{i,j} = \int_{\Omega} \varphi_i^H \varphi_j^H |g^\varepsilon| dx. \quad (4.39)$$

We can calculate that integral for the K element as

$$\int_K \varphi_i^H \varphi_j^H |g^\varepsilon| dx \approx |g^\varepsilon(x_{K_b})| \int_K \varphi_i^H \varphi_j^H dx, \quad (4.40)$$

where x_{K_b} is the barycenter of K . Since $|g^\varepsilon(x_{K_b})|$ need to be computed, we can approximate on the microdomain around x_{K_b} during the integration process. The sampling of $|g^\varepsilon(x_{K_b})|$ can be done in the following way

$$|g^\varepsilon(x_{K_b})| := |R| \sum_{R \in \mathcal{I}_h} |g(x_{K_b}, y_R)|, \quad (4.41)$$

where \mathcal{I}_h is an axiparallel mesh of the unit cell Y with congruent rectangles R of size h and y_R is the barycenter of the rectangle R .

Thus using HMM-FEM discussed in this section we can solve the parabolic equation (4.17)₁ by using the following linear system

$$(\bar{M} + \Delta t \hat{B})C^H(t_n) = \bar{M}C^H(t_{n-1}). \quad (4.42)$$

where \hat{B} is the stiffness matrix $\hat{B} = (\hat{B}(\varphi_i^H, \varphi_j^H))_{ij=1, \dots, M_{mac}}$ and here for abuse of notation we denoted by $C^H(t_n)$ the vector with components $C^H(x_i, t^n)$ for $i = 1, \dots, M_{mac}$ where x_i are the nodes in the mesh \mathcal{T}_H .

A similar methodology can be used for solving the elliptic equation using the HMM-FEM (ABDULLE; NONNENMACHER, 2009).

$$\hat{B}_2 p^H(t_n) = b(C^H(t_{n-1})). \quad (4.43)$$

where the matrix \hat{B}_2 is obtained as before from the operator

$$\hat{B}_2(v^H, w^H) = \sum_{K \in \mathcal{T}_H} \sum_{l=1}^{\mathcal{L}} \frac{\omega_{K_l}}{|K_{\delta_l}|} \int_{K_{\delta_l}} (\nabla v_{K_l}^h) \mathcal{A}^\varepsilon (\nabla w_{K_l}^h)^T dx \quad (4.44)$$

and b a suitable operator for the right-hand side. That contribution can be calculated for the element K as

$$b_K = \int_K f \varphi_i^H dx \approx f(x_{K_b}) \int_K \varphi_i^H dx, \quad (4.45)$$

where $x_{K_b} \in K$ is an integration point located at the barycenter of K .

4.3.1 Approximating \mathcal{A}^0

For numerical purposes, we need to find a way to approximate the homogenized tensor since is not too easy to calculate it analytically. We use rectangular simple domains of edge $\delta = \varepsilon$.

4.3.1.1 Case $\mathcal{A}^\varepsilon(x) = \mathcal{A}(x, \frac{x}{\varepsilon})$

During the implementation of HMM-FEM method, with $\mathcal{A}^\varepsilon(x) = \mathcal{A}(x, \frac{x}{\varepsilon})$, we compute for each quadrature point x_l ($l = 1, \dots, 4$) in the macroelement K the matrix

$$(M_{x_l}^h)_{i,j=1,2} = \frac{1}{|I_{\delta_l}|} \int_{I_{\delta_l}} \mathcal{A}(x_l, y) \nabla \varphi_i^h \nabla \varphi_j^h dy \quad (4.46)$$

that can vary in each element K for each $l = 1, \dots, 4$. I_{δ_l} is a simple domain along the point x_l of edge ε .

We have used previously the microfunctions $\{\varphi_i^h\}$ in K_{δ_l} associated to the nodal macro basis $\{\varphi_i^H\}$ of the rectangular element K and to the quadrature point x_l , that satisfy

$$\varphi_j^h(x) = \varphi_{j,lin_l}^H(x) + \varepsilon \sum_{i=1,2} \chi^{i,h}(x_l, \frac{x}{\varepsilon}) \frac{\partial \varphi_{j,lin_l}^H}{\partial x_i}(x) \quad (4.47)$$

where $\varphi_{j,lin_l}^H(x) = \varphi_j^H(x_l) + (x - x_l) \nabla \varphi_j^H(x_l)$ and $\chi^{i,h}$ are solution of the cell problem whose variational form in $S_{per}^1(Y)$ is:

$$\int_Y \nabla \chi^{i,h} \mathcal{A}(x, y) \nabla v \, dy = - \int_Y (\mathcal{A}(x, y) e_i)^T \cdot \nabla v(y) \, dy, \forall v \in S_{per}^1(Y). \quad (4.48)$$

The following property is valid, see (ABDULLE, 2009),

$$(M_{x_l}^h)_{i,j=1,2} = \mathcal{A}^{0,h}(x_l) \nabla \varphi_i^H(x_l) \nabla \varphi_j^H(x_l), \quad (4.49)$$

with $\mathcal{A}^{0,h}(x_l)$ that is an approximation of $\mathcal{A}^0(x_l)$ defined as follows

$$\mathcal{A}^{0,h}(x_l) = \frac{1}{|I_{\delta_l}|} \int_{I_{\delta_l}} \mathcal{A}(x_l, y) (I + \nabla_y \chi(x_l, y)) \, dy \quad (4.50)$$

In the following we give an easy way to build $\mathcal{A}^{0,h}$ that is based on (4.49). Let consider $\bar{\varphi}_i$ the nodal basis defined in the reference element $\bar{K} = [0, 1]^2$, where

$$\begin{aligned} \bar{\varphi}_1(x_1, x_2) &= (1 - x_1)(1 - x_2), \\ \bar{\varphi}_2(x_1, x_2) &= (1 - x_2)x_1, \\ \bar{\varphi}_3(x_1, x_2) &= x_1x_2, \\ \bar{\varphi}_4(x_1, x_2) &= (1 - x_1)x_2. \end{aligned}$$

We have that $\varphi_i(x) = \bar{\varphi}_i \circ \Phi^{-1}(x)$ where $\Phi : \bar{K} \rightarrow K$ is the linear transformation between \bar{K} and K , that satisfies

$$\Phi(x) = v_1 \bar{\varphi}_1(x) + v_2 \bar{\varphi}_2(x) + v_3 \bar{\varphi}_3(x) + v_4 \bar{\varphi}_4(x), \quad \forall x \in \bar{K}$$

where $v_i, i = 1 \dots r$ are the vertices of K .

Moreover we have

$$\nabla \varphi_i(x) = J_{\Phi^{-1}}^T(x) \nabla \bar{\varphi}_i(\Phi^{-1}(x)).$$

Note that the following relation is also valid $J_{\Phi^{-1}}(x) = (J_{\Phi}(\Phi^{-1}(x)))^{-1} \equiv J_{\Phi}^{-1}(\Phi^{-1}(x))$. Therefore from (4.49) we have

$$(M_{x_l}^h)_{ij} = \xi_i^T J_{\Phi}^{-1} \mathcal{A}^{0,h}(x_l) J_{\Phi}^{-T} \xi_j \quad (4.51)$$

and so

$$M_{x_l}^h = \xi^T J_{\bar{\phi}}^{-1} \mathcal{A}^{0,h}(x_l) J_{\bar{\phi}}^{-T} \xi \quad (4.52)$$

where $\xi = (\nabla \bar{\varphi}_1(\bar{x}_l), \nabla \bar{\varphi}_2(\bar{x}_l))$, (or equivalently $\xi_i \equiv \nabla \bar{\varphi}_i(\bar{x}_l)$) and thus $\xi^T = J_{\bar{\varphi}}(\bar{x}_l)$ that is the Jacobian of $\bar{\varphi} = (\bar{\varphi}_1, \bar{\varphi}_2)$ in the l -th node \bar{x}_l of the reference element \bar{K} . Thus we get

$$M_{x_l}^h = J_{\bar{\varphi}} J_{\bar{\phi}}^{-1} \mathcal{A}^{0,h}(x_l) J_{\bar{\phi}}^{-T} J_{\bar{\varphi}}^T = B^{-1} \mathcal{A}^{0,h}(x_l) B^{-T} \quad (4.53)$$

with $B = J_{\bar{\phi}}(\bar{x}_l) J_{\bar{\varphi}}^{-1}(\bar{x}_l)$.

Using (4.53) we have finally the relation that link $\mathcal{A}^{0,h}$ with the already computed mass matrix

$$\mathcal{A}^{0,h}(x_l) = B M_{x_l}^h B^T \quad (4.54)$$

4.3.1.2 Case $\mathcal{A}^{\varepsilon(x)} = \mathcal{A}\left(\frac{x}{\varepsilon}\right)$ with elements K of same dimension

When \mathcal{A} depends only on the microscale as in our case we have $\mathcal{A} = \mathcal{A}\left(\frac{x}{\varepsilon}\right)$ and then $M_{x_l}^h$ represented in (4.49) or equivalently in (4.53) is constant with respect K , but depends on $m = 1, \dots, 4$ and so it can be represented as $M_{x_l}^h$ and satisfies

$$M_{x_l}^h = \frac{1}{|I_{\delta_l}|} \int_{I_{\delta_l}} \mathcal{A}(y) \nabla \varphi_i^h \nabla \varphi_j^h dy = \mathcal{A}^{0,h} \nabla \varphi_i^H(x_l) \cdot \nabla \varphi_j^H(x_l) \quad (4.55)$$

with

$$\mathcal{A}^{0,h}(x_l) = \frac{1}{|I_{\delta_l}|} \int_{|I_{\delta_l}|} \mathcal{A}(y) (I + \nabla_y \chi^h\left(\frac{x}{\varepsilon}\right)) dy \quad (4.56)$$

that is independent of m and K , then it is an approximation of $\mathcal{A}^0(x_l)$. We note that in (4.56) $\chi^h = (\chi^{j,h})_{j=1,2}$ is the vector of the solution of cell problem (independent of m and K) in $S_{per}^1(Y)$: $\int_Y \nabla \chi^{j,h} \mathcal{A}(y) \nabla v dy = - \int_Y (\mathcal{A}(y) e_j)^T \cdot \nabla v(y) dy, \forall v \in S_{per}^1(Y)$.

Following the same step as in the previous subsection (see (4.50)-(4.53)-(4.54)) we get

$$\mathcal{A}^{0,h}(x_l) = B M_{x_l}^h B^T \quad (4.57)$$

with $B = J_{\bar{\phi}}(\bar{x}_l) J_{\bar{\varphi}}^{-1}(\bar{x}_l)$.

4.4 HMM-FEM approach for multiscale solution

After developing the HMM framework to our problem. In this simulation we fix $H = \frac{1}{48}, T = 0.1, \Delta t = 0.01, \delta = \varepsilon = 1e - 06, \frac{h}{\delta} = \frac{1}{5}$ which provides the results shown in Figure 10

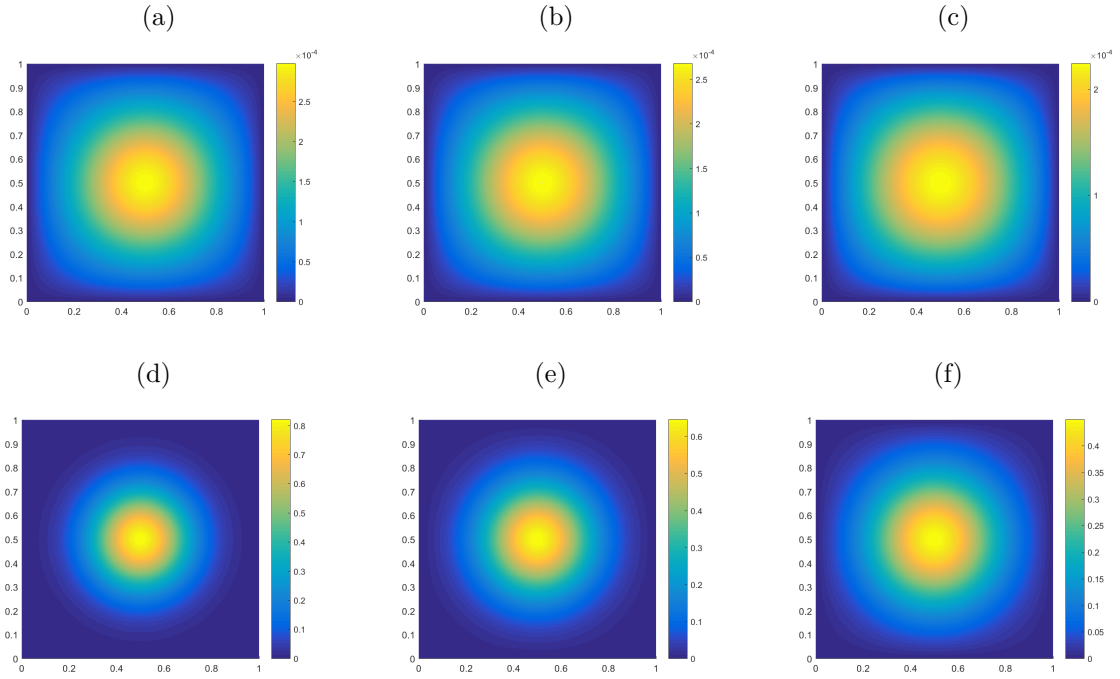


Figure 10 – Numerical solutions of the multiscale problem.

In the top and bottom row we have numerical solutions of the pressure and density at the times $t = 0.01$, $t = 0.04$ and $t = 0.1$ from left to right.

4.4.1 Numerical convergence of HMM-FEM to homogenized solution

Example 1. *In this example, we use the method described in Chapter 5 to get an approximation of the homogenized solution p_0, C_0 to homogenized problem. We are able to compare numerically the HMM-FEM solution with this homogenized solution. To approximate the parameters, present in the homogenized problem and listed below, we use a integration numerical method of high order to not have large errors.*

$$\mathcal{A}^0 = \begin{bmatrix} 1.012724469451771 & 0.0000000000000033 \\ 0.0000000000000011 & 1.012724469451337 \end{bmatrix}, D = 1,$$

$$\langle |g|\beta \rangle = 0.013424520172113,$$

$$\langle |g|\alpha \rangle = 0.008393086150538,$$

$$\langle |g| \rangle = 9.527732571537580.$$

In this simulation we fix an uniform mesh $h = k = \frac{1}{96}$, $T = 0.1$, $\Delta t = 0.01$. following figures shows the plot of the obtained homogenized solution.

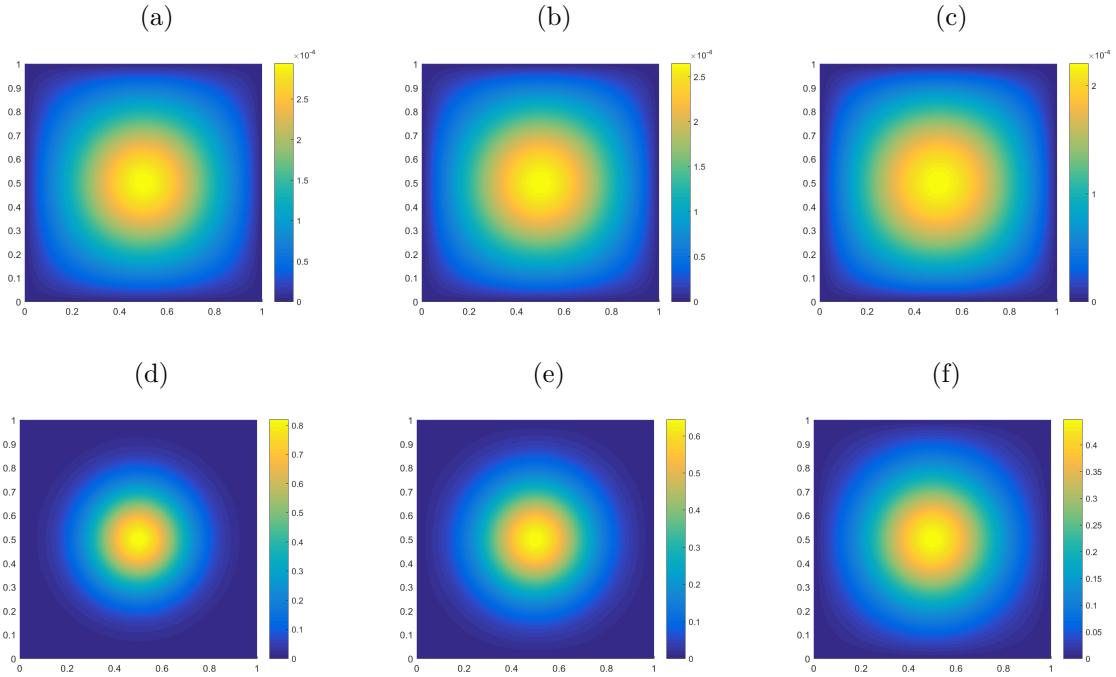


Figure 11 – From top to bottom we have numerical solutions to homogenized problem at the times $t = 0.01, t = 0.04$ and $t = 0.1$.

To compute the HMM-FEM errors into approximating the homogenized solution, we first calculate a fine numerical solution of the homogenized problem using the final system of equations (4.12) and the approximation of the homogenized tensor using HMM described before. Then we solved that system using finite difference (Example 1).

Table 3 – Errors and rate of convergence of the HMM method

H	$\ e_p^H\ _{L^2}$	$\ e_p^H\ _{H^1}$	Rate $_{H^1}$	$\ e_C^H\ _{L^2}$	$\ e_C^H\ _{H^1}$	Rate $_{H^1}$
1/3	9.7270e-03	9.7360e-03	-	1.1662e-01	3.5464e-01	-
1/6	1.4584e-03	3.6590e-03	1.41	4.6964e-02	2.18010e-01	0.70
1/12	4.5137e-04	1.8348e-03	0.99	7.4453e-03	1.1500e-01	0.92
1/24	3.9449e-04	8.8498e-04	1.05	3.7053e-03	5.1204e-02	1.16

That table show us a second order of convergence for pressure and density in L^2 discrete norm and first order of convergence in H^1 discrete norm, where e_p^H and e_C^H are the errors between the HMM approximation and a fine finite difference approximation ($\|e_p^H\|$ and $\|e_C^H\|$ are defined using the discrete norms provided by the next Chapter). Note that these errors are very familiar with (4.11) and (4.14). There are some analytical results that provide convergence rates to simpler elliptic and parabolic problems as (ABDULLE, 2009), (ABDULLE, 2012), (ABDULLE; HUBER, 2014), but there are not works that deal with multiscale coupled problems. For a while in this Chapter we applied the HMM framework to our system and searched for some convergence indicators. Our next step in

a future work is to prove analytically this convergence of HMM-FEM numerical solutions to the homogenized solution.

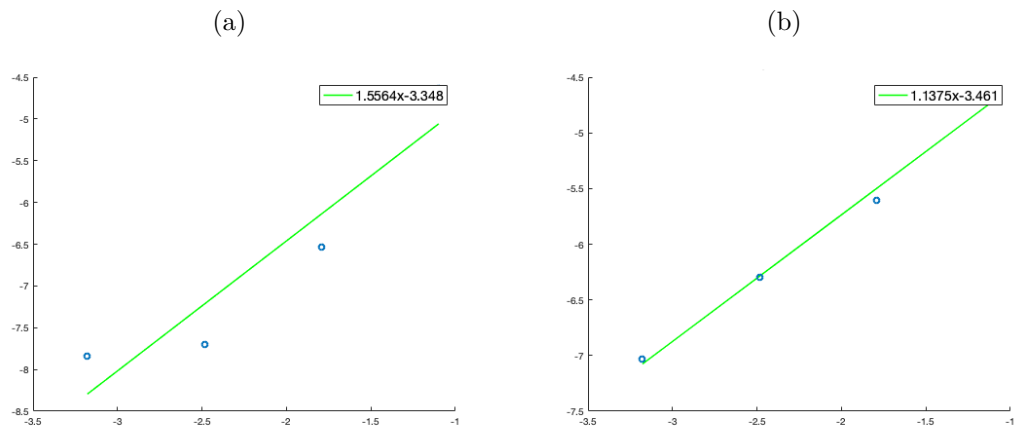


Figure 12 – Convergence rates for HMM approximation (Pressure).

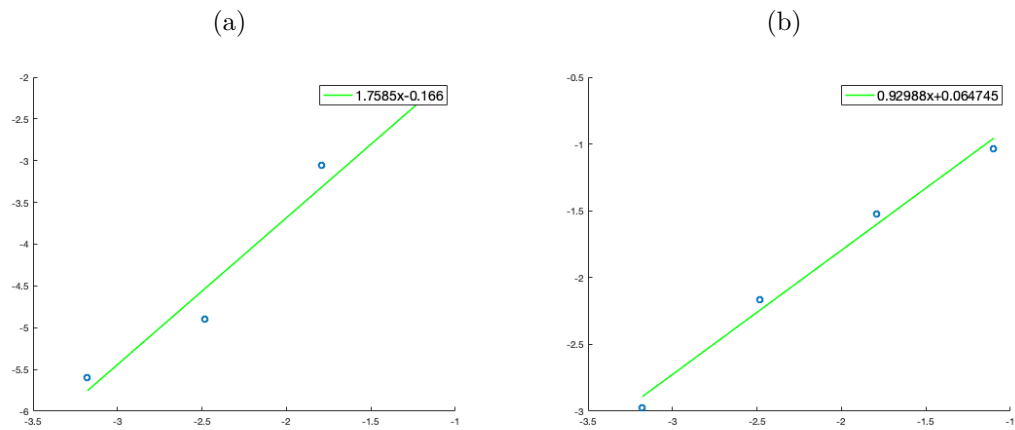


Figure 13 – Convergence rates for HMM approximation (Density).

5 Supraconvergent FDM for the crypt cell dynamics on non uniform meshes

In this Chapter we present a numerical scheme for the cell proliferation problem inside the colonic crypt represented mathematically by the elliptic-parabolic system (2.7) that depends on the cell-cell adhesion $p(x, y, t)$ and proliferative cell density $C(x, y, t)$.

$$\left\{ \begin{array}{ll} |g| \frac{\partial C}{\partial t} & = \nabla \cdot (\mathcal{A} \nabla p C) + \nabla \cdot (D \mathcal{A} \nabla C) + |g| \alpha C, & \text{in } S \times (0, T] \\ -\nabla \cdot (\mathcal{A} \nabla p) & = |g| \beta C, & \text{in } S \times (0, T] \\ C = p & = 0 & \text{on } \partial S \times (0, T] \\ C(\cdot, 0) & = C_0 & \text{in } S. \end{array} \right. \quad (5.1)$$

We solve (5.1) by using a semi-discretization method. The proposed numerical scheme is based on finite differences on nonuniform meshes that provide good convergence and stability properties, which are proved in the following paragraphs. The method has a second order convergence using a discrete norm in $L^2([0, T], H_0^1(\bar{S}))$ norm for the density and second order for the pressure using a discrete norm in $L^\infty([0, T], H_0^1(\bar{S}))$ norm. A such order is not expected since the truncation error decays with second order in L^∞ . For this reason the proposed finite difference method, which is equivalent (see next Chapter) to a finite element method, is supraconvergent (see Appendix B.6). The proof of this supraconvergence is described in the followings Sections in details. A such supraconvergence is here proved to be valid for solutions C, p that belongs in $L^\infty([0, T], C^4(\bar{S}))$. In what follow we solve a semidiscrete problem, with a space discretization using appropriated operators and then the semidiscrete problem is solved by Backward Euler.

5.1 Preliminary results

Let $H = \{(h_i, k_j) \in \mathbb{R}^2 | h_i, k_j > 0, i, j = 1, \dots, N, M; \sum_{i=1}^N h_i = \sum_{j=1}^M k_j = 1\}$, we denote by H_{max} the maximum step size in the two directions: $H_{max} = \max_{(h_i, k_j) \in H} \{h_i, k_j\}$. We suppose that exists $C > 0$ such that $H_{max}/H_{min} \leq C$. Let $(h_i, k_j) \in H$, we define by \bar{S}_H the discrete mesh in $S = (0, 1)^2$, as follows

$$\bar{S}_H = \{(x_i, y_j)_{i,j=0}^{N,M} | (x_i, y_j) = (x_{i-1} + h_i, y_{j-1} + k_j) \in \bar{S}, i, j = 1 \dots, N, M, (x_0, y_0) = (0, 0)\}.$$

We introduce also the following sets

$$\partial S_H = \{(x_i, y_j), i = 0, N; j = 0, \dots, M\} \cup \{(x_i, y_j), i = 0, \dots, N; j = 0, M\}, S_H = \bar{S}_H / \partial S_H.$$

Let $W_{H,0}, W_H$ be the following sets of grid functions

$$\begin{aligned} W_{H,0} &= \{v^H : \overline{S_H} \rightarrow \mathbb{R}, v^H = 0 \text{ in } \partial S_H\}, \\ W_H &= \{v^H : \overline{S_H} \rightarrow \mathbb{R}\}. \end{aligned}$$

In the following we denote by $v_{i,j}^H$ the value $v^H(x_i, y_j)$. We denote also $\nabla_{-H} = (D_{-x}, D_{-y})$ that is $\nabla_{-H} v_{i,j}^H = (D_{-x} v_{i,j}^H, D_{-y} v_{i,j}^H)$ where

$$D_{-x} v_{i,j}^H = \frac{v_{i,j}^H - v_{i-1,j}^H}{x_i - x_{i-1}} \quad (5.2)$$

and

$$D_{-y} v_{i,j}^H = \frac{v_{i,j}^H - v_{i,j-1}^H}{y_j - y_{j-1}}. \quad (5.3)$$

In $W_{H,0}$ we introduce the following inner product

$$(v^H, w^H)_H = \sum_{i,j=1}^{N-1, M-1} h_{i+\frac{1}{2}} k_{j+\frac{1}{2}} v_{i,j}^H w_{i,j}^H,$$

for $v^H, w^H \in W_{H,0}$ and by $\|\cdot\|_H$ we denote the associated induced norm in $W_{H,0}$. In $W_H \times W_H$ we also use the scalar product

$$(\vec{v}^H, \vec{w}^H)_{H,-} = (v^{H,1}, w^{H,1})_{h,-} + (v^{H,2}, w^{H,2})_{k,-} \quad (5.4)$$

where

$$(v^{H,1}, w^{H,1})_{h,-} = \sum_{i,j=1}^{N, M-1} h_i k_{j+\frac{1}{2}} v_{i,j}^{H,1} w_{i,j}^{H,1} \quad (5.5)$$

$$(v^{H,2}, w^{H,2})_{k,-} = \sum_{i,j=1}^{N-1, M} h_{i+\frac{1}{2}} k_j v_{i,j}^{H,2} w_{i,j}^{H,2} \quad (5.6)$$

$\vec{v}^H = (v^{H,1}, v^{H,2}), \vec{w}^H = (w^{H,1}, w^{H,2}) \in W_H \times W_H$, and the induced semi-norm $\|\vec{v}^H\|_{H,-} = \sqrt{(\vec{v}^H, \vec{v}^H)_{H,-}}$.

The centered operator $\nabla_c = (\delta_x, \delta_y)$, uses

$$\delta_x v_{i,j}^H = \frac{v_{i+1,j}^H - v_{i-1,j}^H}{h_i + h_{i+1}}, \delta_y v_{i,j}^H = \frac{v_{i,j+1}^H - v_{i,j-1}^H}{k_j + k_{j+1}}.$$

We consider also the operator $D_H = (\delta_h, \delta_k)$ defined by

$$\delta_h v_{i,j}^H = \frac{h_{i+1} \delta_x^{(1/2)} v_{i-1/2,j}^H + h_i \delta_x^{(1/2)} v_{i+1/2,j}^H}{h_{i+1} + h_i}, \quad (5.7)$$

$$\delta_k v_{i,j}^H = \frac{k_{j+1} \delta_y^{(1/2)} v_{i,j-1/2}^H + k_j \delta_y^{(1/2)} v_{i,j+1/2}^H}{k_{j+1} + k_j}. \quad (5.8)$$

where $\delta_x^{(1/2)} v_{i-1/2,j}^H = D_{-x} v_{i,j}^H$, that is $\delta^{(1/2)}$ is a centered operator of half step. Finally by $M_H = (M_x, M_y)$ we denote the average operator, where $M_x(v^H)_{i,j} = \frac{1}{2}(v_{i,j}^H + v_{i-1,j}^H)$ (respectively for M_y).

Proposition 1. For all $v^H, w^H \in W_{H,0}$ and $a : \overline{S_H} \rightarrow \mathbb{R}$, $\mathcal{A} : \overline{S_H} \rightarrow \mathbb{R}^{2 \times 2}$ bounded we have

$$\|M_x v^H\|_{h,-} \leq \|v^H\|_H, \quad (5.9)$$

$$-(\delta_x^{(1/2)}(a(\mathbf{x}, \mathbf{y})\delta_x^{(1/2)}v^H), w^H)_H = (a(M_x(\mathbf{x}), \mathbf{y})D_{-x}v^H, D_{-x}w^H)_{h,-}, \quad (5.10)$$

$$-(\delta_x v^H, w^H)_H = (v^H, \delta_x w^H)_H, \quad (5.11)$$

$$-(\delta_x v^H, w^H)_H = (M_x(v^H), D_{-x}w^H)_{h,-}, \quad (5.12)$$

$$-(\delta_x v^H, \delta_y v^H)_H \leq \|\nabla_{-H} v^H\|_{H,-}^2, \quad (5.13)$$

$$\|\mathcal{A}D_H v^H\|_H^2 \leq M\|\mathcal{A}\|_\infty^2 \|\nabla_{-H} v^H\|_{H,-}^2. \quad (5.14)$$

where $\mathbf{x} = \{x_i\}_{i=1,\dots,N}$, $\mathbf{y} = \{y_j\}_{j=1,\dots,M}$, with $(x_i, y_j) \in \overline{S}$ and $\frac{H_{max}}{H_{min}} \leq C$.

Proof. For (5.11) we have

$$-(\delta_x v^H, w^H)_H = - \sum_{i,j=1}^{N-1,M-1} h_{i+\frac{1}{2}} k_{j+\frac{1}{2}} \frac{(v_{i+1,j} - v_{i-1,j})}{h_i + h_{i+1}} w_{i,j} \quad (5.15)$$

$$= -\frac{1}{2} \sum_{i,j=1}^{N-1,M-1} k_{j+\frac{1}{2}} (v_{i+1,j} w_{i,j} - v_{i-1,j} w_{i,j}) \quad (5.16)$$

$$= -\frac{1}{2} \sum_{i=2,j=1}^{N,M-1} k_{j+\frac{1}{2}} v_{i,j} w_{i-1,j} + \frac{1}{2} \sum_{i=0,j=1}^{N-2,M-1} k_{j+\frac{1}{2}} v_{i,j} w_{i+1,j} \quad (5.17)$$

$$= (v^H, \delta_x w^H)_H \quad (5.18)$$

using $v_{N,j} = w_{N,j} = 0$ and $v_{0,j} = w_{N,j} = 0$.

For (5.12), continuing from (5.16) we add and subtract

$\sum_{i,j=1}^{N-1,M-1} k_{j+\frac{1}{2}} v_{i-1,j} w_{i-1,j}$ we get

$$-(\delta_x v^H, w^H)_H = -\frac{1}{2} \sum_{i,j=1}^{N,M-1} k_{j+\frac{1}{2}} (v_{i,j} + v_{i-1,j}) w_{i-1,j} \quad (5.19)$$

$$+ \frac{1}{2} \sum_{i,j=1}^{N,M-1} k_{j+\frac{1}{2}} (v_{i-1,j} w_{i-1,j} + v_{i-1,j} w_{i,j}) \quad (5.20)$$

$$= (M_x(v^H), D_{-x}w^H)_{h,-} \quad (5.21)$$

using $v_{N,j} = w_{N,j} = 0$.

For (5.13) we use that for $\varepsilon > 0$

$$\delta_x v_{i,j} \delta_y v_{i,j} \leq \frac{(\delta_x v_{i,j})^2}{4\varepsilon^2} + \varepsilon^2 (\delta_y v_{i,j})^2, \quad (5.22)$$

then we use $\varepsilon = \frac{1}{\sqrt{2}}$.

For (5.14) is enough to show that $\|D_H v^H\|_H^2 \leq C \|\nabla_H v^H\|_{H,-}^2$ where

$$\|D_H v^H\|_H^2 = \sum_{i,j=1}^{N-1,M-1} h_{i+\frac{1}{2}} k_{j+\frac{1}{2}} ((\delta_h v_{i,j})^2 + (\delta_k v_{i,j})^2). \quad (5.23)$$

We have that $\exists M(C) > 0$ such that

$$(\delta_h v_{i,j})^2 = \frac{h_i^2 (D_{-x} v_{i+1,j})^2}{(h_i^2 + h_{i+1}^2)} + \frac{h_i h_{i+1} D_{-x} v_{i,j} D_{-x} v_{i+1,j}}{(h_i^2 + h_{i+1}^2)} + \frac{h_{i+1}^2 (D_{-x} v_{i,j})^2}{(h_i^2 + h_{i+1}^2)} \quad (5.24)$$

$$\leq M(C) ((D_{-x} v_{i,j})^2 + (D_{-x} v_{i+1,j})^2) \quad (5.25)$$

since $\frac{H_{max}}{H_{min}} \leq C$. It's useful to note that $h_i (v_{i,h})^2 \leq C h_k (v_{i,j})^2$ for any i, k . \square

In order to approximate the solution of the elliptic equation in (5.1) we use the elliptic operator

$$\mathcal{L}_A(f^H) = \delta_x^{(1/2)}(\mathcal{A}^{11} \delta_x^{(1/2)}(f^H)) + \delta_x(\mathcal{A}^{21} \delta_y(f^H)) \quad (5.26)$$

$$+ \delta_y(\mathcal{A}^{12} \delta_x(f^H)) + \delta_y^{(1/2)}(\mathcal{A}^{22} \delta_y^{(1/2)}(f^H)), \quad (5.27)$$

associated to the matrix function $\mathcal{A} : [0, 1]^2 \rightarrow \mathbb{R}^{2 \times 2}$. The truncation error of this operator is then $T_{\mathcal{L}_A} = \mathcal{L}_A(R_H f) - \nabla(\mathcal{A} \nabla f)$ where $R_H f$ is the restriction of f in S_H . It satisfies the following proposition

Proposition 2. *Let $f \in C^4(\bar{S})$ and $T_{\mathcal{L}_A} = \mathcal{L}_A(R_H f) - \nabla(\mathcal{A} \nabla f)$ where $R_H f$ is the restriction of f in S_H*

$$T_{\mathcal{L}_A}(x_i, y_j) = (h_{i+1} - h_i)r(x_i, y_j, t) + (k_{j+1} - k_j)s(x_i, y_j, t) + O(H_{max}^2), \quad (5.28)$$

where functions $r(x, y), s(x, y)$ depend on the derivatives of \mathcal{A} and f up to order 3. Furthermore, $T_{\mathcal{L}_A}$ satisfies, for each $\zeta > 0, \forall v^H \in W_{H,0}$

$$(T_{\mathcal{L}_A}, v^H)_H \leq \frac{M}{\zeta^2} H_{max}^4 + \zeta^2 (\|\nabla_{-H} v^H\|_{H,-}^2 + 3\|v^H\|_H^2), \quad (5.29)$$

where M is independent of h_i, k_j .

Proof. It is possible to prove (5.28), then we have

$$\begin{aligned} (T_{\mathcal{L}_A}, v^H)_H &= \underbrace{\sum_{i,j=1}^{N-1,M-1} h_{i+\frac{1}{2}} k_{j+\frac{1}{2}} (h_{i+1} - h_i) r(x_i, y_j, t) v_{i,j}^H}_{\text{first term}} \\ &+ \underbrace{\sum_{i,j=1}^{N-1,M-1} h_{i+\frac{1}{2}} k_{j+\frac{1}{2}} (k_{j+1} - k_j) s(x_i, y_j, t) v_{i,j}^H + (O(H_{max}^2), v^H)_H}_{\text{second term}}. \end{aligned}$$

Using that $v_{0,j} = v_{N,j} = 0$, the first term satisfies

$$\begin{aligned}
& \frac{1}{2} \sum_{i,j=1}^{N-1,M-1} k_{j+\frac{1}{2}} (h_{i+1}^2 - h_i^2) r(x_i, y_j, t) v_{i,j}^H \\
&= \frac{1}{2} \sum_{i,j=1}^{N,M-1} k_{j+\frac{1}{2}} h_i^2 (r(x_{i-1}, y_j, t) v_{i-1,j}^H - r(x_i, y_j, t) v_{i,j}^H) \\
&= -\frac{1}{2} \sum_{i,j=1}^{N,M-1} k_{j+\frac{1}{2}} h_i^3 r(x_{i-1}, y_j, t) D_{-x}(v_{i,j}^H) - \frac{1}{2} \sum_{i,j=1}^{N,M-1} k_{j+\frac{1}{2}} h_i^2 \left(\int_{x_{i-1}}^{x_i} \frac{\partial r}{\partial x}(x, y, t) dx \right) v_{i,j}^H \\
&\leq \frac{\|r\|_\infty H_{max}^2}{2} \sum_{i,j=1}^{N,M-1} k_{j+\frac{1}{2}} h_i |D_{-x}(v_{i,j}^H)| + \frac{\|\frac{\partial r}{\partial x}\|_\infty H_{max}^2}{2} \sum_{i,j=1}^{N,M-1} k_{j+\frac{1}{2}} h_i |v_{i,j}^H| \\
&\leq \frac{M_1 H_{max}^4}{4\zeta^2} + \zeta^2 (\|D_{-x} v^H\|_{h,-}^2 + \|v^H\|_H^2),
\end{aligned}$$

with $M_1 = \max \left\{ \frac{\|r\|_\infty^2}{4}, \left\| \frac{\partial r}{\partial x} \right\|_\infty^2 \right\}$. Analogously we have an upper bound for the second

term : $\frac{M_2 H_{max}^4}{4\zeta^2} + \zeta^2 (\|D_{-y} v^H\|_{k,-}^2 + \|v^H\|_H^2)$, where $M_2 = \max \left\{ \frac{\|s\|_\infty^2}{4}, \left\| \frac{\partial s}{\partial y} \right\|_\infty^2 \right\}$ then since

$(O(H_{max}^2), v^H)_H \leq \frac{M_3 H_{max}^4}{4\zeta^2} + \zeta^2 \|v^H\|_H^2$ we have the thesis (5.29) using $M = \frac{1}{4}(M_1 + M_2 + M_3)$. \square

Analogously we can prove the following proposition

Proposition 3. *Let $f \in L^\infty([0, T], C^4(\bar{S}))$, $g \in L^\infty([0, T], C^3(\bar{S}))$. The discrete operator $\nabla_c(\mathcal{A}D_H(R_H f)R_H g)$ approximates $\nabla((\mathcal{A}\nabla f)g)$ with a truncation error T_{∇_c} that satisfies, for all $\zeta > 0$*

$$(T_{\nabla_c}, v^H)_H \leq \frac{M}{\zeta^2} H_{max}^4 + 4\zeta^2 (\|\nabla_{-H} v^H\|_{H,-}^2 + 2\|v^H\|_H^2), \quad (5.30)$$

where M is independent of h_i, k_j .

Proposition 4 (Discrete Poincaré Inequality). *For all $v^H \in W_{H,0}$ we have*

$$\|v^H\|_H \leq C \|\nabla_{-H} v^H\|_{H,-},$$

where C depends on \bar{S}_H and is independent of h_i, k_j .

In the following we consider the simplified system

$$\begin{cases} -\nabla \cdot (\mathcal{A}\nabla p) &= \alpha C. \\ \frac{\partial C}{\partial t} &= -\nabla \cdot (vC) + \nabla \cdot (D\mathcal{A}\nabla C) + \beta C, \end{cases} \quad (5.31)$$

where $v = -\mathcal{A}\nabla p$ and D is a diffusion coefficient defined in \bar{S} . Note that (5.31) can derive from (5.1) by using $\alpha = |g|\beta$ and $\beta = |g|\alpha$. Note also that since $|g|$ not depends on t

and we are discretizing only the derivatives on space in the PDE system, by a method of lines, we can continue to use $\frac{\partial C}{\partial t}$ instead of $|g|\frac{\partial C}{\partial t}$ in this Chapter that not change the significance of the following results.

By $p^H(t)$ and $C^H(t)$ we represent the semi-discrete approximation for $p(x, y, t)$ and $C(x, y, t)$ defined by the following coupled problem

$$\begin{cases} -\mathcal{L}_{\mathcal{A}}(p^H) = \alpha C^H, & \text{in } S_H \times [0, T], \\ \frac{\partial C^H}{\partial t} - \nabla_c \cdot (\mathcal{A} D_H p^H C^H) = \mathcal{L}_{\mathcal{B}}(C^H) + \beta C^H, & \text{in } S_H \times (0, T], \\ p^H = C^H = 0, & \text{on } \partial S_H, \\ C^H(0) = C_0^H & \text{in } S_H. \end{cases} \quad (5.32)$$

where $\mathcal{B} = D\mathcal{A}$ and $\mathcal{L}_{\mathcal{A}}(\cdot)$, $\mathcal{L}_{\mathcal{B}}(\cdot)$ are defined as in (5.26).

5.2 Convergence analysis and stability

To simplify the notation in the next paragraph we write v^H instead of $v^H(t)$ when it is possible. Let (p^H, C^H) , $(\tilde{p}^H, \tilde{C}^H)$ two solutions of (5.32) with different initial conditions for the parabolic problem. We prove that the stability of the method implemented in (5.32) with respect to the norm $\|\cdot\|_H$ requires the boundness of $\|C^H\|_{\infty}$ and $\|D_H p^H\|_{\infty}$, as it will be shown. Whereas the convergence analysis of (5.32) requires only the boundness of $\|D_H p^H\|_{\infty}$, and since it will be proved that convergence implies stability, then it is sufficient that $\|D_H p^H\|_{\infty}$ is uniformly bounded to have both stability and convergence. Moreover in our demonstration for the convergence of the elliptic problem we requires that matrix \mathcal{A} satisfies $\min_{ij} \{\mathcal{A}_{ij}^{11}, \mathcal{A}_{ij}^{22}\} > \|\mathcal{A}^{12}\|_{\infty} + \|\mathcal{A}^{21}\|_{\infty}$.

Let $v^H = p^H - \tilde{p}^H$, $w^H = C^H - \tilde{C}^H \in W_{H,0}$, using the linearity of the operators defined above, it can be shown that v^H, w^H are solutions of the problem

$$\begin{cases} -\mathcal{L}_{\mathcal{A}}(v^H) = \alpha w^H & \text{in } S_H \times [0, T] \\ \frac{\partial w^H}{\partial t} = \nabla_c \cdot (\mathcal{A}(C^H D_H p^H - \tilde{C}^H D_H \tilde{p}^H)) + \mathcal{L}_{\mathcal{B}}(w^H) + \beta w^H & \text{in } S_H \times (0, T], \\ v^H = w^H = 0 & \text{on } \partial S_H, \\ w^H(0) = w_0^H. & \end{cases} \quad (5.33)$$

5.2.1 Stability for the elliptic equation (5.32)₁

Multiplying (5.33)₁ by $v^H = p^H - \tilde{p}^H$, it can be shown, using the relations (5.12) and (5.13) of Proposition 1, the next estimate: for all $\zeta > 0$

$$a_0 \|\nabla_{-H} v^H\|_{H,-}^2 + ((\mathcal{A}^{12} + \mathcal{A}^{21}) \delta_x v^H, \delta_y v^H)_H \leq \frac{\|\alpha\|_{\infty}^2 \|w^H\|_H^2}{4\zeta^2} + \zeta^2 \|v^H\|_H^2. \quad (5.34)$$

where $\zeta > 0$ and $a_0 = \min\{\mathcal{A}^{11}, \mathcal{A}^{22}\}$. Taking $b_0 = \|\mathcal{A}^{12}\|_\infty + \|\mathcal{A}^{21}\|_\infty$ we get from (5.34), and using Propositions 1₍₅₎

$$(a_0 - b_0 - C\zeta^2)\|\nabla_{-H}v^H\|_{H,-}^2 \leq \frac{\|\alpha\|_\infty^2\|w^H\|_H^2}{4\zeta^2}.$$

Then we have the following stability result for the pressure: if $(a_0 - b_0 - C\zeta^2) > 0, \exists M > 0$, which is independent of H and t , such that

$$\|\nabla_{-H}v^H\|_{H,-}^2 \leq M\|w^H\|_H^2. \quad (5.35)$$

where $M = \frac{\|\alpha\|_\infty^2}{4\zeta^2(a_0 - b_0 - C\zeta^2)}$. Note that the stability result (5.35) for the pressure is obtained when $\min\{\mathcal{A}^{11}, \mathcal{A}^{22}\} > \|\mathcal{A}^{12}\|_\infty + \|\mathcal{A}^{21}\|_\infty$.

5.2.2 Stability for the parabolic equation (5.32)₂

Multiplying the parabolic equation (5.33) by $w^H = C^H - \tilde{C}^H$, we get

$$\frac{1}{2} \frac{\partial \|w^H\|_H^2}{\partial t} + (a_0 - b_0)\|\nabla_{-H}w^H\|_{H,-}^2 \leq (\nabla_c \cdot (\mathcal{A}(C^H D_H p^H - \tilde{C}^H D_H \tilde{p}^H)), w^H)_H + \|\beta\|_\infty \|w^H\|_H^2. \quad (5.36)$$

where $a_0 = \min\{\mathcal{B}^{11}, \mathcal{B}^{22}\}$, $b_0 = \|\mathcal{B}^{12}\|_\infty + \|\mathcal{B}^{21}\|_\infty$.

Firstly we have from Proposition (1)₍₄₎, that

$$\begin{aligned} (\nabla_c \cdot (\mathcal{A}(C^H D_H p^H - \tilde{C}^H D_H \tilde{p}^H)), w^H)_H &= -(M_H(\mathcal{A}C^H D_H p^H), \nabla_{-H}w^H)_{H,-} \\ &+ (M_H(\tilde{C}^H D_H \tilde{p}^H), \nabla_{-H}w^H)_{H,-} \\ &= (M_x(\eta^{1,H}C^H - \tilde{\eta}^{1,H}\tilde{C}^H), D_{-x}w^H)_{h,-} \\ &+ (M_y(\eta^{2,H}C^H - \tilde{\eta}^{2,H}\tilde{C}^H), D_{-x}w^H)_{k,-}, \end{aligned}$$

where $\eta^H = -\mathcal{A}D_H p^H$, $\tilde{\eta}^H = -\mathcal{A}D_H \tilde{p}^H$. Using Proposition (1)₍₁₎ we have

$$\begin{aligned} (M_x(\eta^{1,H}C^H - \tilde{\eta}^{1,H}\tilde{C}^H), \delta_x^{(1/2)}w^H)_{h,-} &\leq \|\eta^{1,H}C^H - \tilde{\eta}^{1,H}\tilde{C}^H\|_H \|D_{-x}w^H\|_{h,-} \\ &\leq \frac{2\|C^H\|_\infty^2 \|\eta^{1,H} - \tilde{\eta}^{1,H}\|_H^2 + 2\|\tilde{\eta}^H\|_\infty^2 \|w^H\|_H^2}{4\zeta^2} \\ &+ \zeta^2 \|D_{-x}w^H\|_{h,-}^2. \end{aligned}$$

Then

$$(M_H(\mathcal{A}(C^H D_H p^H - \tilde{C}^H D_H \tilde{p}^H)), \nabla_{-H}w^H)_{H,-} \leq \frac{2\|C^H\|_\infty^2 \|\mathcal{A}D_H v^H\|_H^2 +}{4\zeta^2} \quad (5.37)$$

$$+ \frac{2\|\mathcal{A}D_H \tilde{p}^H\|_\infty^2 \|w^H\|_H^2}{4\zeta^2} \quad (5.38)$$

$$+ \zeta^2 \|\nabla_{-H}w^H\|_{H,-}^2, \quad (5.39)$$

for some $\zeta > 0$. Using Proposition 1, the pressure stability result (5.35) and (5.37)- (5.39), we get

$$\begin{aligned} (M_H(\mathcal{A}(C^H D_H p^H - \tilde{C}^H D_H \tilde{p}^H)), \nabla_{-H} w^H)_{H,-} &\leq \frac{(M_1 \|C^H\|_\infty^2 + M_2 \|D_H \tilde{p}^H\|_\infty^2) \|w^H\|_H^2}{4\zeta^2} \\ &+ \zeta^2 \|\nabla_{-H} w^H\|_{H,-}^2, \end{aligned}$$

To conclude the stability we need to suppose that the numerical solutions are uniformly bounded that is $\|C^H\|_\infty$ and $\|D_H p^H\|_\infty$ are uniformly bounded with respect to H . Calling $M_3 = (a_0 - b_0 - \zeta^2)$, $M_4(t) = \frac{(M_1(t) \|C^H(t)\|_\infty^2 + M_2(t) \|D_H \tilde{p}^H(t)\|_\infty^2)}{4\zeta^2} + \|\beta\|_\infty$ we have from (5.36)

$$\frac{1}{2} \frac{\partial \|w^H(t)\|_H^2}{\partial t} + M_3 \|\nabla_{-H} w^H\|_{H,-}^2 \leq M_4(t) \|w^H\|_H^2. \quad (5.40)$$

Consequently using the Gronwall lemma we have

$$\|w^H(t)\|_H^2 + \int_0^t \|\nabla_{-H} w^H(s)\|_{H,-}^2 ds \leq \frac{1}{\min\{1, 2M_3\}} \|w^H(0)\|_H^2 e^{K \int_0^t \widehat{M}_4(s) ds} \quad (5.41)$$

where $\widehat{M}_4(s) = \frac{M_4(s)}{\min\{1, 2M_3\}}$.

5.2.3 Convergence

In the following we analyze the behavior of the pressure error $e_p^H = R_H p - p^H$ and density error $e_C^H = R_H C - C^H$, where p, C are the solutions of the density-pressure problem (5.31) and p^H, C^H of (5.32). Let T_p, T_C be the truncation errors induced by the spatial discretization for elliptic and parabolic equations in (5.32) respectively. These errors are related by the system

$$\begin{cases} -\mathcal{L}_A(e_p^H) &= \alpha e_C^H + T_p && \text{in } S_H \times [0, T] \\ \frac{\partial e_C^H}{\partial t} &= (\nabla_c \cdot (\mathcal{A} \nabla p C - \mathcal{A} D_H p^H C^H)) + \mathcal{L}_B(e_C^H) + \beta e_C^H + T_C && \text{in } S_H \times (0, T], \\ e_p^H &= e_C^H = 0 && \text{on } \partial S_H. \end{cases} \quad (5.42)$$

Theorem 3. For $p \in L^\infty([0, T], C^3(\overline{S}))$ and $C \in L^\infty([0, T], C^0(\overline{S}))$, we have the following convergence results for the pressure elliptic problem in the norm $\|\cdot\|_H$

$$\|\nabla_{-H} e_p^H(t)\|_{H,-}^2 \leq M \|e_C^H(t)\|_H^2 + O(H_{max}^4), \quad (5.43)$$

where M is independent of H and t .

Proof. From (5.42) we easily obtain, for $\zeta > 0$, using a demonstration similar to that done to get the stability result (5.35) for the pressure

$$(a_0 - b_0) \|\nabla_{-H} e_p^H\|_{H,-}^2 \leq \frac{\|\alpha\|_\infty^2}{4\zeta^2} \|e_C\|_H^2 + \zeta^2 \|e_p\|_H^2 + (T_p, e_p)_H. \quad (5.44)$$

where $a_0 = \min\{\mathcal{A}^{11}, \mathcal{A}^{22}\}$, $b_0 = \|\mathcal{A}^{12}\|_\infty + \|\mathcal{A}^{21}\|_\infty$.

Using the Propositions 2 and 4 with $v^H = e_p^H$, we get

$$(a_0 - b_0)\|\nabla_{-H}e_p^H\|_{H,-}^2 \leq \frac{\|\alpha\|_\infty^2}{4\zeta^2}\|e_C^H\|_H^2 + 4\zeta^2\|e_p^H\|_H^2 + \frac{M}{\zeta^2}H_{max}^4 + \zeta^2\|\nabla_{-H}e_p^H\|_{H,-}^2. \quad (5.45)$$

Supposing that $(a_0 - b_0 - \zeta^2(1 + 4C)) > 0$ we prove the theorem. \square

Proposition 5. Suppose that $\|\nabla_{-H}e_p^H\|_{H,-}^2 \leq MH_{max}^4$, $p \in C^0(\bar{S})$ and $\frac{H_{max}}{H_{min}} \leq M(\bar{S})$, then $\|D_{HP}^H\|_\infty$ is bounded.

Proof. Since $\|\nabla_{-H}e_p^H\|_{H,-}^2 \leq MH_{max}^4$ then $\|\nabla_{HP}^H\|_\infty$ is bounded. We have that

$$(\delta_h p_{i,j}^H)^2 = \left(\frac{h_{i+1}\delta_x^{1/2}p_{i,j}^H + h_i\delta_x^{1/2}p_{i+1,j}^H}{h_{i+1} + h_i} \right)^2 \quad (5.46)$$

$$\leq \frac{M(\bar{S})^2}{4}\|D_{-x}p^H\|_\infty^2. \quad (5.47)$$

\square

Theorem 4. For $C \in L^2([0, T], C^4(\bar{S})) \cap L^\infty([0, T], C^3(\bar{S})) \cap C^1([0, T], C^0(\bar{S}))$. Let $\|D_{HP}^H\|_\infty$ uniformly bounded with respect to H , then we have the convergence for density parabolic problem, that is

$$\|e_C^H(t)\|_H^2 + \int_0^t \|\nabla_{-H}e_C^H(s)\|_{H,-}^2 ds \leq M(H_{max}^4 + \|e_C^H(0)\|_H^2). \quad (5.48)$$

where M is independent of h and k .

Proof. We can get this result using a similar demonstration of that used to get the result (5.41). In this demonstration we use $w^H = R^H C - C^H$, and we are always supposing that the restriction of the solution is uniformly bounded by $\|C\|_\infty$.

\square

Corollary 2. The elliptic pressure problem and the parabolic density problem are convergent if and only if $\|D_{HP}^H\|_\infty$ is bounded.

Corollary 3. For the density-pressure numerical problem (5.33) convergence implies stability.

Proof. Convergence for the density problem implies that $\|C^H\|_\infty$ is bounded and for the Theorem 5.43 also implies convergence for the pressure problem. Such convergence for Proposition (5) implies that $\|D_{HP}^H\|_\infty$ is bounded. Then from the uniform bounding of $\|C^H\|_\infty$ and $\|D_{HP}^H\|_\infty$ we obtain the stability of the density pressure problem (5.34). \square

5.3 Numerical results

We measure the errors of the numerical solution p^H, C^H of (5.33) with respect to the solution p, C of (5.31) by using the following norms:

$$\|e_C\|_H = \max_{n=1, \dots, N_T} \sqrt{\|e_C^H(t_n)\|_H^2 + \sum_{j=1}^n \Delta t \|\nabla_{-H} e_C^H(t_j)\|_{H,-}^2}. \quad (5.49)$$

$$\|e_p\|_H = \max_{n=0, \dots, M} \|e_p^H(t_n)\|_H. \quad (5.50)$$

Here we consider the time interval $[0, T]$ with constant time steps $\Delta t = T/N_T$.

We proved in the Section 5.2 that using these different norms for measuring the pressure and density approximation error of the method the approximations p^H and C^H converges to p and C with a second order when p, C are in $L^2([0, T], C^4(\bar{S}))$ as one can see in Examples 2 and 3. In this section we prove numerically that this second order is obtained in the example 4 when we use solutions p, C in $L^2([0, T], C^4(\bar{S}))$. However in example 3 we prove that this order is obtained also for functions in $L^2([0, T], C^3(\bar{S}))$. This have motivated us to further examine in Chapter 6 the numerical method where we proved that a such second order of convergence is valid also for functions less regular that are in fact in $L^2([0, T], H^3(\bar{S}))$.

The non uniform mesh is built using a small and random perturbation of an uniform one. For some purposes we always impose the condition $\frac{H_{max}}{H_{min}} \leq C$. To avoid the non linearity of the problem, we decouple the system by solving firstly the elliptic equation and then the parabolic one. The final semi discrete problem is solved using backward Euler in time and the rate of convergence is computed using the following expression.

$$Rate_i = \frac{\log\left(\frac{\|e_i\|_H}{\|e_i\|_{\tilde{H}}}\right)}{\log\left(\frac{H_{max}}{\tilde{H}_{max}}\right)}, \quad (5.51)$$

for $i = p, C$.

Example 2. We start by considering a regular $C^4(\bar{S})$ solution of (5.31)

$$p(x, y, t) = C(x, y, t) = e^{-t} \text{sen}(\pi x) \text{sen}(\pi y),$$

defined in $[0, 1]^2 \times (0, T]$, with $T = 0.1$ and $\Delta t = 1e - 04$.

$$\mathcal{A}(x, y) = \begin{bmatrix} 4 + \text{sen}(\pi y)^2 & -\text{sen}(\pi x) \text{sen}(\pi y) \\ -\text{sen}(\pi x) \text{sen}(\pi y) & 4 + \text{sen}(\pi x)^2 \end{bmatrix}, D = \frac{1}{8\pi^2},$$

Table 4 – Numerical errors and convergence rates for Example 2

H_{max}	$\ e_p\ _H$	Rate _p	$\ e_C\ _H$	Rate _C
2.503216e-01	1.706188e-01	-	3.505003e-01	-
1.252408e-01	3.605839e-02	2.244438	7.620294e-02	2.203528
8.342393e-02	1.541813e-02	2.091040	3.357726e-02	2.017093
6.255882e-02	8.574553e-03	2.038528	1.906057e-02	1.967243
5.023403e-02	5.469237e-03	2.049362	1.224774e-02	2.015729
4.204243e-02	3.793964e-03	2.054495	8.511195e-03	2.044562

Example 3. We consider the following solution that is in $C^3(\bar{S})$

$$p(x, y, t) = \begin{cases} e^{8-t} \left((x - \frac{1}{10})(x - \frac{9}{10})(y - \frac{1}{10})(y - \frac{9}{10}) \right)^4 & \text{if } \frac{1}{10} \leq x, y \leq \frac{9}{10} \\ 0 & \text{otherwise.} \end{cases} \quad (5.52)$$

$$C(x, y, t) = e^{-t} \text{sen}(\pi x) \text{sen}(\pi y), \quad (5.53)$$

with $T = 0.1$ and $\Delta t = 1e - 04$.

$$A(x, y) = \begin{bmatrix} 1 + \text{sen}(\pi y)^2 & -\text{sen}(\pi x) \text{sen}(\pi y) \\ -\text{sen}(\pi x) \text{sen}(\pi y) & 1 + \text{sen}(\pi x)^2 \end{bmatrix}, D = \frac{1}{2\pi^2}$$

Table 5 – Numerical errors and convergence rates for Example 3

H_{max}	$\ e_p\ _H$	Rate _p	$\ e_C\ _H$	Rate _C
8.340501e-02	4.244955e-04	-	1.855296e-03	-
7.699766e-02	3.614419e-04	2.011679	1.590796e-03	1.924220
7.149196e-02	3.127291e-04	1.951262	1.381933e-03	1.897174
6.673173e-02	2.732260e-04	1.959786	1.209120e-03	1.938781
6.254805e-02	2.412143e-04	1.924663	1.069797e-03	1.890848
5.900608e-02	2.144615e-04	2.016581	9.522958e-04	1.995874
5.560734e-02	1.909160e-04	1.960324	8.492288e-04	1.930827
5.280920e-02	1.713778e-04	2.091092	7.651417e-04	2.019521

In the next example we are solving the cell dynamics problem in a single scale, basically, we choose $\bar{S} = Y$. In the last Chapter, we do something similar but with other boundary conditions and other purposes.

Example 4. We consider the problem of cell proliferation in a colonic crypt described by the system (5.1) with initial condition for the cell density

$$C_0(x, y) = \frac{xy(x-1)(y-1)}{(0.5)^4} e^{-\left(\frac{R(x, y)}{0.03}\right)^2}, \quad (x, y) \in [0, 1]^2 \quad (5.54)$$

see figure 14 for its graph in three dimension depicted on the crypt Γ with $h = 7$ and $\sigma = 0.03$.

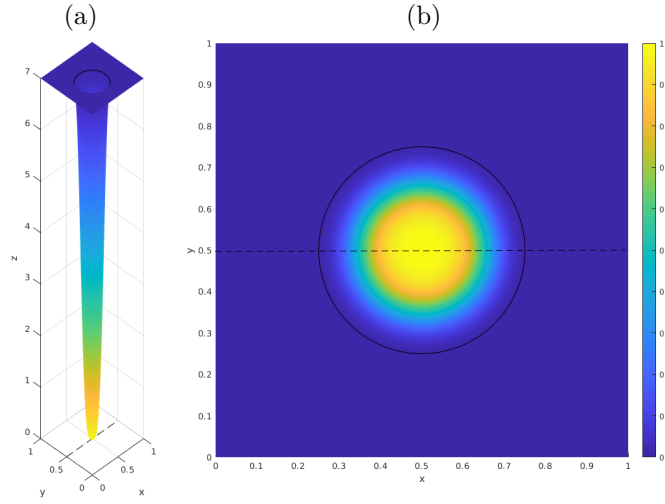


Figure 14 – Initial density distribution C_0 defined in (5.54) on the crypt Γ graph of the function f defined in (5.55). Three dimensional plot of the initial density $C_0(x, y)$ in the points $(x, y, f(x, y))$. Two dimensional plot of $C_0(x, y)$ with $(x, y) \in [0, 1]^2$.

In this example we use $D = 1$ and functions $\mathcal{A}_\xi = \xi \mathcal{A}$ ($\xi = 4.17451 \cdot 10^3$), $|g|, \alpha, \beta$ ($\tau = 2.22627 \cdot 10^{-3}$) and with the crypt geometry defined as described previously in Chapter 2 with

$$h = 7, \sigma = 0.03, \quad f(x, y) = h(1 - e^{-\left(\frac{R(x, y)}{\sigma}\right)^2}), \quad R(x, y) = (x - 1/2)^2 + (y - 1/2)^2, \quad (5.55)$$

where $\mathcal{A}, |g|$ are given respectively in (2.14), (2.13) and α, β are those given in (2.3) and (2.2).

For $T = 1$ we solve (5.1) in $(0, 1)^2 \times (0, T]^2$ by the Backward Euler method with time step $\Delta t = 1e - 01$ applied to the initial value problem (5.32). The accuracy results applying the IVP (5.32) to this example on non uniform meshes are given in Table 6, where a fine solution of (5.1) associated to $H_{max} = 1/480 = 2.2083 \cdot 10^{-3}$ is used as exact solution.

Table 6 – Numerical errors and convergence rates in Example 4

H_{max}	$\ e_p\ _H$	Rate _p	$\ e_C\ _H$	Rate _C
1.6667e-02	3.9386e-07	-	1.9956	-
1.2500e-02	3.5188e-07	0.3917	9.7944e-01	0.7047
1.0000e-02	3.1160e-07	0.5449	8.0811e-01	0.8617
8.3333e-03	2.7443e-07	0.6967	6.7472e-01	0.9895
7.1429e-03	2.4080e-07	0.8480	5.6788e-01	1.1182
6.2500e-03	2.1062e-07	1.0026	4.8177e-01	1.2320
5.5556e-03	1.8370e-07	1.1610	4.0992e-01	1.3708
5.0000 e-03	1.5975e-07	1.3263	3.4983e-01	1.5042
4.5455e-03	1.3846e-07	1.5004	2.9876e-01	1.6560
4.1667e-03	1.1956e-07	1.6870	2.5521e-01	1.8107
3.8462e-03	1.0268e-07	1.9010	2.1686e-01	2.0341
3.5714e-03	8.7652e-08	2.1355	1.8369e-01	2.2401

Since the density and pressure depends only on their distance with respect the bottom of the crypt that is respect the point $(x, y, 0) = (0.5, 0.5, 0)$ we can analyze only one direction along this point ot analyze the evolution of the pressure and density along the time interval $[0, T]$. In figures 15-16 we plot the value measure for the cell density and pressure along the line $y = 0.5$. We observe that the cell density of transit cells diffuse away from the bottom of the crypt filling slowly the above regions along the crypt walls.

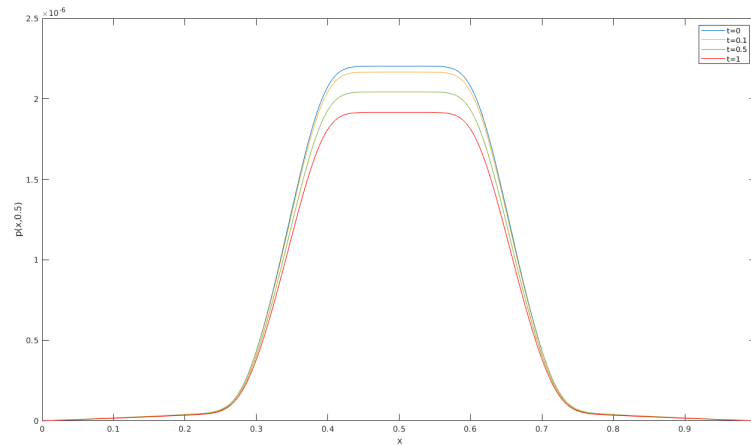


Figure 15 – Pressure in the points located in the line $y = 0.5$ during the numerical simulation in the time interval $[0, 1]$. Plots are referred to the times $t = 0, 0.1, 0.5, 1$.

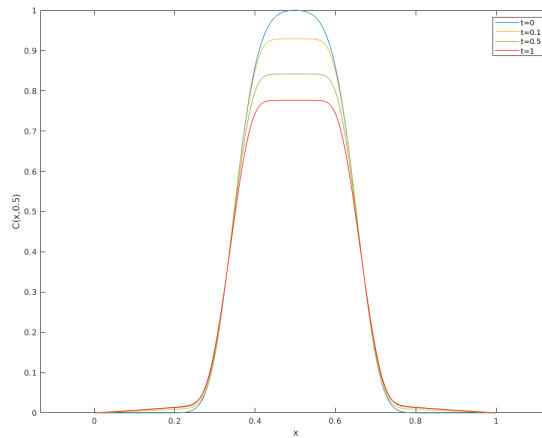


Figure 16 – Pressure in the points located in the line $y = 0.5$ during the numerical simulation in the time interval $[0, 1]$. Plots are referred to the times $t = 0, 0.1, 0.5, 1$.

We note a decreasing of pressure at the bottom and of its gradient along the crypt axis, this yield to a significant decrease of the velocity, as you can see in figure 17, where the maximum is always obtained along the line $y = 0.5$ for $x = 0.6773$ that corresponds to the crypt quote $z = \frac{2}{3}h$.

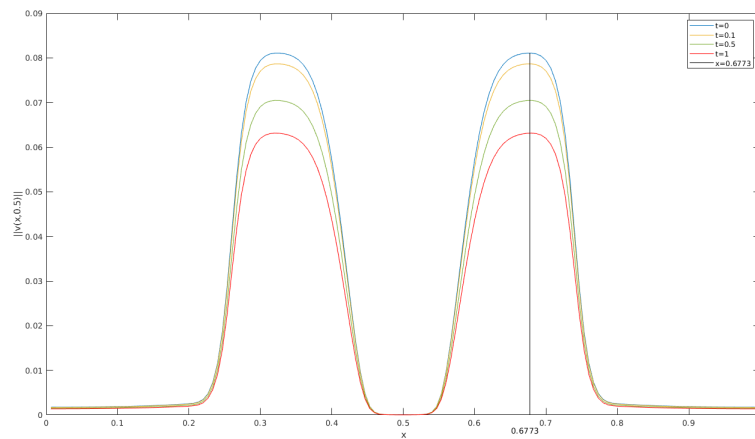


Figure 17 – Euclidean Norm for the velocity $\|v\| = \xi \|\nabla p\|$ in the points located in the line $y = 0.5$ during the numerical simulation in the time interval $[0, 1]$. Plots are referred to the times $t = 0, 0.1, 0.5, 1$.

6 An equivalent FEM with second order accuracy for solutions in $L^\infty([0, T], H^3(\bar{S}))$

In the previous Chapter we have seen that the finite difference method (5.32) on nonuniform meshes converges with order two using a discrete norm in $L^2([0, T], H_0^1(\bar{S}))$ for the density and second order in the $L^\infty([0, T], H_0^1(\bar{S}))$ discrete norm for the pressure. Since we were using centered schemes a such order was unexpected, thus we called the method as supraconvergent. The convergence theorem seen in the previous Chapter guarantees a such convergence order when the solutions p, C belong to $L^\infty([0, T], C_0^4(\bar{S}))$. However in the Example 3 of previous Chapter we have seen numerically that a such convergence order is reached in a case when p, C belong to $L^\infty([0, T], C_0^3(\bar{S}))$. We will prove in this Chapter that for any C, p in $L^\infty([0, T], H_0^3(\bar{S}))$ the finite difference method have order 2 using the same norms. This Chapter is an application of the method presented in (FERREIRA; GRIGORIEFF, 2006) for a two-dimensional coupled elliptic-parabolic problems. See also (FERREIRA; PINTO, 2013; FERREIRA; NO; OLIVEIRA, 2013; FERREIRA; BARBEIRO; GRIGORIEFF, 2005).

6.1 Approximating the variational problem

We will work with the usual Sobolev spaces $W_q^r(\bar{S})$ for $r \in \mathbb{N} \cup \{0\}$ where $S = (0, 1)^2$ and $q \in [2, \infty]$ with semi-norms, respectively, given by

$$|v|_{W_q^r(\bar{S})} = \left(\sum_{|\alpha|=r} \|D^\alpha v\|_{L^q(\bar{S})}^q \right)^{1/q}, \quad \|v\|_{W_q^r(\bar{S})} = \left(\sum_{j=0}^r |v|_{W_q^j(\bar{S})}^q \right)^{1/q},$$

with the usual interpretation in case $q = \infty$ and $\|\cdot\|_{L^q(\bar{S})}$ denoting the usual norm in the Sobolev space $L^q(\bar{S})$. We often write $H^r(\bar{S})$ in place of $W_2^r(\bar{S})$ and denote by $\|\cdot\|_r$ for its norm. By $(\cdot, \cdot)_0$ we denote the standard inner product on $L^2(\bar{S})$ and we use the notation $H_0^1(\bar{S}) = \{v \in H^1(\bar{S}); v = 0 \text{ on } \partial S\}$.

We now write down the variational formulation of (5.1) in H_0^1 using the L^2 inner product. Let $\bar{S} \subset \mathbb{R}^2$ be a simple polygonal domain (in this case $\bar{S} = [0, 1]^2$). The variational formulation of our problem is: find $p, C \in H_0^1(\bar{S})$ such that

$$\begin{cases} a_{\mathcal{A}}(p, v) = (\alpha C, v)_0, & \text{for } v \in H_0^1(\bar{S}) \\ (C_t, w)_0 + b_z(C, w) = -a_{D\mathcal{A}}(C, w) + (\beta C, w)_0, & \text{for } w \in H_0^1(\bar{S}), \end{cases} \quad (6.1)$$

where $z = -\mathcal{A}\nabla p$, the diffusion coefficient $D > 0$ is supposed to be constant, and

$a_{\mathcal{B}}(\cdot, \cdot), b_z(\cdot, \cdot)$ are defined by

$$a_{\mathcal{A}}(v, w) = (\mathcal{A}^{11}v_x, w_x)_0 + (\mathcal{A}^{21}v_x, w_y)_0 + (\mathcal{A}^{12}v_y, w_x)_0 + (\mathcal{A}^{22}v_y, w_y)_0, \quad (6.2)$$

$$b_z(v, w) = ((z)_1v, w_x)_0 + ((z)_2v, w_y)_0, \quad (6.3)$$

for $v, w \in H^1(\bar{S})$. $(z)_1$ and $(z)_2$ are respectively the first and the second component

The discretization of (6.2)-(6.3) is obtained in the following way. As done in Chapter 5 let $\mathbf{h} = (h_i)_{\mathbb{Z}}$ and $\mathbf{k} = (k_j)_{\mathbb{Z}}$ be two sequences of mesh sizes. We define by \bar{S}_H the discrete mesh in $\bar{S} = [0, 1]^2$,

$$\bar{S}_H = \{(x_i, y_j)_{i,j=0}^{N,M} | (x_i, y_j) = (x_{i-1} + h_i, y_{j-1} + k_j), (x_0, y_0) = (0, 0)\}.$$

We introduce the following sets

$$\partial S_H = \{(x_i, y_j), i = 0, N; j = 0, \dots, M\} \cup \{(x_i, y_j), i = 0, \dots, N; j = 0, M\}, S_H = \bar{S}_H / \partial S_H.$$

By W_H we denote the space of grid functions on \bar{S}_H and by $W_{H,0}$ the subspace of grid functions vanishing on ∂S_H . For convenience, we assume that functions in W_H are also defined outside of \bar{S}_H with function values equal to zero. For $(x_i, y_j) \in \bar{S}_H$ let $\square_{i,j} := (x_{i-1/2}, x_{i+1/2}) \times (y_{j-1/2}, y_{j+1/2}) \cap S$ and $\omega_{i,j} = |\square_{i,j}|$, the measure of $\square_{i,j}$.

In W_H we introduce the following inner product

$$(v^H, w^H)_H := \sum_{(x_i, y_j) \in S_H} \omega_{i,j} v_{i,j} \bar{w}_{i,j}, \text{ for } v^H, w^H \in W_H$$

that defines an inner product in W_H where $v^H = \{v_{ij}\}$ and $w^H = \{w_{ij}\}$.

In this Chapter we apply the following method that approximate the variational formulation of the cell dynamics problem (5.33) in the space $W_{H,0}$ using the scalar product $(\cdot, \cdot)_H$. The benefit of the method (6.4) is that it is written as a finite element method and this provide use numerical properties that allow to prove that the method is second order accurate also for solutions in $L^2([0, T], H^3(\bar{S}))$.

The discrete problem has the form: find $p^H, C^H \in W_H$ such that

$$\begin{aligned} a_{\mathcal{A},H}(p^H, v^H) &= (\alpha C^H, v^H)_H, \\ (\partial_t C^H, w^H)_H &= -b_{z_H,H}(C^H, w^H) - a_{D,\mathcal{A},H}(C^H, w^H) + (\beta C^H, w^H)_H, \end{aligned} \quad (6.4)$$

for $v^H, w^H \in W_{H,0}$, where $z_H = -\mathcal{A}D_H p^H$, where $D_H = (\delta_h, \delta_k)$ with δ_h, δ_k are the operator defined below and $p^H = C^H = 0$ on ∂S_H .

Let \mathcal{T}_H be a triangularization of S using the set \bar{S}_H as vertices. By $P_H v^H$ we denote the continuous piecewise linear interpolation of v^H with respect to \mathcal{T}_H . The $a_{\mathcal{A},H}(\cdot, \cdot), b_{z_H,H}(\cdot, \cdot)$ are defined as follows

$$a_{\mathcal{A},H} = a + b + c \quad (6.5)$$

$$b_{z_H,H} = d \quad (6.6)$$

where a, b, c, d are defined bellow. These terms derives from the terms in the variational problem (6.1) that are rewritten in an equivalent formulation using the piecewise linear interpolation of grid functions in W_H .

Let $\Delta \in \mathcal{T}_H$ with a $\frac{\pi}{2}$ angle, we define $\mathcal{A}_{\Delta,x}^{11}$ to be the value of the coefficient \mathcal{A}^{11} in the midpoint of the side of Δ parallel to the x -axis. Then let

$$a(v^H, w^H) := \sum_{\Delta \in \mathcal{T}_H} \mathcal{A}_{\Delta,x}^{11} \int_{\Delta} (P_H v^H)_x (P_H \bar{w}^H)_x \, dx \, dy. \quad (6.7)$$

Similarly, with $\mathcal{A}_{\Delta,y}^{22}$, denoting the value of \mathcal{A}^{22} in the midpoint of the side of Δ parallel to the y -axis,

$$c(v^H, w^H) := \sum_{\Delta \in \mathcal{T}_H} \mathcal{A}_{\Delta,y}^{22} \int_{\Delta} (P_H v^H)_y (P_H \bar{w}^H)_y \, dx \, dy. \quad (6.8)$$

For the discretization of the mixed derivatives, we consider two special triangularizations of S , which we call $\mathcal{T}_H^{(1)}$ and $\mathcal{T}_H^{(2)}$ that have as vertices all the grid points x_{ij} of \bar{S}_H . They are obtained from the disjoint decomposition

$$\bar{S}_H = \bar{S}_H^{(1)} \cup \bar{S}_H^{(2)},$$

where the sum $i + j$ of the indices of the points (x_i, y_j) in $\bar{S}_H^{(1)}$ and $\bar{S}_H^{(2)}$ is even and odd, respectively. $\mathcal{T}_H^{(1)}$ (and $\mathcal{T}_H^{(2)}$) has triangles with angle $\pi/2$, each triangle has two vertices in $\bar{S}_H^{(1)}$ (respectively in $\bar{S}_H^{(2)}$) and the third is that associated to the $\pi/2$ angle. For a triangle Δ in a triangularization, denote by (x_Δ, y_Δ) the vertex of Δ associated with the angle $\pi/2$ of Δ . We define the value of \mathcal{A}^{12} and $(z_H)_s v^H$ in the points Δ, x and Δ, y as follows

$$\mathcal{A}_{\Delta,x}^{12} = \mathcal{A}_{\Delta,y}^{12} := \mathcal{A}^{12}(x_\Delta, y_\Delta), ((z_H)_s v^H)_{\Delta,x} = ((z_H)_s v^H)_{\Delta,y} := ((z_H)_s v^H)(x_\Delta, y_\Delta), s = 1, 2.$$

We use

$$b(v^H, w^H) := \frac{1}{2} (b^{(1)}(v^H, w^H) + b^{(2)}(v^H, w^H)), \quad (6.9)$$

$$d(v^H, w^H) := \frac{1}{2} (d^{(1)}(v^H, w^H) + d^{(2)}(v^H, w^H)), \quad (6.10)$$

for $v^H, w^H \in W_{H,0}$, where

$$\begin{aligned} b^{(l)}(v^H, w^H) &:= \sum_{\Delta \in \mathcal{T}_H^{(l)}} \int_{\Delta} [\mathcal{A}_{\Delta,x}^{21} (P_H^{(l)} v^H)_x (P_H^{(l)} \bar{w}^H)_y + \mathcal{A}_{\Delta,y}^{12} (P_H^{(l)} v^H)_y (P_H^{(l)} \bar{w}^H)_x] \, dx \, dy \\ &=: b_{xy}^{(l)} + b_{yx}^{(l)}, \\ d^{(l)}(v^H, w^H) &:= - \sum_{\Delta \in \mathcal{T}_H^{(l)}} [((z_H)_1 v^H)_{\Delta,x} \int_{\Delta} (P_H^{(l)} \bar{w}^H)_x \, dx \, dy \\ &\quad + ((z_H)_2 v^H)_{\Delta,y} \int_{\Delta} (P_H^{(l)} \bar{w}^H)_y \, dx \, dy], \\ &=: d_x^{(l)} + d_y^{(l)}, \end{aligned}$$

where $z_H = -\mathcal{A}D_H p^H$, $l = 1, 2$ and $P_H^{(l)}$ is the piecewise linear interpolant operator. The operator $D_H = (\delta_h, \delta_k)$ will be defined later.

The method (6.4) can be seen as a finite element method with standard piecewise linear basis in \mathcal{T}_H . This method is similar to the finite difference method in the non uniform grid Ω_H defined in the previous Chapter (5.32). For its formulation we use the following centered finite difference operators

$$\delta_x^{(1/2)} v_{i,j} = \frac{v_{i+1/2,j} - v_{i-1/2,j}}{x_{i+1/2} - x_{i-1/2}}, \quad \delta_x^{(1/2)} v_{i+1/2,j} = \frac{v_{i+1,j} - v_{i,j}}{x_{i+1} - x_i}, \quad (6.11)$$

$$\delta_x v_{i,j} = \frac{v_{i+1,j} - v_{i-1,j}}{x_{i+1} - x_{i-1}}, \quad (6.12)$$

$$\delta_h v_{i,j} = \frac{h_i \delta_x^{(1/2)} v_{i+1/2,j} + h_{i+1} \delta_x^{(1/2)} v_{i-1/2,j}}{h_i + h_{i+1}}, \quad (6.13)$$

in the x -direction and also correspondingly we get the defined quantities in y -direction. By M_x we denote the average operator, where $M_x(v^H)_{i,j} = \frac{1}{2}(v_{i,j} + v_{i-1,j})$ (respectively for M_y).

In the following we use the discrete operator

$$\mathcal{L}_B(u^H) := -\delta_x^{(1/2)}(\mathcal{B}^{11} \delta_x^{(1/2)}(u^H)) - \delta_x(\mathcal{B}^{12} \delta_y(u^H)) - \delta_y(\mathcal{B}^{21} \delta_x(u^H)) - \delta_y^{(1/2)}(\mathcal{B}^{22} \delta_y^{(1/2)}(u^H)). \quad (6.14)$$

Proposition 6. For all $v^H \in W_H, w^H \in W_{H,0}$ and $a : [0, 1]^2 \rightarrow \mathbb{R}$ we have

$$\begin{aligned} -(\delta_x^{(1/2)}(a \delta_x^{(1/2)} v^H), w^H)_H &= \sum_{(x_i, y_j) \in \bar{S}_H} h_i k_{j+1/2} a(x_{i-1/2}, y_j) \delta_x^{(1/2)} v_{i-1/2,j} \delta_x^{(1/2)} \bar{w}_{i-1/2,j} \\ -(\delta_x v^H, w^H)_H &= \sum_{(x_i, y_j) \in \bar{S}_H} h_i k_{j+1/2} M_x(v^H)_{i,j} \delta_x^{(1/2)} \bar{w}_{i-1/2,j}. \end{aligned}$$

Proof. This proposition presents the same results (5.11) and (5.12) that are here rewritten using an explicit expression in order to help in the proof of the next proposition. \square

Proposition 7. Let $a_{\mathcal{A},H}$ and the operator $\mathcal{L}_{\mathcal{A}}$ be defined by (6.5) and (7.5), respectively. We have

$$a_{\mathcal{A},H}(v^H, w^H) = (\mathcal{L}_{\mathcal{A}}(v^H), w^H)_H, \text{ for } v^H \in W_H, w^H \in W_{H,0}.$$

Proof. Consider the following triangles in \mathcal{T}_H

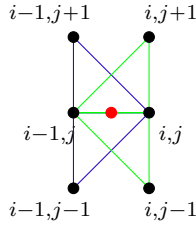


Figure 18 – Triangles representation

Triangles of different colors are in different triangularization, then fixing the segment from (x_{i-1}, y_j) to (x_i, y_j) we have since $w^H \in W_{H,0}$

$$\begin{aligned} \mathcal{A}_{\Delta_1, x}^{11} \int_{\Delta_1} (P_H v^H)_x (P_H \bar{w}^H)_x dx dy + \mathcal{A}_{\Delta_2, x}^{11} \int_{\Delta_2} (P_H v^H)_x (P_H \bar{w}^H)_x dx dy = \\ h_i k_{j+1/2} \mathcal{A}_{i-1/2, j}^{11} \delta_x^{(1/2)} v_{i-1/2, j} \delta_x^{(1/2)} \bar{w}_{i-1/2, j}. \end{aligned}$$

The same holds to Δ_1, Δ_2 . Then using Proposition 6 for any triangularization

$$\begin{aligned} a(v^H, w^H) &:= \sum_{\Delta \in \mathcal{T}_H} \mathcal{A}_{\Delta, x}^{11} \int_{\Delta} (P_H v^H)_x (P_H \bar{w}^H)_x dx dy \\ &= \sum_{i, j=1}^{N, M-1} h_i k_{j+1/2} \mathcal{A}_{i-1/2, j}^{11} \delta_x^{(1/2)} v_{i-1/2, j} \delta_x^{(1/2)} \bar{w}_{i-1/2, j} \\ &= - \sum_{i, j=1}^{N-1, M-1} h_{i+1/2} k_{j+1/2} \delta_x^{(1/2)} (\mathcal{A}^{11} \delta_x^{(1/2)}(v))_{i, j} \bar{w}_{i, j} \\ &= (-\delta_x^{(1/2)} (\mathcal{A}^{11} \delta_x^{(1/2)}(v^H)), w^H)_H. \end{aligned}$$

Now, considering both triangularizations, we have using Proposition 6

$$\begin{aligned} &\frac{1}{2} (\mathcal{A}_{\Delta_1, y}^{12} \int_{\Delta_1} (P_H^{(1)} v^H)_y (P_H^{(1)} w^H)_x dx dy + \mathcal{A}_{\Delta_2, y}^{12} \int_{\Delta_2} (P_H^{(1)} v^H)_y (P_H^{(1)} w^H)_x dx dy \\ &+ \mathcal{A}_{\Delta_1, y}^{12} \int_{\Delta_1} (P_H^{(2)} v^H)_y (P_H^{(2)} w^H)_x dx dy + \mathcal{A}_{\Delta_2, y}^{12} \int_{\Delta_2} (P_H^{(2)} v^H)_y (P_H^{(2)} w^H)_x dx dy) \\ &= \frac{1}{2} \left(\frac{h_i k_{j+1}}{2} \mathcal{A}_{i-1, j}^{12} \delta_y^{(1/2)} v_{i-1, j+1/2} \delta_x^{(1/2)} \bar{w}_{i-1/2, j} + \frac{h_i k_j}{2} \mathcal{A}_{i-1, j}^{12} \delta_y^{(1/2)} v_{i-1, j-1/2} \delta_x^{(1/2)} \bar{w}_{i-1/2, j} \right. \\ &+ \left. \frac{h_i k_{j+1}}{2} \mathcal{A}_{i, j}^{12} \delta_y^{(1/2)} v_{i, j+1/2} \delta_x^{(1/2)} \bar{w}_{i-1/2, j} + \frac{h_i k_j}{2} \mathcal{A}_{i, j}^{12} \delta_y^{(1/2)} v_{i, j-1/2} \delta_x^{(1/2)} \bar{w}_{i-1/2, j} \right). \end{aligned}$$

Then

$$\begin{aligned}
& \frac{1}{2}(b_{yx}^{(1)} + b_{yx}^{(2)})(v^H, w^H) = \frac{1}{2} \sum_{l=1}^2 \sum_{\Delta \in \mathcal{T}_H^l} \mathcal{A}_{\Delta_y}^{12} \int_{\Delta} (P_H^{(l)} v^H)_y (P_H^{(l)} w^H)_x \, dx \, dy \\
&= \frac{1}{4} \sum_{i,j=1}^{N,M-1} (h_i \mathcal{A}_{i,j}^{12} (k_{j+1} \delta_y^{(1/2)} v_{i,j+1/2} + k_j \delta_y^{(1/2)} v_{i,j-1/2}) \delta_x^{(1/2)} \bar{w}_{i-1/2,j} \\
&+ h_i \mathcal{A}_{i-1,j}^{12} (k_{j+1} \delta_y^{(1/2)} v_{i-1,j+1/2} + k_j \delta_y^{(1/2)} v_{i-1,j-1/2}) \delta_x^{(1/2)} \bar{w}_{i-1/2,j}) \\
&= \frac{1}{2} \sum_{i,j=1}^{N,M-1} h_i k_{j+1/2} (\mathcal{A}_{i,j}^{12} \delta_y v_{i,j} + \mathcal{A}_{i-1,j}^{12} \delta_y v_{i-1,j}) \delta_x^{(1/2)} \bar{w}_{i-1/2,j} \\
&= \sum_{i,j=1}^{N,M-1} h_i k_{j+1/2} M_x (\mathcal{A}^{12} \delta_y v)_{i,j} \delta_x^{(1/2)} \bar{w}_{i-1/2,j} \\
&= - \sum_{i,j=1}^{N-1,M-1} h_{i+1/2} k_{j+1/2} \delta_x (\mathcal{A}^{12} \delta_y (v))_{i,j} \bar{w}_{i,j} \\
&= - (\delta_x (\mathcal{A}^{12} \delta_y (v^H)), w^H)_H.
\end{aligned}$$

□

Proposition 8. The operator $b_{z_H, H}$ defined in (6.6) satisfies the following equality

$$b_{z_H, H}(v^H, w^H) = (\delta_x((z_H)_1 v^H) + \delta_y((z_H)_2 v^H), w^H)_H, \text{ for } v^H \in W_H, w^H \in W_{H,0}.$$

Proof. Consider the term d and the two triangularizations $\mathcal{T}_H^{(1)}, \mathcal{T}_H^{(2)}$ we have for all $i = 1, \dots, N$ and $j = 1, \dots, M-1$

$$\begin{aligned}
& \frac{1}{2}(((z_H)_1 v^H)_{\Delta_{1,x}} \int_{\Delta_1} (P_H^{(1)} w^H)_x \, dx \, dy + ((z_H)_1 v^H)_{\Delta_{2,x}} \int_{\Delta_2} (P_H^{(1)} w^H)_x \, dx \, dy \\
&+ ((z_H)_1 v^H)_{\Delta_{1,x}} \int_{\Delta_1} (P_H^{(2)} w^H)_x \, dx \, dy + ((z_H)_1 v^H)_{\Delta_{2,x}} \int_{\Delta_2} (P_H^{(2)} w^H)_x \, dx \, dy) \\
&= \frac{1}{2} \left(\frac{h_i k_{j+1}}{2} ((z_H)_1 v^H)_{i-1,j} \delta_x^{(1/2)} \bar{w}_{i-1/2,j} + \frac{h_i k_j}{2} ((z_H)_1 v^H)_{i-1,j} \delta_x^{(1/2)} \bar{w}_{i-1/2,j} \right. \\
&+ \left. \frac{h_i k_{j+1}}{2} ((z_H)_1 v^H)_{i,j} \delta_x^{(1/2)} \bar{w}_{i-1/2,j} + \frac{h_i k_j}{2} ((z_H)_1 v^H)_{i,j} \delta_x^{(1/2)} \bar{w}_{i-1/2,j} \right).
\end{aligned}$$

Then

$$\begin{aligned}
\frac{1}{2}(d_x^{(1)} + d_x^{(2)})(v^H, w^H) &= - \sum_{i,j=1}^{N,M-1} (h_i k_{j+1/2} M_x ((z_H)_1 v^H)_{i,j} \delta_x^{(1/2)} \bar{w}_{i-1/2,j} \\
&= \sum_{i,j=1}^{N-1,M-1} h_{i+1/2} k_{j+1/2} \delta_x ((z_H)_1 v^H)_{i,j} \bar{w}_{i,j} \\
&= (\delta_x ((z_H)_1 v^H), w^H)_H.
\end{aligned}$$

Thus we have the thesis $\frac{1}{2}(d_y^{(1)} + d_y^{(2)})(v^H, w^H) = (\delta_y((z_H)_2 v^H), w^H)_H$.

□

6.2 Estimating the method error

In this section we estimate the errors between the discretized operator used in the numerical method (6.4) with respect the corresponding integrals appearing in the variational formulation of the elliptic-parabolic problem (6.1). Such estimates are of second order of consistency for functions u in $H^3(\bar{S})$ as it is proved in this section. Then following the same theorems done in Section 5.2 it can be proved that this finite element method is a superconvergent method in the context of finite elements methods theory. Our method will result in fact to be of second order of convergence for the pressure using the norm $L^\infty([0, T], H^1(\bar{S}))$ and second order of convergence for the density using the norm $C^1([0, T], H^1(\bar{S}))$.

Lemma 2. *Let $u \in H^3(\bar{S})$ and the coefficient $\mathcal{A}^{11} \in W_\infty^2(\bar{S})$. Then the part*

$$\tau_H^{(a)}(v^H) := a(R_H u, v^H) - \sum_{(x_i, y_j) \in S_H} \int_{\square_{ij}} (-\mathcal{A}^{11} u_x)_x \, dx \, dy \bar{v}_{ij}. \quad (6.15)$$

satisfies the following estimate

$$|\tau_H^{(a)}(v^H)| \leq C \left(\sum_{\Delta \in \mathcal{T}_H} (\text{diam} \Delta)^4 \|u_x\|_{H^2(\Delta)}^2 \right)^{1/2} \|P_H v^H\|_1, \forall v^H \in W_{H,0}.$$

where $\text{diam} \Delta$ is the diameter of the triangle $\Delta \in \mathcal{T}_H$, where \mathcal{T}_H is a regular triangulation of \bar{S} as that represented in blue or green in Figure 18 with triangles with a angle of $\pi/2$.

Proof. Let consider the interval $I_j := (y_{j-1/2}, y_{j+1/2})$ and define $\tilde{\square}_{i,j} = (x_{i-1}, x_i) \times I_j$. Using the definition of a , we get

$$\tau_H^{(a)}(v^H) = \sum_{i,j} \left(|I_j| (\mathcal{A}^{11} \delta_x^{(1/2)} u)_{i-1/2,j} - \int_{I_j} (\mathcal{A}^{11} u_x)(x_{i-1/2}, y) \, dy \right) \Delta_x \bar{v}_{i,j}. \quad (6.16)$$

Adding and subtracting $(\mathcal{A}^{11} u_x)(x_{i-1/2}, y_j)$, we obtain

$$\begin{aligned} \tau_H^{(a)}(v^H) &= \sum_{i,j} |I_j| \left((\mathcal{A}^{11} \delta_x^{(1/2)} u)_{i-1/2,j} - (\mathcal{A}^{11} u_x)(x_{i-1/2}, y_j) \right) \Delta_x \bar{v}_{i,j} \\ &+ \sum_{i,j} \left(|I_j| (\mathcal{A}^{11} u_x)(x_{i-1/2}, y_j) - \int_{I_j} (\mathcal{A}^{11} u_x)(x_{i-1/2}, y) \, dy \right) \Delta_x \bar{v}_{i,j} \\ &= \tau_H^{(a,1)}(v^H) + \tau_H^{(a,2)}(v^H). \end{aligned}$$

We rewrite the first term $\tau_H^{(a,1)}(v^H)$ as follows $\tau_H^{(a,1)}(v^H) = \sum_{i=1, j=1}^{N, M-1} |I_j| F_{i,j}(u) \Delta_x \bar{v}_{i,j}$ where

$$\begin{aligned} F_{i,j}(u) &= (\mathcal{A}^{11} \delta_x^{(1/2)} u)_{i-1/2,j} - (\mathcal{A}^{11} u_x)(x_{i-1/2}, y_j) \\ &= \mathcal{A}^{11}(x_{i-1/2}, y_j) \left(\frac{1}{h_i} \int_{x_{i-1}}^{x_i} u_x(x, y_j) \, dx - u_x(x_{i-1/2}, y_j) \right). \end{aligned}$$

as a linear bounded functional in the function $u_x \in H^2(\tilde{\square}_{i,j})$ that vanishes for the functions 1, x and y , see Remark 1. The Bramble-Hilbert lemma furnishes the bound

$$\begin{aligned} |F(u)| &\leq C \sup_{\tilde{\square}_{i,j}} |\mathcal{A}^{11}(x, y)| \left(\frac{1}{h_i |I_j|} \int_{\tilde{\square}_{i,j}} h_i^4 |u_{xxx}|^2 + h_i^2 |I_j|^2 |u_{xxy}|^2 + h_i^2 |I_j|^2 |u_{xyx}|^2 \right. \\ &\quad \left. + |I_j|^4 |u_{xyy}|^2 \right)^{1/2} \\ &\leq C \sup_{\tilde{\square}_{i,j}} |\mathcal{A}^{11}(x, y)| (h_i |I_j|)^{-1/2} (h_i^2 + |I_j|^2) |u_x|_{H^2(\tilde{\square}_{i,j})}. \end{aligned}$$

and we obtain

$$\left| \sum_{i,j} |I_j| (\mathcal{A}^{11} \delta_x^{(1/2)} u - \mathcal{A}^{11} u_x)(x_{i-1/2}, y_j) \Delta_x \bar{v}_{i,j} \right| \leq C \left(\sum_{\Delta \in \mathcal{T}_H} (\text{diam} \Delta)^4 |u_x|_{H^2(\Delta)}^2 \right)^{1/2} \|P_H v^H\|_1. \quad (6.17)$$

Note that since $\exists C > 0$ such that $\frac{h_i}{k_j} \leq C$ then $|I_j|^2 = \left(\frac{k_j}{2} + \frac{k_{j+1}}{2}\right)^2 \leq k_j^2 + k_{j+1}^2$. Using the previous equation and Cauchy Schwartz, we can estimate $\tau_H^{(a,1)}$ as follows

$$|\tau_H^{(a,1)}| \leq C \left(\sum_{\Delta \in \mathcal{T}_H} (\text{diam} \Delta)^4 |u_x|_{H^2(\Delta)}^2 \right)^{1/2} \|P_H v^H\|_{H^1(\bar{S})}. \quad (6.18)$$

Remark 1. Define the operator

$$\lambda(g) := \int_0^1 g(\xi, \eta) d\xi - g\left(\frac{1}{2}, \eta\right), \quad (6.19)$$

which vanishes for 1, ξ and η . From Bramble-Hilbert lemma

$$|\lambda(g)| \leq C \|g^{(2)}\|_{L^2((0,1)^2)}.$$

Now we estimate the term $\tau_H^{(a,2)}(u)$

$$\begin{aligned} &\sum_{i,j} (|I_j| (\mathcal{A}^{11} u_x)(x_{i-1/2}, y_j) - \int_{I_j} (\mathcal{A}^{11} u_x)(x_{i-1/2}, y) dy) \Delta_x \bar{v}_{i,j} \\ &= \sum_{i,j} \left(\frac{k_{j+1}}{2} (\mathcal{A}^{11} u_x)(x_{i-1/2}, y_j) - \int_{y_j}^{y_{j+1/2}} (\mathcal{A}^{11} u_x)(x_{i-1/2}, y) dy \right) \Delta_x \bar{v}_{i,j} \\ &\quad + \sum_{i,j} \left(\frac{k_j}{2} (\mathcal{A}^{11} u_x)(x_{i-1/2}, y_j) - \int_{y_{j-1/2}}^{y_j} (\mathcal{A}^{11} u_x)(x_{i-1/2}, y) dy \right) \Delta_x \bar{v}_{i,j} \\ &= \sum_{i,j} T_{i,j+1}^{(1)} \Delta_x \bar{v}_{i,j} + T_{i,j}^{(2)} \Delta_x \bar{v}_{i,j} \end{aligned}$$

where

$$T_{i,j+1}^{(1)} = \frac{k_{j+1}}{2} (\mathcal{A}^{11} u_x)(x_{i-1/2}, y_j) - \int_{y_j}^{y_{j+1/2}} (\mathcal{A}^{11} u_x)(x_{i-1/2}, y) dy, \quad (6.20)$$

$$T_{i,j}^{(2)} = \frac{k_j}{2} (\mathcal{A}^{11} u_x)(x_{i-1/2}, y_j) - \int_{y_{j-1/2}}^{y_j} (\mathcal{A}^{11} u_x)(x_{i-1/2}, y) dy. \quad (6.21)$$

Since $v^H \in W_{H,0}$ we have

$$\begin{aligned} \tau_H^{a,2} &= \sum_{i,j} (T_{ij}^{(1)}) \Delta_x \bar{v}_{i,j-1} + (T_{ij}^{(2)}) \Delta_x \bar{v}_{i,j} \\ &= \frac{1}{2} \left(\sum_{i,j} (T_{ij}^{(2)} + T_{ij}^{(1)}) (\Delta_x \bar{v}_{i,j} + \Delta_x \bar{v}_{i,j-1}) + (T_{ij}^{(2)} - T_{ij}^{(1)}) (\Delta_x \bar{v}_{i,j} - \Delta_x \bar{v}_{i,j-1}) \right) \\ &:= Q_1 + Q_2. \end{aligned}$$

We start estimating Q_1 . Consider

$$F(u) = \frac{k_j}{2} ((\mathcal{A}^{11} u_x)(x_{i-1/2}, y_j) + (\mathcal{A}^{11} u_x)(x_{i-1/2}, y_{j-1})) - \int_{y_{j-1}}^{y_j} (\mathcal{A}^{11} u_x)(x_{i-1/2}, y) dy. \quad (6.22)$$

The Bramble-Hilbert lemma furnishes, see Remark 2

$$|F(u)| \leq C \left(\frac{k_j}{h_i} \right)^{1/2} (h_i^2 + k_j^2) |\mathcal{A}^{11} u_x|_{H^2(\hat{\delta}_{i,j})} \leq C \left(\frac{k_j}{h_i} \right)^{1/2} (h_i^2 + k_j^2) \|u_x\|_{H^2(\hat{\delta}_{i,j})}, \quad (6.23)$$

where $\hat{\delta}_{i,j} = (x_{i-1}, x_i) \times (y_{j-1}, y_j)$ and we took $\mathcal{A}^{11} \in W_\infty^2(\bar{S})$.

Remark 2. Define the operator

$$\lambda(g) := \frac{1}{2} (g(\frac{1}{2}, 0) + g(\frac{1}{2}, 1)) - \int_0^1 g(\frac{1}{2}, \eta) d\eta, \quad (6.24)$$

which vanishes for $1, \xi$ and η . From Bramble-Hilbert lemma

$$|\lambda(g)| \leq C \|g^{(2)}\|_{L^2((0,1)^2)}. \quad (6.25)$$

Then

$$|F(u)| \leq C k_j \left(\frac{1}{h_i k_j} \right)^{1/2} (h_i^2 + k_j^2) |\mathcal{A}^{11} u_x|_{H^2(\hat{\delta}_{i,j})} \leq C \left(\frac{k_j}{h_i} \right)^{1/2} (h_i^2 + k_j^2) \|u_x\|_{H^2(\hat{\delta}_{i,j})}. \quad (6.26)$$

Then it follows that

$$|Q_1| \leq C \left(\sum_{\Delta \in \mathcal{T}_H} (\text{diam} \Delta)^4 \|u_x\|_{H^2(\Delta)}^2 \right)^{1/2} \|P_H v^H\|_1. \quad (6.27)$$

We are now going to estimate Q_2 . A summation by parts with respect to i leads to the representation

$$Q_2 = \frac{1}{2} \sum_{i,j} (T_{i,j}^{(2)} - T_{i+1,j}^{(2)} - T_{i,j}^{(1)} + T_{i+1,j}^{(1)}) \Delta_y \bar{v}_{i,j}. \quad (6.28)$$

since $\Delta_x v_{i,j} - \Delta_x v_{i,j-1} = (v_{i,j} - v_{i-1,j}) - (v_{i,j-1} - v_{i-1,j-1}) = \Delta_y v_{i,j} - \Delta_y v_{i-1,j}$. Using (6.20) and (6.21) it is seen that

$$\begin{aligned}
& T_{i+1,j}^{(1)} - T_{i,j}^{(1)} + T_{i,j}^{(2)} - T_{i+1,j}^{(2)} \\
&= \frac{k_j}{2} \int_{x_{i-1/2}}^{x_{i+1/2}} \left((\mathcal{A}^{11} u_x)_x(x, y_{j-1}) - \int_{y_{j-1}}^{y_{j-1/2}} (\mathcal{A}^{11} u_x)_x(x, y) dy \right) dx \\
&- \frac{k_j}{2} \int_{x_{i-1/2}}^{x_{i+1/2}} \left((\mathcal{A}^{11} u_x)_x(x, y_j) - \int_{y_{j-1/2}}^{y_j} (\mathcal{A}^{11} u_x)_x(x, y) dy \right) dx \\
&= \int_{x_{i-1/2}}^{x_{i+1/2}} \left(\int_{y_{j-1/2}}^{y_j} (\mathcal{A}^{11} u_x)_x(x, y) dy - \int_{y_{j-1}}^{y_{j-1/2}} (\mathcal{A}^{11} u_x)_x(x, y) dy \right) dx \\
&+ \frac{k_j}{2} (\mathcal{A}^{11} u_x)_x(x, y_{j-1}) - \frac{k_j}{2} (\mathcal{A}^{11} u_x)_x(x, y_j) dx.
\end{aligned}$$

We obtain for almost all $x \in (x_{i-1/2}, x_{i+1/2})$

$$\begin{aligned}
& \left| \left(\int_{y_{j-1/2}}^{y_j} - \int_{y_{j-1}}^{y_{j-1/2}} \right) (\mathcal{A}^{11} u_x)_x dy - \left(\frac{k_j}{2} (\mathcal{A}^{11} u_x)_x(x, y_j) - \frac{k_j}{2} (\mathcal{A}^{11} u_x)_x(x, y_{j-1}) \right) \right| \\
&\leq C k_j^{3/2} \left(\int_{y_{j-1}}^{y_j} |(\mathcal{A}^{11} u_x)_{xy}(x, y)|^2 dy \right)^{1/2}.
\end{aligned}$$

This last estimate can be proved using the following remark

Remark 3. Taking

$$F(u) = \left(\int_{y_{j-1/2}}^{y_j} - \int_{y_{j-1}}^{y_{j-1/2}} \right) (\mathcal{A}^{11} u_x)_x dy - \left(\frac{k_j}{2} (\mathcal{A}^{11} u_x)_x(x, y_j) - \frac{k_j}{2} (\mathcal{A}^{11} u_x)_x(x, y_{j-1}) \right). \quad (6.29)$$

Define the operator

$$\lambda(g) := \left(\int_{1/2}^1 - \int_0^{1/2} \right) g(\xi) d\xi - \frac{1}{2} (g(1) - g(0)), \quad (6.30)$$

which vanishes for 1. From Bramble-Hilbert lemma

$$|\lambda(g)| \leq C \|g^{(1)}\|_{L^2((0,1))}.$$

Then

$$|F(u)| \leq C k_j^{3/2} \|(\mathcal{A}^{11} u_x)_{xy}(x, y)\|_{L^2((y_{j-1}, y_j))}. \quad (6.31)$$

After integrating with respect to x and an application of Cauchy-Schwartz's inequality for integrals

$$|T_{i+1,j}^{(1)} - T_{i,j}^{(1)} + T_{i,j}^{(2)} - T_{i+1,j}^{(2)}| \leq C k_j^{3/2} (h_i^{1/2} \|u_x\|_{H^2(\bar{\Omega}_{i,j})} + h_{i+1}^{1/2} \|u_x\|_{H^2(\bar{\Omega}_{i+1,j})})$$

follows. Then Q_2 satisfies the same bound as Q_1 . \square

Lemma 3. Let $u \in H^3(\bar{S})$ and the coefficient $\mathcal{A}^{12} = \mathcal{A}^{21} \in W_\infty^2$. Then the part

$$\tau_H^{(b)}(v^H) := b(R_H u, v^H) - \sum_{i,j} \int_{\square_{i,j}} (-\mathcal{A}^{12} u_y)_x + (-\mathcal{A}^{21} u_x)_y \, dx \, dy \bar{v}_{i,j}, \quad (6.32)$$

satisfies the estimate

$$|\tau_H^{(b)}(v^H)| \leq C \left(\sum_{\Delta \in \mathcal{T}_H} (\text{diam} \Delta)^4 \|u\|_{H^3(\Delta)}^2 \right)^{1/2} \|P_H v^H\|_1, \quad (6.33)$$

for $v^H \in W_{H,0}$.

Proof. We estimate only the error of the discretization of $(\mathcal{A}^{12} u_y)_x$. Analogously we get the estimate for the error associated to $(\mathcal{A}^{21} u_x)_y$. Our strategy is to rewrite the integral term coming from the variational form

$$\tilde{b}_{yx} = - \sum_{i,j} \int_{\square_{i,j}} (\mathcal{A}^{12} u_y)_x \, dx \, dy \bar{v}_{i,j} \quad (6.34)$$

and its approximation $b_{yx}(R_H u, v^H) := \frac{1}{2} (b_{yx}^{(1)}(R_H u, v^H) + b_{yx}^{(2)}(R_H u, v^H))$ in a similar way in function of the elementary displacements $\Delta_x v_{i,j} \Delta_y v_{i,j}$. By a partial integration of a summation by part we obtain

$$\tilde{b}_{yx} = \sum_{i,j} \int_{\square_{i,j}} (-\mathcal{A}^{12} u_y)_x \, dx \, dy \bar{v}_{i,j} = \sum_{i,j} \int_{I_j} (\mathcal{A}^{12} u_y)(x_{i-1/2}, y) \, dy \Delta_x \bar{v}_{i,j}. \quad (6.35)$$

Next we want to evaluate (a similar expression is valid also for b_{xy})

$$b_{yx}(R_H u, v^H) := \frac{1}{2} (b_{yx}^{(1)}(R_H u, v^H) + b_{yx}^{(2)}(R_H u, v^H)) = -(\delta_x (\mathcal{A}^{12} \delta_y R_H u), v^H)_H,$$

for $v^H \in W_{H,0}$.

It is easy to see that

$$\begin{aligned} b_{yx}(R_H u, v^H) &= - \sum_{i,j} h_{i+1/2} k_{j+1/2} \delta_x (\mathcal{A}^{12} \delta_y R_H u)_{i,j} \bar{v}_{i,j} \\ &= \frac{1}{2} \sum_{i,j} k_{j+1/2} ((\mathcal{A}^{12} \delta_y R_H u)_{i-1,j} - (\mathcal{A}^{12} \delta_y R_H u)_{i+1,j}) \bar{v}_{i,j} \\ &= \frac{1}{4} \sum_{i,j} (\mathcal{A}_{i-1,j}^{12} (u_{i-1,j+1} - u_{i-1,j-1}) \\ &\quad - \mathcal{A}_{i+1,j}^{12} (u_{i+1,j+1} - u_{i+1,j-1})) \bar{v}_{i,j} \\ &= \frac{1}{4} \sum_{i,j} (\mathcal{A}_{i-1,j}^{12} (k_{j+1} \delta_y(1/2) u_{i-1,j+1} + k_j \delta_y(1/2) u_{i-1,j}) \\ &\quad - \mathcal{A}_{i+1,j}^{12} (k_{j+1} \delta_y^{(1/2)} u_{i+1,j+1} + k_j \delta_y^{(1/2)} u_{i+1,j})) \bar{v}_{i,j} \\ b_{yx}(R_H u, v^H) &= \frac{1}{4} \sum_{i,j} (k_j (\mathcal{A}_{i,j}^{12} \delta_y^{(1/2)} u_{i,j-1/2} + \mathcal{A}_{i-1,j}^{12} \delta_y^{(1/2)} u_{i-1,j-1/2}) \\ &\quad + k_{j+1} (\mathcal{A}_{i,j}^{12} \delta_y^{(1/2)} u_{i,j+1/2} + \mathcal{A}_{i-1,j}^{12} \delta_y^{(1/2)} u_{i-1,j+1/2})) \Delta_x \bar{v}_{i,j}. \end{aligned}$$

We can rewrite it using

$$\begin{aligned} k_j(\mathcal{A}_{i,j-1/2}^{12}\delta_y^{(1/2)}u_{i,j-1/2} + \mathcal{A}_{i-1,j}^{12}\delta_y^{(1/2)}u_{i-1,j-1/2}) &= 2M_x(\mathcal{A}_{i,j}^{12}\int_{y_{j-1}}^{y_j} u_y(x_i, y) dy) \\ k_{j+1}(\mathcal{A}_{i,j}^{12}\delta_{-y}^{(1/2)}u_{i,j+1/2} + \mathcal{A}_{i-1,j}^{12}\delta_y^{(1/2)}u_{i-1,j+1/2}) &= 2M_x(\mathcal{A}_{i,j}^{12}\int_{y_j}^{y_{j+1}} u_y(x_i, y) dy). \end{aligned}$$

Then summing and subtracting

$$\frac{1}{4}\sum_{i,j} M_x(\mathcal{A}_{i,j}^{12}\int_{y_{j-1}}^{y_j} u_y dy)\Delta_x v_{i,j-1} + \frac{1}{4}\sum_{i,j} M_x(\mathcal{A}_{i,j-1}^{12}\int_{y_{j-1}}^{y_j} u_y dy)\Delta_x v_{i,j} \quad (6.36)$$

and using after the relation we can write $b_{yx}(R_H u, v^H)$ as follows

$$\begin{aligned} b_{yx}(R_H u, v^H) &= \frac{1}{2}\sum_{i,j} (M_x(\mathcal{A}_{i,j}^{12}\int_{y_{j-1}}^{y_j} u_y(x_i, y) dy) \\ &+ M_x(\mathcal{A}_{i,j}^{12}\int_{y_j}^{y_{j+1}} u_y(x_i, y) dy))\Delta_x \bar{v}_{i,j} \\ &= \frac{1}{4}(\sum_{i,j} M_x(\mathcal{A}_{i,j}^{12}\int_{y_{j-1}}^{y_j} u_y(x_i, y) dy \\ &+ \mathcal{A}_{i,j-1}^{12}\int_{y_{j-1}}^{y_j} u_y(x_i, y) dy)(\Delta_x \bar{v}_{i,j} + \Delta_x \bar{v}_{i,j-1}) \\ &+ \sum_{i,j} (M_x(\mathcal{A}_{i,j}^{12}\int_{y_{j-1}}^{y_j} u_y(x_i, y) dy \\ &- \mathcal{A}_{i,j-1}^{12}\int_{y_{j-1}}^{y_j} u_y(x_i, y) dy)(\Delta_x \bar{v}_{i,j} - \Delta_x \bar{v}_{i,j-1})) \\ &= \frac{1}{4}(\sum_{i,j} M_x(\mathcal{A}_{i,j}^{12}\int_{y_{j-1}}^{y_j} u_y(x_i, y) dy \\ &+ \mathcal{A}_{i,j-1}^{12}\int_{y_{j-1}}^{y_j} u_y(x_i, y) dy)(\Delta_x \bar{v}_{i,j} + \Delta_x \bar{v}_{i,j-1}) \\ &+ \frac{1}{2}\sum_{i,j} ((\mathcal{A}_{i-1,j}^{12} - \mathcal{A}_{i-1,j-1}^{12})\int_{y_{j-1}}^{y_j} u_y(x_{i-1}, y) dy \\ &- (\mathcal{A}_{i+1,j}^{12} - \mathcal{A}_{i+1,j-1}^{12})\int_{y_{j-1}}^{y_j} u_y(x_{i+1}, y) dy)\Delta_y \bar{v}_{i,j}) \\ &:= \sum_{i,j} B_{i,j}^{(1)}(\Delta_x \bar{v}_{i,j} + \Delta_x \bar{v}_{i,j-1}) + \sum_{i,j} B_{i,j}^{(2)}\Delta_y \bar{v}_{i,j}, \end{aligned}$$

since

$$\Delta_x \bar{v}_{i,j} - \Delta_x \bar{v}_{i,j-1} = (\bar{v}_{i,j} - \bar{v}_{i-1,j}) - (\bar{v}_{i,j-1} - \bar{v}_{i-1,j-1}) = \Delta_y \bar{v}_{i,j} - \Delta_y \bar{v}_{i-1,j}.$$

Now we obtain a similar expression for \tilde{b}_{yx} by using (6.14), decomposing the integrals

$$\begin{aligned}
\tilde{b}_{yx} &= \sum_{i,j} \int_{I_j} (\mathcal{A}^{12} u_y)(x_{i-1/2}, y) dy \Delta_x \bar{v}_{i,j} \\
&= \frac{1}{2} \left(\sum_{i,j} \int_{y_{j-1}}^{y_j} (\mathcal{A}^{12} u_y)(x_{i-1/2}, y) dy (\Delta_x \bar{v}_{i,j} + \Delta_x \bar{v}_{i,j-1}) \right. \\
&\quad \left. + \left(\int_{y_{j-1/2}}^{y_j} - \int_{y_{j-1}}^{y_{j-1/2}} \right) (\mathcal{A}^{12} u_y)(x_{i-1/2}, y) dy (\Delta_x \bar{v}_{i,j} - \Delta_x \bar{v}_{i,j-1}) \right) \\
&= \frac{1}{2} \left(\sum_{i,j} \int_{y_{j-1}}^{y_j} (\mathcal{A}^{12} u_y)(x_{i-1/2}, y) dy (\Delta_x \bar{v}_{i,j} + \Delta_x \bar{v}_{i,j-1}) \right. \\
&\quad \left. + \sum_{i,j} \left(\int_{y_{j-1/2}}^{y_j} - \int_{y_{j-1}}^{y_{j-1/2}} \right) ((\mathcal{A}^{12} u_y)(x_{i-1/2}, y) - (\mathcal{A}^{12} u_y)(x_{i+1/2}, y)) dy (\Delta_y \bar{v}_{i,j}) \right) \\
&:= \sum_{i,j} S_{i,j}^{(1)} (\Delta_x \bar{v}_{i,j} + \Delta_x \bar{v}_{i,j-1}) + \sum_{i,j} S_{i,j}^{(2)} \Delta_y \bar{v}_{i,j}.
\end{aligned}$$

Now we begin with estimating the corresponding quantities starting with $B_{i,j}^{(1)} - S_{i,j}^{(1)}$. First we concentrate on $B_{i,j}^{(1)}$ alone

$$\mathcal{A}_{i,j}^{12} u_y(x_i, y) + \mathcal{A}_{i-1,j}^{12} u_y(x_{i-1}, y) \quad (6.37)$$

An application of Bramble-Hilbert lemma and taking $\mathcal{A}^{12} \in W_\infty^2(\bar{S})$ into account yields that uniformly for $y \in (y_j, y_{j-1})$

$$|\mathcal{A}_{i,j}^{12} u_y(x_i, y) + \mathcal{A}_{i-1,j}^{12} u_y(x_{i-1}, y) - 2\mathcal{A}_{i-1/2,j}^{12} u_y(x_{i-1/2}, y)| \leq Ch_i^{3/2} |\mathcal{A}^{12}(\cdot, y) u_y(\cdot, y)|_{H^2(x_{i-1}, x_i)}. \quad (6.38)$$

Remark 4. In order to get (6.38) we consider the functional $\lambda(g) = g(1) - g(0) - 2g(\frac{1}{2})$ that vanishes for 1 and ξ . Thus using $\tilde{g}(\xi) := \mathcal{A}^{12}(x_{i-1} + \xi h_i, y) u_y(x_{i-1} + \xi h_i, y)$ for the Bramble Hilbert Lemma $|\lambda(\tilde{g})| \leq \|\tilde{g}^{(2)}\|_{L^2(0,1)}$ and thus we obtain (6.38).

Integration of the last inequality over (y_{j-1}, y_j) provides an additional factor $k_j^{1/2}$ and we end up with

$$\begin{aligned}
& \left| \int_{y_{j-1}}^{y_j} (\mathcal{A}_{i,j}^{12} u_y(x_i, y) + \mathcal{A}_{i-1,j}^{12} u_y(x_{i-1}, y) - 2\mathcal{A}_{i-1/2,j}^{12} u_y(x_{i-1/2}, y)) dy \right| \\
& \leq C k_j^{1/2} h_i^{3/2} \|\mathcal{A}^{12}(x_{i-1/2}, y_j) u_y(x_{i-1/2}, y)\|_{H^2(\hat{\sigma}_{i,j})} \leq C(h_i^2 + k_j^2) \|u_y\|_{H^2(\hat{\sigma}_{i,j})}
\end{aligned}$$

(the same holds for $j-1$ in place of j). The last inequality is obtained using that

$$2k_j h_i^{\frac{3}{2}} = \left(\frac{k_j}{h_i}\right)^{\frac{1}{2}} h_i^2 + \left(\frac{h_i}{k_j}\right)^{\frac{1}{2}} k_j^2 \leq h_i^2 + k_j^2. \quad (6.39)$$

Remark 5. Define

$$\mathcal{A}_{i,j}^{12} u_y(x_i, y) + \mathcal{A}_{i-1,j}^{12} u_y(x_{i-1}, y) = F_j(x_i, y) + F_j(x_{i-1}, y), \quad (6.40)$$

where $F_j(x, y) := \mathcal{A}^{12}(x, y_j)u_y(x, y)$. The following operator

$$\lambda(g) = g(1) + g(0) - 2g\left(\frac{1}{2}\right), \quad (6.41)$$

vanishes for 1 and ξ , then we get easily (6.38).

Now we estimate the two terms added

$$\frac{1}{4}(\mathcal{A}_{i-1/2,j}^{12} \int_{y_{j-1}}^{y_j} u_y(x_{i-1/2}, y) dy + \mathcal{A}_{i-1/2,j-1}^{12} \int_{y_{j-1}}^{y_j} u_y(x_{i-1/2}, y) dy). \quad (6.42)$$

as before we have

$$|\mathcal{A}_{i-1/2,j}^{12} + \mathcal{A}_{i-1/2,j-1}^{12} - 2\mathcal{A}_{i-1/2,j-1/2}^{12}| \int_{y_{j-1}}^{y_j} u_y(x_{i-1/2}, y) dy| \leq Ck_j^2 \left(\frac{k_j}{h_i}\right)^{1/2} \|u_y\|_{H^1(\hat{\Theta}_{i,j})} \quad (6.43)$$

Now, adding and subtracting $k_j(\mathcal{A}^{12}u_y)_{i-1/2,j-1/2}$, we get from Bramble-Hilbert lemma

$$|\mathcal{A}_{i-1/2,j-1/2}^{12} \left(\int_{y_{j-1}}^{y_j} u_y(x_{i-1/2}, y) dy - k_j(u_y)(x_{i-1/2}, y_{j-1/2}) \right)| \leq C(h_i^2 + k_j^2) \left(\frac{k_j}{h_i}\right)^{1/2} |u_y|_{H^2(\hat{\Theta}_{i,j})} \quad (6.44)$$

Next we consider $S_{i,j}^{(1)}$ and derive the following estimate:

$$\begin{aligned} \left| \left(\int_{y_{j-1}}^{y_j} (\mathcal{A}^{12}u_y)(x_{i-1/2}, y) dy - k_j(\mathcal{A}^{12}u_y)_{i-1/2,j-1/2} \right) \right| &\leq C(h_i^2 + k_j^2) \left(\frac{k_j}{h_i}\right)^{1/2} |\mathcal{A}^{12}u_y|_{H^2(\hat{\Theta}_{i,j})} \\ &\leq C(h_i^2 + k_j^2) \left(\frac{k_j}{h_i}\right)^{1/2} \|u_y\|_{H^2(\hat{\Theta}_{i,j})}. \end{aligned}$$

Combining this bounds, it follows that

$$\begin{aligned} \left| \sum_{i,j} (B_{i,j}^{(1)} - S_{i,j}^{(1)}) (\Delta_x \bar{v}_{i,j} + \Delta_x \bar{v}_{i,j-1}) \right| &\leq \sum_{i,j} (h_i^2 + k_j^2) \left(\frac{k_j}{h_i}\right)^{\frac{1}{2}} \|u_y\|_{H^2(\hat{\Theta}_{i,j})} (\Delta_x v_{i,j} + \Delta_x v_{i,j-1}) \\ &\leq C \left(\sum_{\Delta \in \mathcal{T}_H} (\text{diam} \Delta)^4 \|u_y\|_{H^2(\Delta)}^2 \right)^{1/2} \|P_H v^H\|_1. \end{aligned}$$

We are now going to estimate $B_{i,j}^{(2)}$ and $S_{i,j}^{(2)}$. Starting from the of $S_{i,j}^{(2)}$, we obtain with the aid of Bramble-Hilbert lemma

$$\begin{aligned} |S_{i,j}^{(2)}| &= \frac{1}{2} \left| \left(\int_{y_{j-1/2}}^{y_j} - \int_{y_{j-1}}^{y_{j-1/2}} \right) ((\mathcal{A}^{12}u_y)(x_{i-1/2}, y) - (\mathcal{A}^{12}u_y)(x_{i+1/2}, y)) dy \right| \\ &\leq \frac{1}{2} \left| \int_{x_{i-1/2}}^{x_{i+1/2}} \left(\int_{y_{j-1/2}}^{y_j} - \int_{y_{j-1}}^{y_{j-1/2}} \right) (\mathcal{A}^{12}u_y)_x(x, y) dy dx \right| \\ &\leq C \left((h_{i+1} + k_j)(h_{i+1}k_j)^{\frac{1}{2}} |(\mathcal{A}^{12}u_y)_x|_{H^1(\hat{\Theta}_{i+1,j})} + (h_i + k_j)(h_i k_j)^{\frac{1}{2}} |(\mathcal{A}^{12}u_y)_x|_{H^1(\hat{\Theta}_{i,j})} \right). \end{aligned}$$

We use $|(\mathcal{A}^{12}u_y)_x|_1 \leq C\|u_y\|_2$ and derive

$$\left| \sum_{i,j} S_{i,j}^{(2)} \Delta_y \bar{v}_{i,j} \right| \leq C \left(\sum_{\Delta \in \mathcal{T}_H} (\text{diam} \Delta)^4 \|u_y\|_{H^2(\Delta)}^2 \right)^{1/2} \|P_H v^H\|_1. \quad (6.45)$$

Recalling the definition of $B_{i,j}^{(2)}$

$$\begin{aligned} |B_{i,j}^{(2)}| &= \frac{1}{8} \left| \int_{x_{i-1}}^{x_{i+1}} \int_{y_{j-1}}^{y_j} [(\mathcal{A}^{12}(x, y_j) - \mathcal{A}^{12}(x, y_{j-1}))u_y(x, y)]_x dy dx \right| \\ &\leq C \int_{x_{i-1}}^{x_{i+1}} \int_{y_{j-1}}^{y_j} k_j \|\mathcal{A}^{12}\|_{2,\infty} (|u_y(x, y)| + |u_{yx}(x, y)|) dy dx \\ &\leq C k_j (h_i k_j)^{1/2} \|u_y\|_{H^1(\hat{\Omega}_{i,j})} + k_j (h_{i+1} k_j)^{1/2} \|u_y\|_{H^1(\hat{\Omega}_{i+1,j})}. \end{aligned}$$

It follows that

$$\left| \sum_{i,j} B_{i,j}^{(2)} \Delta_y \bar{v}_{i,j} \right| \leq C \left(\sum_{\Delta \in \mathcal{T}_H} (\text{diam} \Delta)^4 \|u_y\|_{H^1(\Delta)}^2 \right)^{1/2} \|P_H v^H\|_1. \quad (6.46)$$

Then we have

$$\left| \sum_{ij} (B_{ij}^{(2)} - S_{ij}^{(2)}) \Delta_y v_{i,j} \right| \leq C \left(\sum_{\Delta \in \mathcal{T}_H} ((\text{diam} \Delta)^4 \|u_y\|_{H^2(\Delta)}^2) \right)^{1/2} \|P_H v^H\|_1 \quad (6.47)$$

and thus this lemma is proved. \square

Lemma 4. Let $u \in H^3(\bar{S})$, $p_x u, p_y u \in H^2(\bar{S})$ and the coefficients $\mathcal{A}^{ij} \in W_\infty^2$, for $i, j = 1, 2$. Then

$$\tau_H^{(d)}(v^H) := d(R_H u, v^H) - \sum_{i,j} \int_{\square_{i,j}} -((\mathcal{A} \nabla p)_1 u)_x - ((\mathcal{A} \nabla p)_2 u)_y dx dy \bar{v}_{i,j}, \quad (6.48)$$

satisfies the estimate

$$|\tau_H^{(d)}(v^H)| \leq C \left(\sum_{\Delta \in \mathcal{T}_H} (\text{diam} \Delta)^4 (\|p_x u\|_{H^2(\Delta)}^2 + \|p_y u\|_{H^2(\Delta)}^2) \right)^{1/2} \|P_H v^H\|_1, \quad (6.49)$$

for $v^H \in W_{H,0}$.

Proof. We concentrate on estimating the error of the discretization $((\mathcal{A} \nabla p)_1 u)_x = ((\mathcal{A}^{11} p_x + \mathcal{A}^{12} p_y)u)_x$. By a partial integration of a summation by parts we obtain

$$\tilde{d}_x = \sum_{i,j} \int_{\square_{i,j}} -(\mathcal{A} \nabla p)_1 u)_x dx dy \bar{v}_{i,j} = \sum_{i,j} \int_{I_j} ((\mathcal{A} \nabla p)_1 u)(x_{i-1/2}, y) dy \Delta_x \bar{v}_{i,j}$$

Next we want to evaluate

$$\begin{aligned} d_x(R_H u, v^H) &:= \frac{1}{2} (d_x^{(1)}(R_H u, v^H) + d_x^{(2)}(R_H u, v^H)) \\ &= -(\delta_x((\mathcal{A} D_H p)_1 R_H u), v^H)_H, \text{ for } v^H \in W_{H,0}. \end{aligned}$$

It is easy to see that

$$\begin{aligned} d_x(R_H u, v^H) &= - \sum_{i,j} h_{i+1/2} k_{j+1/2} \delta_x^{(1/2)} ((\mathcal{A} D_H p)_1 R_H u)_{i,j} \bar{v}_{i,j} \\ &= \sum_{i,j} k_{j+1/2} M_x ((\mathcal{A} D_H p)_1 R_H u)_{i,j} \Delta_x \bar{v}_{i,j} \\ &= \sum_{i,j} k_{j+1/2} M_x ((\mathcal{A}^{11} \delta_h p + \mathcal{A}^{12} \delta_k p) R_H u)_{i,j} \Delta_x \bar{v}_{i,j}, \end{aligned}$$

then

$$\begin{aligned} d_x(R_H u, v^H) - \tilde{d}_x(R_H u, v^H) &= \sum_{i,j} (|I_j| M_x((\mathcal{A}^{11} \delta_h p + \mathcal{A}^{12} \delta_k p) R_H u))_{i,j} \\ &\quad - \int_{I_j} ((\mathcal{A} \nabla p)_1 u)(x_{i-1/2}, y) dy \Delta_x \bar{v}_{i,j} \\ &:= B_1 + B_2. \end{aligned}$$

Starting with B_1 (B_2 is equivalent), we have

$$B_1 = \sum_{i,j} (|I_j| M_x(\mathcal{A}^{11} \delta_h p R_H u))_{i,j} - \int_{I_j} ((\mathcal{A}^{11} p_x R_H u)(x_{i-1/2}, y) dy) \Delta_x \bar{v}_{i,j} \quad (6.50)$$

Adding and subtracting $|I_j|(\mathcal{A}^{11} p_x R_H u)(x_{i-1/2}, y_j)$, we get

$$\begin{aligned} B_1 &= \sum_{i,j} |I_j| (M_x(\mathcal{A}^{11} \delta_h p R_H u))_{i,j} - (\mathcal{A}^{11} p_x R_H u)(x_{i-1/2}, y_j) \Delta_x \bar{v}_{i,j} \\ &\quad + \sum_{i,j} (|I_j| (\mathcal{A}^{11} p_x R_H u)(x_{i-1/2}, y_j) - \int_{I_j} ((\mathcal{A}^{11} p_x R_H u)(x_{i-1/2}, y) dy) \Delta_x \bar{v}_{i,j} \end{aligned}$$

The quantity

$$\sum_{i,j} (|I_j| (\mathcal{A}^{11} p_x R_H u)(x_{i-1/2}, y_j) - \int_{I_j} ((\mathcal{A}^{11} p_x R_H u)(x_{i-1/2}, y) dy) \Delta_x \bar{v}_{i,j},$$

as before, can be divided in $Q_1 + Q_2$, where we can estimate Q_1 with the aid of

$$\begin{aligned} F(u) &= \frac{k_j}{2} (((\mathcal{A}^{11} \nabla p)_1 u)(x_{i-1/2}, y_j) + ((\mathcal{A}^{11} \nabla p)_1 u)(x_{i-1/2}, y_{j-1})) \\ &\quad - \int_{y_{j-1}}^{y_j} ((\mathcal{A}^{11} \nabla p)_1 u)(x_{i-1/2}, y) dy, \end{aligned}$$

then from Bramble-Hilbert we get

$$|F(u)| \leq C \left(\frac{k_j}{h_i}\right)^{1/2} (h_i^2 + k_j^2) |\mathcal{A}^{11} p_x u|_{H^2(\hat{\sigma}_{i,j})}, \quad (6.51)$$

(Q_2 has a similar bound). Now we need to bound the quantity

$$\sum_{i,j} |I_j| (M_x(\mathcal{A}^{11} \delta_h p u))_{i,j} - (\mathcal{A}^{11} p_x u)(x_{i-1/2}, y_j) \Delta_x \bar{v}_{i,j}. \quad (6.52)$$

It is easy to see that

$$|M_x(\mathcal{A}^{11} p_x u)_{i,j} - (\mathcal{A}^{11} p_x u)(x_{i-1/2}, y_j)| \leq C \frac{h_i^2 + |I_j|^2}{(h_i |I_j|)^{1/2}} |\mathcal{A}^{11} p_x u|_{H^2(\bar{\sigma}_{i,j})},$$

then the remain quantity is

$$\sum_{i,j} |I_j| (M_x(\mathcal{A}^{11} \delta_h p u))_{i,j} - M_x(\mathcal{A}^{11} p_x u)_{i,j} \Delta_x \bar{v}_{i,j},$$

which can be bounded by

$$\begin{aligned} |M_x(\mathcal{A}^{11}\delta_h p u)_{i,j} - M_x(\mathcal{A}^{11}p_x u)_{i,j}| &\leq C \left(\frac{(h_{i-1} + h_i)^2 + |I_j|^2}{(h_{i-1/2}|I_j|)^{1/2}} |\mathcal{A}^{11}p_x u|_{H^2(\square_{i-1,j})} \right. \\ &\quad \left. + \frac{(h_{i+1} + h_i)^2 + |I_j|^2}{(h_{i+1/2}|I_j|)^{1/2}} |\mathcal{A}^{11}p_x u|_{H^2(\square_{i,j})} \right). \end{aligned}$$

□

Remark 6. The 1D the operator

$$\lambda(g) = \frac{\xi_i}{\xi_{i+1}} \left(g(1) - g\left(\frac{\xi_i}{\xi_i + \xi_{i+1}}\right) \right) + \frac{\xi_{i+1}}{\xi_i} \left(g\left(\frac{\xi_i}{\xi_i + \xi_{i+1}}\right) - g(0) \right) - g_\xi\left(\frac{\xi_i}{\xi_i + \xi_{i+1}}\right),$$

vanishes for $g = 1, \xi$ and $g = \xi^2$. Then, from Bramble-Hilbert lemma

$$|\delta_h g_i - g_x(x_i)| \leq C |g|_{H^3((0,1))}.$$

We can also rewrite λ as

$$\lambda(g_\xi) = \frac{\xi_i}{\xi_{i+1}} \left(\int_{\frac{\xi_i}{\xi_i + \xi_{i+1}}}^1 g_\xi d\xi \right) + \frac{\xi_{i+1}}{\xi_i} \left(\int_0^{\frac{\xi_i}{\xi_i + \xi_{i+1}}} g_\xi d\xi \right) - g_\xi\left(\frac{\xi_i}{\xi_i + \xi_{i+1}}\right),$$

which vanishes for $g_\xi = 1$ and $g_\xi = \xi$, then

$$|\delta_h g_i - g_x(x_i)| \leq C |g_\xi|_{H^2((0,1))}. \quad (6.53)$$

Lemma 5. Let $u \in H^3(\bar{S})$ and the coefficient $\gamma \in W_\infty^2$, for $i, j = 1, 2$. Then the part

$$\tau_H^{(u)}(v^H) := (R_H(\gamma u), v^H)_H - \sum_{i,j} \int_{\square_{i,j}} \gamma u(x, y) dx dy \bar{v}_{i,j}, \quad (6.54)$$

satisfies the estimate

$$|\tau_H^{(u)}(v^H)| \leq C \left(\sum_{\Delta \in \mathcal{T}_H} (\text{diam} \Delta)^4 \|u\|_{H^2(\Delta)}^2 \right)^{1/2} \|P_H v^H\|_1, \quad (6.55)$$

for $v^H \in W_{H,0}$.

Proof. We know that

$$\begin{aligned} \tau_H^{(u)}(v^H) &= \sum_{i,j} (h_{i+1/2} k_{j+1/2} (\gamma u)_{i,j} - \int_{\square_{i,j}} \gamma u(x, y) dx dy) \bar{v}_{i,j} \\ &= \sum_{i,j} \left(\frac{h_i}{2} k_{j+1/2} (\gamma u)_{i,j} \bar{v}_{i,j} + \frac{h_i}{2} k_{j+1/2} (\gamma u)_{i-1,j} \bar{v}_{i-1,j} \right) \\ &\quad - \sum_{i,j} \left(\int_{I_j} \int_{x_{i-1/2}}^{x_i} \gamma u(x, y) dx dy \bar{v}_{i,j} + \int_{I_j} \int_{x_{i-1}}^{x_{i-1/2}} \gamma u(x, y) dx dy \bar{v}_{i-1,j} \right) \\ &= \sum_{i,j} \left(h_i k_{j+1/2} M_x(\gamma u)_{i,j} \bar{v}_{i,j} - \frac{h_i}{2} k_{j+1/2} (\gamma u)_{i-1,j} \Delta_x \bar{v}_{i,j} \right) \\ &\quad - \sum_{i,j} \left(\int_{I_j} \int_{x_{i-1}}^{x_i} \gamma u(x, y) dx dy \bar{v}_{i,j} - \int_{I_j} \int_{x_{i-1}}^{x_{i-1/2}} \gamma u(x, y) dx dy \Delta_x \bar{v}_{i,j} \right) \\ &=: \sum_{i,j} S_{i,j}^1 \bar{v}_{i,j} + \sum_{i,j} S_{i,j}^2 \Delta_x \bar{v}_{i,j} \end{aligned}$$

With the aid of Bramble-Hilbert lemma, we can bound $S_{i,j}^1$ using

$$|M_x(\gamma u)_{i,j} - \frac{1}{h_i} \int_{x_{i-1}}^{x_i} \gamma u(x, y) dx| \leq Ch_i^{3/2} \left(\int_{x_{i-1}}^{x_i} |(\gamma u)_{xx}|^2 dx \right)^{1/2}.$$

Integrating over I_j we get

$$|S_{i,j}^1| \leq C \int_{I_j} h_i h_i^{3/2} \left(\int_{x_{i-1}}^{x_i} |(\gamma u)_{xx}|^2 dx \right)^{1/2} \leq C(h_i |I_j|)^{1/2} h_i^2 \|u\|_{H^2(\bar{\omega}_{i,j})},$$

then

$$\left| \sum_{i,j} S_{i,j}^1 \bar{v}_{i,j} \right| \leq C \left(\sum_{\Delta \in \mathcal{T}_H} (\text{diam} \Delta)^4 \|u\|_{H^2(\Delta)}^2 \right)^{1/2} \|P_H v^H\|_0. \quad (6.56)$$

Using Bramble-Hilbert again we have

$$|(\gamma u)_{i-1,j} - \frac{2}{h_i} \int_{x_{i-1}}^{x_{i-1/2}} \gamma u(x, y) dx| \leq Ch_i^{1/2} \left(\int_{x_{i-1}}^{x_i} |(\gamma u)_x|^2 dx \right)^{1/2}.$$

Integrating over I_j we get

$$|S_{i,j}^2| \leq C \int_{I_j} h_i h_i^{1/2} \left(\int_{x_{i-1}}^{x_i} |(\gamma u)_x|^2 dx \right)^{1/2} \leq C(h_i |I_j|)^{1/2} h_i \|u\|_{H^1(\bar{\omega}_{i,j})},$$

then

$$\left| \sum_{i,j} S_{i,j}^2 \Delta \bar{v}_{i,j} \right| \leq C \left(\sum_{\Delta \in \mathcal{T}_H} (\text{diam} \Delta)^4 \|u\|_{H^1(\Delta)}^2 \right)^{1/2} \|P_H v^H\|_1. \quad (6.57)$$

□

6.3 Numerical results

In this section we prove numerically that the method is convergent with second order when C, p stays in $H^3(\bar{S})$ using many examples.

We consider a uniform discretization in time of $[0, T]$ with N_T time steps of width $\Delta t = T/N_T$. Then for each $t_n = n\Delta t$ with $n = 1, \dots, N_T$ we measure the numerical errors $e_C^H(t_n) = R_H C(t_n) - C^H(t_n)$, $e_p^H(t_n) = R_H p(t_n) - p^H(t_n)$ of the numerical method (6.4) by using the following norms defined by the mesh H :

We illustrate the behavior of the errors

$$\|e_C\|_H = \max_{n=1, \dots, N_T} \sqrt{\|e_C^H(t_n)\|_H^2 + \sum_{j=1}^n \Delta t \|\nabla_{-H} e_C^H(t_j)\|_{H,-}^2}. \quad (6.58)$$

$$\|\nabla e_p\|_H = \max_{n=1, \dots, N_T} \sqrt{\|e_p^H(t_n)\|_H^2 + \|\nabla_{-H} e_p^H(t_j)\|_{H,-}^2}. \quad (6.59)$$

$$\|e_p\|_H = \max_{n=0, \dots, N_T} \|e_p^H(t_n)\|_H. \quad (6.60)$$

The rate of convergence is numerically obtained by the formula

$$Rate = \frac{\log\left(\frac{\|\cdot\|_H}{\|\cdot\|_{\tilde{H}}}\right)}{\log\left(\frac{H_{max}}{\tilde{H}_{max}}\right)}. \quad (6.61)$$

Let

$$\psi(x, y, t) = 4e^t \text{sen}(xy)(x-1)(y-1)(|2y-1|^{(1+\sigma)} + |2x-1|^{(1+\sigma)}) \quad (6.62)$$

defined in $S \times (0, T] = [0, 1]^2 \times (0, T]$ we observe that

- If $\sigma > 1.5$ then $\psi \in H^3(\bar{S})$;
- If $1.5 \geq \sigma > 0.5$ ($\sigma \neq 1$) then $\psi \in H^2(\bar{S})$;

To illustrate the convergence rate we introduce functions f_1, f_2 in (5.31), such that, the exact solution of problem (5.31) is given by

$$p(x, y, t) = C(x, y, t) = \psi(x, y, t). \quad (6.63)$$

In this first example, the exact solution matches with the assumption $p, C \in H^3$, then the $O(H_{max}^2)$ rate of convergence is expected.

Example 5. *Let*

$$\mathcal{A} = \begin{bmatrix} 1 + \text{sen}(\pi y)^2 & -\text{sen}(\pi x)\text{sen}(\pi y) \\ -\text{sen}(\pi x)\text{sen}(\pi y) & 1 + \text{sen}(\pi x)^2 \end{bmatrix}, \alpha = 1, \beta = -1, \sigma = 1.6, \quad (6.64)$$

with initial condition $C(x, y, 0) = p(x, y, 0) = 0$.

Note that we obtain, as expected, a second order of convergence in all the considered norms.

Table 7 – Numerical approximation p, C ($T = 0.01, dt = 5e - 04$) Example 5

H	$\ e_p\ _H$	Rate	$\ \nabla e_p\ _H$	Rate	$\ e_C\ _H$	Rate
5.0025e-02	8.7543e-04	-	4.6994e-03	-	3.1635e-04	-
4.1687e-02	6.0893e-04	1.9910	3.2763e-03	1.9785	2.2130e-04	1.9598
3.5762e-02	4.4755e-04	2.0085	2.4114e-03	1.9991	1.6335e-04	1.9805
3.1266e-02	3.4263e-04	1.9882	1.8478e-03	1.9815	1.2550e-04	1.9620
2.7798e-02	2.7085e-04	1.9998	1.4618e-03	1.9932	9.9370e-05	1.9856
2.5012e-02	2.1941e-04	1.9948	1.1849e-03	1.9892	8.0618e-05	1.9807
2.2750e-02	1.8137e-04	2.0083	9.7989e-04	2.0035	6.6701e-05	1.9990

In the next example we analyse what happens with the problem (5.31) when the solution is in H^2 and not in H^3

Example 6. Let

$$\mathcal{A} = \begin{bmatrix} 1 + \text{sen}(\pi y)^2 & -\text{sen}(\pi x)\text{sen}(\pi y) \\ -\text{sen}(\pi x)\text{sen}(\pi y) & 1 + \text{sen}(\pi x)^2 \end{bmatrix}, \alpha = 1, \beta = -1, \sigma = 0.51. \quad (6.65)$$

We obtain the errors and rate of convergence given in Table 8

Table 8 – Numerical approximation $p, C(T = 0.01, dt = 5e - 04)$ Example 6

H	$\ e_p\ _H$	Rate	$\ \nabla e_p\ _H$	Rate	$\ e_C\ _H$	Rate
2.7793e-02	1.7721e-04	-	1.9498e-03	-	2.1546e-04	-
2.5047e-02	1.4403e-04	1.9928	1.7161e-03	1.2275	1.9190e-04	1.1132
2.2772e-02	1.1915e-04	1.9914	1.5312e-03	1.1971	1.7293e-04	1.0929
2.0931e-02	1.0033e-04	2.0393	1.3840e-03	1.1993	1.5752e-04	1.1074
1.9290e-02	8.5821e-05	1.9128	1.2643e-03	1.1073	1.4475e-04	1.0349
1.7920e-02	7.4013e-05	2.0102	1.1609e-03	1.1592	1.3366e-04	1.0825
1.6687e-02	6.4466e-05	1.9365	1.0745e-03	1.0841	1.2430e-04	1.0186
1.5671e-02	5.6740e-05	2.0320	1.0004e-03	1.1374	1.1616e-04	1.0778

We observe that only the convergence rate associated to the L^2 norm $\|e_p\|_H$ continue to be of second order as expected for finite element method with linear piecewise basis, instead in other norms we lost the second order and we obtain the first order. The method is then not superconvergent for functions that not belong in H^3 . This is confirming that this class of functions is the largest possible space that permit to have a superconvergent method for our problem.

The next one give us an indication of convergence of $O(H^s)$ if $p, C \in H^{1+s}$ with $s \in (1/2, 2]$. One can see that it is achieved in (FERREIRA; BARBEIRO; GRIGORIEFF, 2005). Decreasing σ we show the convergence rate decay for p, C belonging in a less regular space.

Example 7. In this case p, C are not in $H^2(\bar{S})$.

$$\mathcal{A} = \begin{bmatrix} 1 + \text{sen}(\pi y)^2 & -\text{sen}(\pi x)\text{sen}(\pi y) \\ -\text{sen}(\pi x)\text{sen}(\pi y) & 1 + \text{sen}(\pi x)^2 \end{bmatrix}, \alpha = 1, \beta = -1, \sigma = 0.3. \quad (6.66)$$

Table 9 – Numerical approximation $p, C(T = 0.01, dt = 5e - 04)$ Example 7

H	$\ e_p\ _H$	Rate	$\ \nabla e_p\ _H$	Rate	$\ e_C\ _H$	Rate
2.5107e-02	1.3781e-04	-	2.2619e-03	-	2.7196e-04	-
2.2739e-02	1.1414e-04	1.9020	2.0521e-03	0.9828	2.4841e-04	0.9143
2.0843e-02	9.6692e-05	1.9062	1.8876e-03	0.9599	2.2947e-04	0.9115
1.9240e-02	8.2606e-05	1.9671	1.7446e-03	0.9841	2.1301e-04	0.9297
1.7910e-02	7.1992e-05	1.9204	1.6298e-03	0.9501	1.9944e-04	0.9190
1.6675e-02	6.2461e-05	1.9870	1.5227e-03	0.9511	1.8697e-04	0.9032
1.5650e-02	5.5360e-05	1.9029	1.4341e-03	0.9456	1.7641e-04	0.9167

These error estimates allow us to conclude that the method studied leads to $O(H^s)$ for the pressure and density as expected for $s \in (1/2, 2]$.

7 Supraconvergent multiscale scheme

The main idea of this Chapter is to show how we can use the supraconvergent finite difference method of Chapter 5 (or equivalently the finite element method of Chapter 6) to get an approximation for the homogenized solution of system (3.78) and also for the multiscale solution of the systems (2.21). The method is here presented only for solving the problems (3.78) and (2.21) in a one dimensional domain. However a simple method extension can be implemented to solve also two-dimensional multiscale and homogenized problems. The proposed scheme is based on approximating the homogenized solution obtained by supposing that the solutions C, p satisfies an asymptotic expansion in the micro dimension ε . Basically, we solve the microproblem (3.24) to provide an approximation at the macro-scale with mesh sizes H_i for the homogenized tensor and then we obtain with the method of Chapter 5 the approximated homogenized solution $u^{0,H}$ and then through a reconstructed $u^{0,H} + \varepsilon u^{1,H}$ we can approximate the multiscale solution. Here $u^{0,H}$ is the numerical homogenized solution and $u^{1,H}$ approximates the spatial derivatives of $u^{0,H}$ and depends on the cell microproblem in the periodically distributed domain Y . One can see more details about homogenization in Chapter 3 and Appendix B.4.

The homogenization for multiscale systems as (2.21) has been discussed in Chapter 3 and further details on the homogenization of PDE systems are presented in Appendix B.4. In fact despite we proved in Chapter 6 a second order using a norm in $L^2([0, T], H^1(\bar{S}))$ when Dirichlet conditions were used here we prove that when we use micro cell problems with a Y -periodic conditions the discussed process to build the homogenized numerical solution and multiscale solution is also a second order method using a macroscale norm in $L^2([0, T], H^1(\bar{S}))$ and a microscale norm in $L^2([0, T], H^1(\bar{S}))$.

The second order in $L^2([0, T], H^1(\bar{S}))$ proved for single-scale problems in Chapter 5 and 6 is thus conserved also for solving multiscale problems (2.21) with proposed multiscale strategy proposed in this Chapter.

7.1 Cell problem

The periodicity of the micro-problem in the multiscale problem is a good feature for numerical multiscale methods since we can solve the microproblem once in a reference domain Y and then its solution can be replicated periodically in the macroscale domain Ω . In this section we approximate the solution χ in the reference domain $Y = [0, 1]$ of the

cell problem that is

$$\begin{cases} -\frac{\partial}{\partial y}(\mathcal{K}(y)\frac{\partial \chi}{\partial y}) = -\frac{\partial \mathcal{K}}{\partial y}(y) & \text{in } Y \\ \chi(y) \text{ } Y\text{-periodic,} \\ \langle \chi \rangle = 0. \end{cases} \quad (7.1)$$

We remember that a function v is called Y -periodic if and only if

$$v(y + k|Y|) = v(y) \quad \forall y \in Y \forall k \in \mathbb{Z}. \quad (7.2)$$

Let $\mathbf{h} = (h_i)_{i=0,\dots,N+1}$ with $h_0 = h_{N+1}$ be the sequence nonuniform mesh sizes with a maximum $h_{max} = \max\{h_i | i = 0, \dots, N\}$. We define by \bar{Y}_h the discrete mesh in $Y = [0, 1]$,

$$\bar{Y}_h = \{\{y_i\}_{i=0}^N | y_i = y_{i-1} + h_i, y_0 = 0, y_N = 1\}$$

As before, we introduce the following sets

$$\partial Y_h = \{y_i, i = 0, N\}, Y_h = \bar{Y}_h / \partial Y_h.$$

By $W_{per}^h(Y)$ we denote the space of Y -periodic grid functions v^h on \bar{Y}_h and $W_{per,0}^h(Y)$ the subspace of Y -periodic grid functions with “zero mean”. For $y_i \in \bar{Y}_h$ let $I_i := (y_{i-1/2}, y_{i+1/2}) \cap Y$ and $|I_i| = h_{i+1/2} = \frac{h_i + h_{i+1}}{2}$.

In $W_{per}^h(Y)$ we introduce the inner products

$$\begin{aligned} (v^h, w^h)_h &:= \sum_{y_i \in \bar{Y}_h} |I_i| v_i \bar{w}_i \\ (v^h, w^h)_{h,-} &:= \sum_{i=1}^N h_i v_i \bar{w}_i \end{aligned}$$

and the associated norms $\|v^h\|_h = \sqrt{(v^h, v^h)_h}$ and $\|v^h\|_{h,-} = \sqrt{(v^h, v^h)_{h,-}}$

The discrete problem has the form: find $\chi^h \in W_{per,0}^h$ such that

$$a_{\mathcal{K},h}(\chi^h, v^h) = -\left(\left(\frac{\partial \mathcal{K}}{\partial y}\right)_h, v^h\right)_h. \quad (7.3)$$

for $v^h \in W_{per,0}^h(Y)$ and $a_{\mathcal{K},h}(v^h, w^h) = -(\delta_y^{(1/2)}(\mathcal{K}\delta_y^{(1/2)}v^h), w^h)_h$ (see Chapter 6 and 7.1.1).

7.1.1 The finite difference scheme

The discretized variational problem (7.3) is equivalent to a standard FDM for (7.1) on a nonuniform grid, which we will derive in this section. To formulate, as in

Chapter 5, the finite difference method in nonuniform meshes we use the following finite difference operators

$$\delta_y^{(1/2)}v_i = \frac{v_{i+1/2} - v_{i-1/2}}{y_{i+1/2} - y_{i-1/2}}, \quad \delta_y^{(1/2)}v_{i+1/2} = D_{-y}v_i = \frac{v_{i+1} - v_i}{y_{i+1} - y_i}. \quad (7.4)$$

Then denoted by

$$\mathcal{L}_{\mathcal{K}}(u^h) := -\delta_y^{(1/2)}(\mathcal{K}\delta_y^{(1/2)}(u^h)) \quad (7.5)$$

the finite difference method used to solve the cell problem (7.1) is find $\chi^h \in W_{per,0}^h$ such that:

$$\mathcal{L}_{\mathcal{K}}(\chi^h) = \left(\frac{\partial \mathcal{K}}{\partial y} \right)_h \quad (7.6)$$

where $\left(\frac{\partial \mathcal{K}}{\partial y} \right)_h = \left\{ \frac{1}{|I_i|} \int_{I_i} \frac{\partial \mathcal{K}}{\partial y} \right\}_i$ is a local approximation for $\frac{\partial \mathcal{K}}{\partial y}$ on the nodes y_i .

7.1.2 Equivalent FE method for the cell problem 7.1

As in Chapter 6 we are able to show here the equivalence of the FD scheme to a FE method. Let $\mathcal{T}_h = \bigcup_{i=1}^N \Delta_i$ a partition of Y using the set \bar{Y}_h as extremes of each subinterval Δ . We define by $K_{\Delta,y}$ the value of \mathcal{K} in the midpoint of Δ . Note that we use this notations in order to be easy to extend the problem in two dimensions.

We define the following discrete operator : $\forall v^h, w^h \in W_{per}^h(Y)$

$$a(v^h, w^h) = \sum_{\Delta \in \mathcal{T}_h} K_{\Delta,y} \int_{\Delta} (P_h v^h)_y (P_h w^h)_y \, dy. \quad (7.7)$$

Thus we can get an approximation of the solution χ of the cell problem through the variational problem: find $\chi^h \in W_{per,0}^h$ such that

$$a(\chi^h, v^h) = -\left(\left(\frac{\partial \mathcal{K}}{\partial y} \right)_h, v^h \right)_h \forall v^h \in W_{per,0}^h \quad (7.8)$$

The next proposition show the equivalence of (7.6) and (7.8)

Proposition 9. For all $v^h, w^h \in W_{per}^h(Y)$ and $\mathcal{K}(y)$ Y -periodic, we have

$$-\left(\delta_y^{(1/2)}(\mathcal{K}\delta_y^{(1/2)}v^h), w^h \right)_h = \sum_{i=1}^N h_i K_{i-1/2} \delta_y^{(1/2)}v_{i-1/2} \delta_y^{(1/2)}\bar{w}_{i-1/2}. \quad (7.9)$$

Proof. Since $\mathcal{K}_{N+1/2}\delta_y^{(1/2)}v_{N+1/2}\bar{w}_N = \mathcal{K}_{1/2}\delta_y^{(1/2)}v_1\bar{w}_0$ for periodicity we have

$$-(\delta_y^{(1/2)}(\mathcal{K}\delta_y^{(1/2)}v^h), w^h)_h = -\sum_{i=1}^N |I_i| \delta_y^{(1/2)}(\mathcal{K}\delta_y^{(1/2)}v)_i \bar{w}_i \quad (7.10)$$

$$= -\sum_{i=1}^N (\mathcal{K}_{i+1/2}\delta_y^{(1/2)}v_{i+1/2} - \mathcal{K}_{i-1/2}\delta_y^{(1/2)}v_{i-1/2}) \bar{w}_i \quad (7.11)$$

$$= \sum_{i=1}^N h_i \mathcal{K}_{i-1/2} \delta_y^{(1/2)}v_{i-1/2} \delta_y^{(1/2)}\bar{w}_{i-1/2}. \quad (7.12)$$

□

Now we can prove using Proposition 6 and Lemma 2 in Chapter 6 that the finite difference method (7.6) is of second order of consistency, that is its truncation error decays of order two. In order to help the reader we rewrite in the following the Lemma 2 of Chapter 6 for our cell problem in one dimension.

Lemma 6. *Let $u \in H_{per}^3(Y)$ and the coefficient $\mathcal{K} \in W_{per}^{2,\infty}(Y)$. Then the part*

$$\tau_h^{(a)}(v^h) := a(R_h u, v^h) - \sum_{y_i \in Y_h} \int_{I_i} (-\mathcal{K}u_y)_y \, dy \bar{v}_i. \quad (7.13)$$

satisfies the estimate

$$|\tau_h^{(a)}(v^h)| \leq C \left(\sum_{\Delta \in \mathcal{T}_h} (\text{diam} \Delta)^4 \|u_y\|_{H^2(\Delta)}^2 \right) \|P_h v^h\|_1, \text{ for } v^h \in W_{per,0}^h(Y),$$

where R_h is the restriction operator.

7.2 Approximating the homogenized coefficient

By $mean_Y(\cdot)$ we denote a discrete mean operator in $W_{per}^h(Y)$ that approximate the arithmetic mean over Y defined by

$$\langle v \rangle = \frac{1}{|Y|} \int_Y v \, dy, \quad (7.14)$$

for instance, we use Midpoint rule to construct $mean_Y(\cdot)$.

Proposition 10. *For all $v^h \in W_{per}^h(Y)$ we have*

$$\|v^h - mean_Y(v^h)\|_h \leq C \|\nabla_{-y} v^h\|_{h,-},$$

where C depends on \bar{Y}_h .

Proof. Firstly,

$$\begin{aligned} v_i &= \sum_{j=1}^i (v_j - v_{j-1}) + v_0 = \sum_{j=1}^i (h_i \nabla_{-y} v_j) + v_0, \\ \text{mean}_Y(v^h) &= \frac{1}{|Y|} \sum_{i=1}^N |I_i| v_i = \frac{1}{|Y|} \sum_{i=1}^N |I_i| \left(\sum_{j=1}^i (h_i \nabla_{-y} v_j) + v_0 \right) \\ &= \frac{1}{|Y|} \sum_{i=1}^N |I_i| \left(\sum_{j=1}^i h_j \nabla_{-y} v_j \right) + v_0 \end{aligned}$$

then using that $\forall a, b \in \mathbb{R} \quad (a + b)^2 \leq a^2 + b^2$ and that $\forall a_j \in \mathbb{R} \quad \left(\sum_{j=1}^i a_j \right)^2 \leq i \sum_{j=1}^i a_j^2$

$$\begin{aligned} \|v^h - \text{mean}_Y(v^h)\|_h^2 &= \sum_{i=1}^N |I_i| (v_i - \text{mean}_Y(v^h))^2 \\ &= \sum_{i=1}^N |I_i| \left(\sum_{j=1}^i h_j \nabla_{-y} v_j - \frac{1}{|Y|} \sum_{k=1}^N |I_k| \left(\sum_{l=1}^k h_l \nabla_{-y} v^h(y_k) \right) \right)^2 \\ &\leq 2 \left(\sum_{i=1}^N |I_i| (i h_{\max} \sum_{j=1}^i h_j (\nabla_{-y} v_j)^2 + \frac{N}{|Y|^2} \sum_{k=1}^N |I_k|^2 k \sum_{l=1}^k h_l^2 (\nabla_{-y} v_k)^2) \right) \\ &\leq 2C(Y) (\|D_{-y} v^h\|_{h,-}^2 + \|D_{-y} v^h\|_{h,-}^2) \\ &\leq C(Y) \|\nabla_{-y} v^h\|_{h,-}^2 \end{aligned}$$

Corollary 4. *The Poincaré inequality holds for $v^h \in W_{\text{per}}^h(Y)$ if $v_0 = 0$ or $\text{mean}_Y(v^h) = 0$.*

□

We can use the approximated solution χ^h of the cell problem solution χ , obtained by the finite difference method 7.6 with $\text{mean}_Y(\chi^h) = 0$ that is such that

$$\begin{cases} -\mathcal{L}\mathcal{K}(\chi^h) = -\left(\frac{\partial \mathcal{K}}{\partial y}\right)_h & \text{in } \bar{Y}_h \\ \chi^h \text{ is } Y\text{-periodic} \\ \text{mean}_Y(\chi^h) = 0. \end{cases} \quad (7.15)$$

to build an approximation of the homogenized coefficient

$$q = \frac{1}{|Y|} \int_Y (\mathcal{K} - \mathcal{K} \frac{\partial \chi}{\partial y} dy). \quad (7.16)$$

The approximated homogenized coefficient q^h used is given by

$$q^h = \text{mean}_Y(R_h \mathcal{K} - R_h \mathcal{K} \nabla_{-y} \chi^h). \quad (7.17)$$

Note that the right hand-side of (7.15) is not available in general, but it can be replaced by the discrete derivative of \mathcal{K} without loss of convergence.

Proposition 11. q^h approximates the homogenized coefficient with a second order consistency, that is

$$|q - q^h| \leq Ch_{max}^2.$$

Proof. Since for hypothesis $h_{N+1} := h_1$ then for the Y -periodicity of $\mathcal{K} - \mathcal{K} \frac{\partial \chi}{\partial y}$ we have that its integral in $[y_N, y_{N+1/2}]$ is equal to that in $[y_0, y_{1/2}]$. Thus we obtain

$$q = \frac{1}{|Y|} \int_Y (\mathcal{K} - \mathcal{K} \frac{\partial \chi}{\partial y}) dy = \frac{1}{|Y|} \sum_{i=1}^N \int_{I_i} (\mathcal{K} - \mathcal{K} \frac{\partial \chi}{\partial y}) dy. \quad (7.18)$$

From Bramble-Hilbert Lemma

$$|\sum_{i=1}^N \int_{I_i} (f dy - |I_i| f_i)| \leq C \left(\sum_{\Delta \in \mathcal{T}_H} (\text{diam} \Delta)^4 \|f\|_{H^2(\Delta)}^2 \right)^{1/2}, \quad (7.19)$$

then if $\chi \in H_{per}^3(Y)$

$$|q - q^h| \leq |\text{mean}_Y(R_h \mathcal{K} (\frac{\partial \chi}{\partial y} - \nabla_{-y} \chi^h))| + Ch_{max}^2 \quad (7.20)$$

$$\leq \|\mathcal{K}\|_{\infty} |\text{mean}_Y(R_h \frac{\partial \chi}{\partial y} - \nabla_{-y} R_h \chi + \nabla_{-y} R_h \chi - \nabla_{-y} \chi^h)| + Ch_{max}^2. \quad (7.21)$$

From Bramble-Hilbert Lemma

$$|\sum_{i=1}^N |I_i| (\frac{\partial \chi(y_i)}{\partial y} - \nabla_{-y} \chi_i)| \leq C \left(\sum_{\Delta \in \mathcal{T}_H} (\text{diam} \Delta)^4 \|\chi\|_{H^2(\Delta)}^2 \right)^{1/2}, \quad (7.22)$$

then we obtain

$$|q - q^h| \leq \|\mathcal{K}\|_{\infty} |\text{mean}_Y(\nabla_{-y} R_h \chi - \nabla_{-y} \chi^h)| + Ch_{max}^2 \quad (7.23)$$

$$\leq Ch_{max}^2, \quad (7.24)$$

where C depends on \mathcal{K} and χ . □

We verify now with two examples that effectively our approximated homogenized coefficient is second order accurate.

Example 8. Taking

$$\mathcal{K}(y) = \frac{1}{2 + \cos(2\pi y)},$$

we have that $q = \frac{1}{2}$.

Using formula (7.17) we build varying the non uniform mesh the value q^h that has shown in the Table 10 it converges to q with order two when h_{max} tends to zero.

Table 10 – Numerical approximation for homogenized coefficient

h_{max}	q^h	$ q - q^h $	Rate
2.5051e-01	5.243247e-01	2.4325e-02	-
1.2514e-01	5.058797e-01	5.8797e-03	2.0460
6.2555e-02	5.014967e-01	1.4967e-03	1.9732
3.1278e-02	5.003722e-01	3.7217e-04	2.0078
1.5640e-02	5.000931e-01	9.3094e-05	1.9994
7.8200e-03	5.000235e-01	2.3523e-05	1.9846
3.9596e-03	5.000060e-01	5.9780e-06	2.0129
1.9551e-03	5.000015e-01	1.4860e-06	1.9725
9.7754e-04	5.000004e-01	3.6813e-07	2.0131
4.8877e-04	5.000001e-01	9.8083e-08	1.9081
2.4438e-04	5.000000e-01	2.3477e-08	2.0628
1.2219e-04	5.000000e-01	5.6048e-09	2.0665

Example 9. Taking

$$\mathcal{K}(y) = \frac{2 + |2x - 1|^{2.1}}{2 + \cos(2\pi y)},$$

we have that $q = 1.1930597352384201837$.

The associated numerical results are shown in Table 11, showing a gain a second order of convergence of q^h to the homogenized coefficient q .

Table 11 – Numerical approximation for homogenized coefficient

h_{max}	q^h	$ q - q^h $	Rate
2.5017e-01	1.244211e+00	5.1151e-02	-
1.2510e-01	1.205424e+00	1.2364e-02	2.0491
6.2565e-02	1.196208e+00	3.1479e-03	1.9743
3.1314e-02	1.193846e+00	7.8638e-04	2.0040
1.5640e-02	1.193257e+00	1.9708e-04	1.9933
7.8202e-03	1.193108e+00	4.8481e-05	2.0234
3.9440e-03	1.193072e+00	1.2534e-05	1.9761
1.9955e-03	1.193063e+00	3.1958e-06	2.0060
9.7754e-04	1.193060e+00	7.5597e-07	2.0201
4.9948e-04	1.193060e+00	1.8905e-07	2.0641
2.6163e-04	1.193060e+00	4.9999e-08	2.0569
1.2219e-04	1.193060e+00	1.0459e-08	2.0550

7.3 Approximating the solution of multiscale elliptic problems

In this section we propose a numerical method to approximate the solution of the multiscale one dimensional elliptic equation

$$\begin{cases} -\frac{\partial}{\partial x} \left(\mathcal{K}^\varepsilon \frac{\partial u^\varepsilon}{\partial x} \right) = f^\varepsilon & \text{in } \Omega \\ u|_\Omega = 0 \end{cases} \quad (7.25)$$

associated to a multiscale tensor (coefficient) \mathcal{K}^ε and multiscale function f^ε . This equation is a simpler case of the multiscale pressure equation analyzed and determined in Chapter 3 in a two dimensional colon domain.

An important feature of the proposed multiscale method is to approximate u^ε starting by approximating the solution u^0 of the associated homogenized problem

$$\begin{cases} -\frac{\partial}{\partial x} \left(q \frac{\partial u^0}{\partial x} \right) = \int_Y f^0(x, y) dy & \text{in } \Omega \\ u^0|_\Omega = 0 \end{cases} \quad (7.26)$$

with the homogenized coefficient $q = \frac{1}{|Y|} \int_Y (\mathcal{K} - \mathcal{K} \frac{\partial \chi}{\partial y} dy)$ given in the previous section 7.2.

The approximation $u^{0,H}$ of u^0 is obtained by the high order method finite difference method

$$\begin{cases} \mathcal{L}_{q^h} u^{0,H} = \text{mean}_Y(f^0) & \text{in } \Omega_H \\ u^{0,H}|_{\partial\Omega_H} = 0 \end{cases}, \quad (7.27)$$

where as usual

$$\mathcal{L}_{q^h}(u^{0,H}) = -\delta_x^{1/2}(q^h \delta_x^{(1/2)} u^{0,H}), \quad (7.28)$$

f^0 is the ε^0 component of the asymptotic expansion of f^ε and q^h is the approximated homogenization coefficient given by (7.16).

In (7.27) Ω_H is a one dimensional mesh in $\Omega \subset \mathbb{R}$ that is given by the macroscale non uniform mesh sizes $H = \{H_i\}_{i=1,\dots,M}$ with a maximum mesh size H_{max} that is given

$$\bar{\Omega}_H = \{x_i \in \Omega | x_i = x_{i-1} + H_i, i = 1, \dots, M\},$$

$$\partial\Omega_H = \{x_0, x_M\}, \quad \Omega_H = \bar{\Omega}_H / \partial\Omega_H.$$

Proposition 12. *Let $e^{0,H} = R_H u^0 - u^{0,H}$ with u^0 , $u^{0,H}$ solution of (7.26) and (7.27) respectively then the following convergence result is valid*

$$\|\nabla_{-x} e^{0,H}\|_{H,-}^2 \leq C(H_{max}^4 + h_{max}^4), \quad (7.29)$$

since $|q - q^h| \leq Ch_{max}^2$ and $|\langle f^0 \rangle - \text{mean}_Y(f^0)| \leq Ch_{max}^2$.

Proof. We have that $u^{0,H}$ verifies the following equation

$$\mathcal{L}_{q^h} u^{0,H} = \text{mean}_Y(f^0). \quad (7.30)$$

Furthermore $R_H u^0$ verifies the same equation with addition of an $O(H_{max}^2)$ term

$$\mathcal{L}_q R_H u^0 = \langle f^0 \rangle + O(H_{max}^2). \quad (7.31)$$

Subtracting both (7.30) and (7.31) and multiplying by $e^{0,H}$ we get

$$\begin{aligned} (-\delta_x^{1/2}(q\delta_x^{(1/2)} R_H u^0) + \delta_x^{1/2}(q^h \delta_x^{(1/2)} u^{0,H}), e^{0,H})_H &= (O(h_{max}^2) + O(H_{max}^2), e^{0,H})_H, \\ (qD_{-x} R_H u^0 - q^h D_{-x} u^{0,H}, D_{-x} e^{0,H})_H &= \\ (q^h D_{-x} e^{0,H} + (q - q^h) D_{-x} R_H u^0, D_{-x} e^{0,H})_H &= \end{aligned}$$

then using that q^h is constant with respect to H and the discrete Poincaré inequality

$$\begin{aligned} q^h \|\nabla_{-x} e^{0,H}\|_{H,-}^2 &\leq ((q^h - q) D_{-x} R_H u^0, D_{-x} e^{0,H})_H + O(h_{max}^4) + O(H_{max}^4) \\ &+ C \|\nabla_{-x} e^{0,H}\|_{H,-}^2 \\ &\leq O(h_{max}^4) \|\nabla_{-x} u^0\|_{H,-}^2 + \|\nabla_{-x} e^{0,H}\|_{H,-}^2 \\ &+ O(h_{max}^4) + O(H_{max}^4) + C \|\nabla_{-x} e^{0,H}\|_{H,-}^2 \end{aligned}$$

We obtain that if $(q^h - C) > 0$,

$$\|\nabla_{-x} e^{0,H}\|_{H,-}^2 \leq C(h_{max}^4 + H_{max}^4) \quad (7.32)$$

□

In the next example, we test numerically the validity of the convergence result in Proposition 12.

Example 10. *Using the parameters*

$$\mathcal{K}(y) = \frac{1}{2 + \cos(2\pi y)}, f^\varepsilon(x, y) = \cos(2\pi x),$$

and solving the numerical homogenized associated problem (7.27) we get the numerical results of Table 12.

In Table 12 we note a second order of convergence with respect H . This is obtained since we used a sufficient small micro-scale mesh size h .

Table 12 – Numerical errors

H_{max}	$\ e_0^H\ _H$	Rate	$\ \nabla_{-x}e_0^H\ _{H,-}$	Rate
2.5032e-01	8.3717e-03	-	4.7358e-02	-
1.2517e-01	1.9029e-03	2.1375e+00	1.1651e-02	2.0233e+00
6.2562e-02	4.6355e-04	2.0364e+00	2.8940e-03	2.0083e+00
3.1278e-02	1.1531e-04	2.0069e+00	7.2339e-04	1.9999e+00
1.5639e-02	2.8768e-05	2.0031e+00	1.8069e-04	2.0013e+00
7.8774e-03	7.1965e-06	2.0205e+00	4.5213e-05	2.0201e+00
3.9200e-03	1.7974e-06	1.9877e+00	1.1294e-05	1.9876e+00
1.9551e-03	4.4842e-07	1.9958e+00	2.8176e-06	1.9957e+00
1.0005e-03	1.1119e-07	2.0815e+00	6.9865e-07	2.0815e+00
4.9633e-04	2.7121e-08	2.0128e+00	1.7041e-07	2.0128e+00

Numerical error in approximating on nonuniform meshes the homogenized solution of (7.26) by using the method (7.27) varying in H_{max} and fixing $h = 5e - 03$.

In the next Table 13 we do the opposite in the sense that we fix H and vary h_{max} .

Table 13 – Numerical errors

h_{max}	$\ e_0^H\ _H$	Rate	$\ \nabla_{-x}e_0^H\ _{H,-}$	Rate
2.5014e-01	1.6683e-03	-	1.0483e-02	-
1.2512e-01	4.1596e-04	2.0051e+00	2.6136e-03	2.0051e+00
6.2557e-02	1.0618e-04	1.9698e+00	6.6719e-04	1.9698e+00
3.1281e-02	2.6624e-05	1.9960e+00	1.6729e-04	1.9960e+00
1.5641e-02	6.6140e-06	2.0092e+00	4.1557e-05	2.0092e+00
7.8829e-03	1.6900e-06	1.9914e+00	1.0619e-05	1.9914e+00
3.9101e-03	4.2508e-07	1.9686e+00	2.6709e-06	1.9686e+00
1.9551e-03	1.0575e-07	2.0070e+00	6.6448e-07	2.0070e+00
9.8381e-04	2.5197e-08	2.0886e+00	1.5832e-07	2.0886e+00
4.8877e-04	5.6460e-09	2.1383e+00	3.5475e-08	2.1383e+00

Numerical error in approximating on nonuniform meshes the homogenized solution of (7.26) by using the method (7.27) varying in h_{max} and fixing $H = 1e - 04$.

Now, we are able to construct an approximation for the multiscale solution by distributing the domain of reference Y periodically in Ω . The numerical multiscale solution is built by using the following formula

$$u_\varepsilon^H = u^{0,H} - \varepsilon \chi^H \nabla_{-x} u^{0,H}, \quad (7.33)$$

where χ^H is the macroscale function obtained by linear interpolating χ^h in the Ω_H nodes. This interpolation is obtained after by distributing periodically Y in Ω_H . Note that a such multiscale numerical solution approximate the first two terms of the ε asymptotic expansion of $u^\varepsilon = u^0 + \varepsilon u^1 + \dots$

One can find a post-processing scheme similar to (7.33) in (ABDULLE, 2009) that satisfies the following error estimate

$$\|u^\varepsilon - u_{p,\varepsilon}\|_{\bar{H}^1(\Omega)} \leq C(H + \frac{h}{\varepsilon} + \sqrt{\varepsilon}). \quad (7.34)$$

In (ABDULLE, 2009) they use the numerical homogenized solution provided by the HMM-FEM method in place of $u^{0,H}$. That is done by extending the small scale solution locally on the macro element K .

We assert that our multiscale approximation (7.33) satisfies

$$\begin{aligned} \|\nabla_{-x} e_\varepsilon^H\|_{H,-} &\leq C(H^2 + h^2 + \varepsilon + f_1(H, h, \varepsilon)) \\ \|e_\varepsilon^H\|_H &\leq C(H^2 + h^2 + \varepsilon^2 + f_2(H, h, \varepsilon)) \end{aligned} \quad (7.35)$$

where $e_\varepsilon^H = R_H u^\varepsilon - u_\varepsilon^H$. Despite we are not able to prove the convergence result in (7.35), we can obtain numerically a second order for H and h and a first order for ε on non uniform meshes as shown in the next Examples.

Example 11. Taking in (7.25)

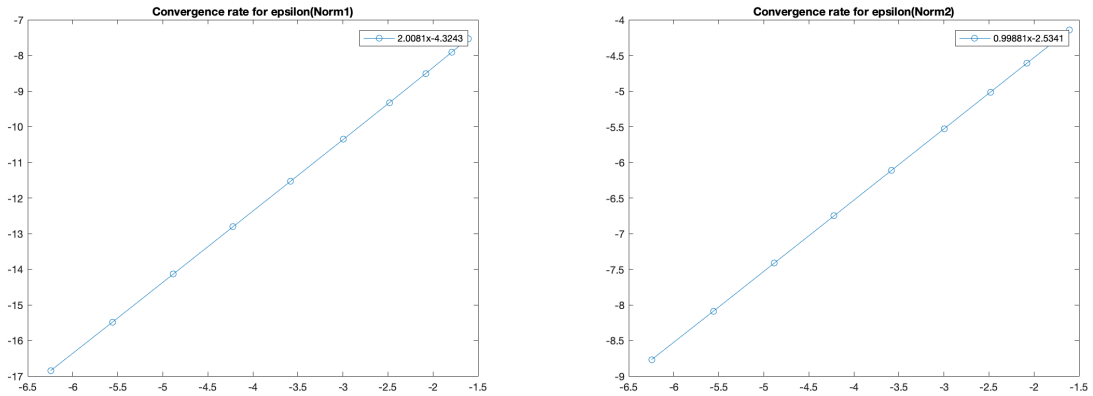
$$\mathcal{K}(y) = \frac{1}{2 + \cos(2\pi y)}, f^\varepsilon = \sin(2\pi x), \quad (7.36)$$

we obtain, varying ε and h , the approximation errors shown in Tables 14 and 15, respectively.

As we can see, in Table 14 and associated plots we have a first order of convergence in the $\|\cdot\|_{H,-}$ norm with respect to ε .

Table 14 – Convergence rate for $\varepsilon(H = h = 1e - 04)$

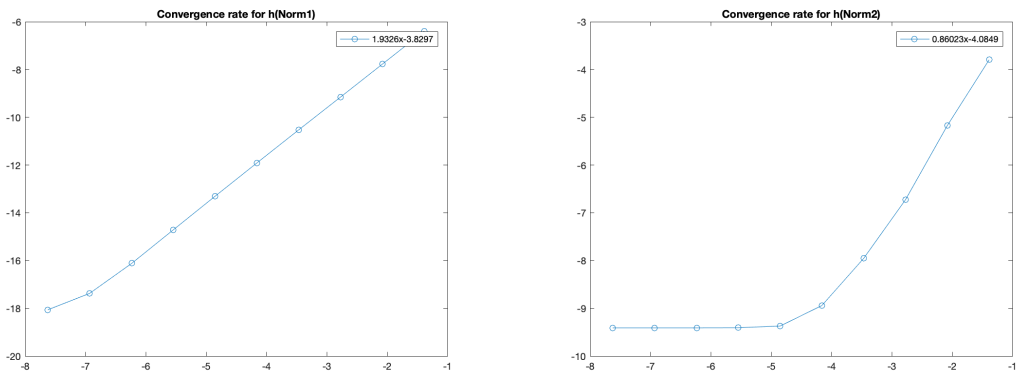
ε	$\ e_\varepsilon^H\ _H$	Rate	$\ \nabla_{-x} e_\varepsilon^H\ _{H,-}$	Rate
2.0000e-01	5.3816e-04	-	1.5916e-02	-
1.6667e-01	3.6685e-04	2.10	1.3263e-02	1.00
1.2500e-01	2.0259e-04	2.06	9.9472e-03	1.00
8.3333e-02	8.8875e-05	2.03	6.6315e-03	0.99
5.0000e-02	3.1782e-05	2.01	3.9789e-03	0.99
2.7778e-02	9.7844e-06	2.00	2.2106e-03	0.99
1.4706e-02	2.7405e-06	2.00	1.1704e-03	0.99

Figure 19 – Convergence for ε .

In the next we choose a quite large ε to see how it affects the errors. Note that in Table and Figure 15 the error in $\|\cdot\|_{H,-}$ norm decreases up to reach a lower limit. We think that this happens due to presence of a term f_1 in (7.35) that depends on ε , H and h .

Table 15 – Convergence rate for $h(H = 1e - 04, \varepsilon = 1e - 03)$

h_{max}	$\ e_\varepsilon^H\ _H$	Rate	$\ \nabla_{-x} e_\varepsilon^H\ _{H,-}$	Rate
2.5021e-01	1.67150e-03	-	2.2469e-02	-
1.2512e-01	4.19674e-04	1.99	5.6681e-03	1.98
6.2560e-02	1.05793e-04	1.98	1.2000e-03	2.23
3.1280e-02	2.67972e-05	1.98	3.5142e-04	1.77
1.5640e-02	6.70333e-06	1.99	1.3087e-04	1.42
7.8384e-03	1.66984e-06	2.01	8.5213e-05	0.62
3.9156e-03	4.07688e-07	2.03	8.2261e-05	0.05
1.9667e-03	1.00208e-07	2.03	8.2035e-05	0.00
9.7753e-04	2.84471e-08	1.80	8.2048e-05	-0.00
4.8877e-04	1.43107e-08	0.99	8.2047e-05	0.00

Figure 20 – Convergence rate for h .

In the following example we can analyze the influence of the magnitude of ε in the convergence analysis varying the macroscale mesh size H . A similar analysis can be done varying h .

Example 12. Taking in (7.25)

$$\mathcal{K}(y) = \frac{1}{2 + \cos(2\pi y)}, f^\varepsilon = e^x + \cos^2(2\pi x), \varepsilon = 0.05, 0.01 \text{ and } 0.001, \quad (7.37)$$

we obtain the numerical errors shown in the next Tables 16, 17 and 18.

Firstly for $\varepsilon = 0.05$ we have

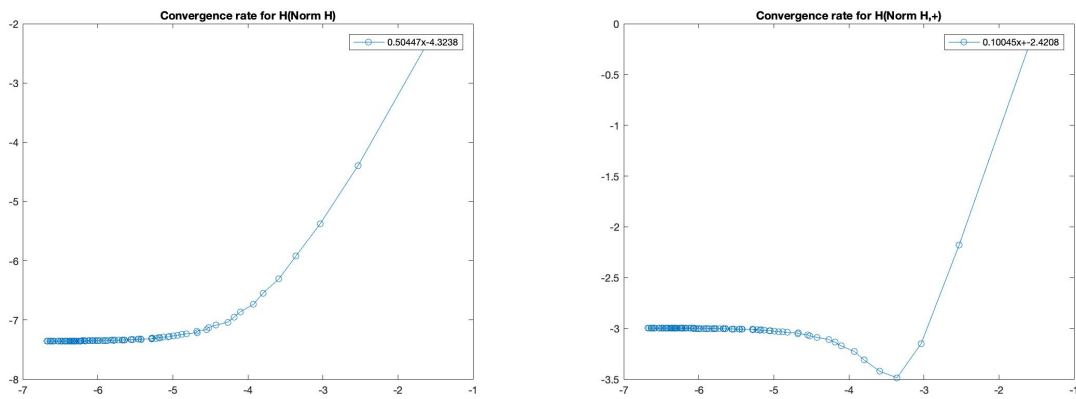


Figure 21 – From left to right we can see the behavior of the errors for $\varepsilon = 0.05$.

Table 16 – Convergence rate for $H(h = 1e - 04, \varepsilon = 0.05)$

H_{max}	$\ e_\varepsilon^H\ _H$	Rate	$\ \nabla_{-x} e_\varepsilon^H\ _{H,-}$	Rate
2.0138e-01	9.8645e-02	-	8.0082e-01	-
7.9540e-02	1.2352e-02	2.2366e+00	1.1302e-01	2.1078e+00
4.8022e-02	4.6284e-03	1.9453e+00	4.2921e-02	1.9188e+00
3.4798e-02	2.6877e-03	1.6874e+00	3.0623e-02	1.0482e+00
2.7675e-02	1.8237e-03	1.6933e+00	3.2657e-02	-2.8082e-01
\vdots	\vdots	\vdots	\vdots	\vdots
1.3202e-03	6.3838e-04	6.0425e-03	4.9943e-02	-1.0861e-03
1.3081e-03	6.3827e-04	5.3403e-04	4.9945e-02	-3.8638e-05
1.2737e-03	6.3823e-04	2.0257e-03	4.9946e-02	-5.9153e-04
1.2610e-03	6.3818e-04	7.7969e-03	4.9947e-02	-2.5189e-03

For $\varepsilon = 0.01$ we have

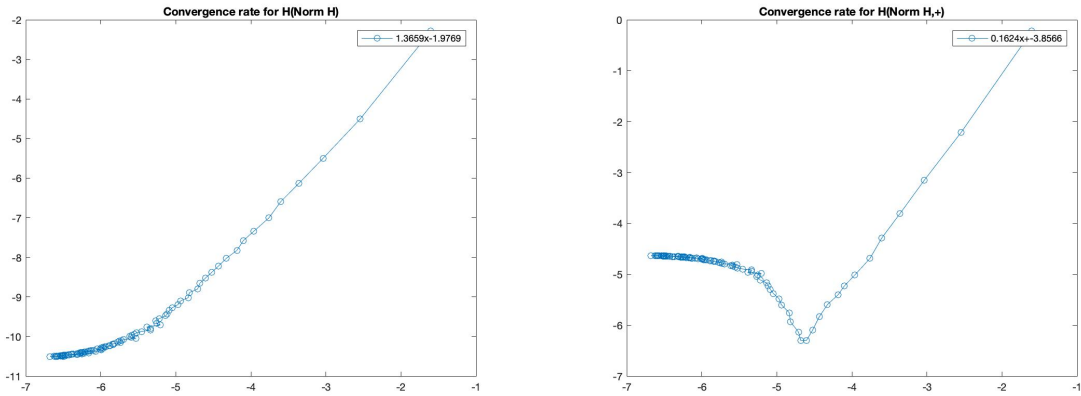


Figure 22 – From left to right we can see the behavior of the errors for $\varepsilon = 1e - 2$.

Table 17 – Convergence rate for $H(h = 1e - 04, \varepsilon = 0.01)$

H_{max}	$\ e_\varepsilon^H\ _H$	Rate	$\ \nabla_{-x} e_\varepsilon^H\ _{H,-}$	Rate
2.0162e-01	1.0184e-01	-	8.0216e-01	-
7.8452e-02	1.1012e-02	2.3568e+00	1.0927e-01	2.1120e+00
4.7961e-02	4.0982e-03	2.0085e+00	4.2582e-02	1.9150e+00
3.4819e-02	2.1854e-03	1.9634e+00	2.2266e-02	2.0248e+00
2.7260e-02	1.3671e-03	1.9168e+00	1.3731e-02	1.9748e+00
⋮	⋮	⋮	⋮	⋮
1.3639e-03	2.7532e-05	-3.6428e-02	9.7231e-03	2.8402e-02
1.5003e-03	2.7465e-05	-2.5288e-02	9.7283e-03	5.6779e-03
1.3486e-03	2.7430e-05	1.2086e-02	9.7331e-03	-4.5617e-03
1.3870e-03	2.7372e-05	-7.5536e-02	9.7403e-03	2.6541e-02
1.2610e-03	2.7331e-05	1.5773e-02	9.7420e-03	-1.8105e-03

Then, for $\varepsilon = 0.001$

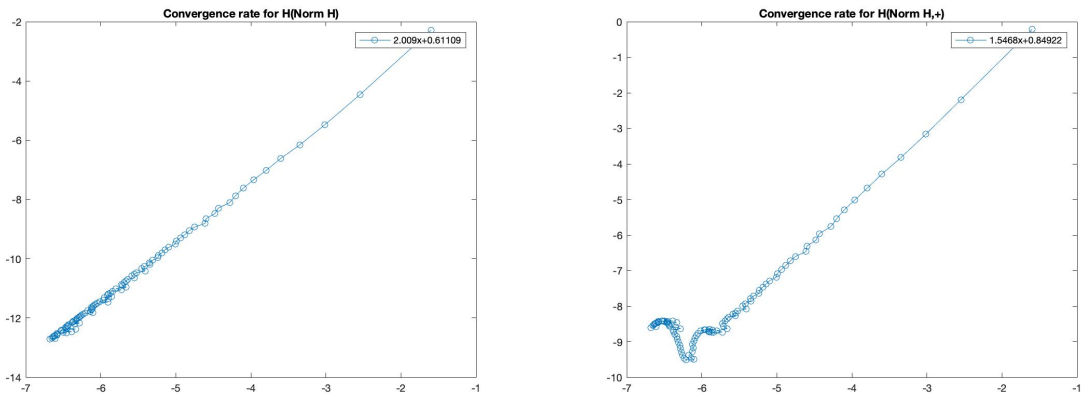


Figure 23 – From left to right we can see the behavior of the errors for $\varepsilon = 1e - 3$.

Table 18 – Convergence rate for $H(h = 1e - 04, \varepsilon = 1e - 3)$

H_{max}	$\ e_\varepsilon^H\ _H$	Rate	$\ \nabla_{-x}e_\varepsilon^H\ _{H,-}$	Rate
2.0199e-01	1.0138e-01	-	8.0507e-01	-
7.8301e-02	1.1523e-02	2.2946e+00	1.1159e-01	2.0852e+00
4.9199e-02	4.2003e-03	2.1718e+00	4.2433e-02	2.0808e+00
3.5164e-02	2.1173e-03	2.0396e+00	2.1825e-02	1.9796e+00
2.7264e-02	1.3388e-03	1.8013e+00	1.3721e-02	1.8238e+00
\vdots	\vdots	\vdots	\vdots	\vdots
1.3202e-03	3.2941e-06	1.3806e+00	2.0274e-04	1.7373e+00
1.3066e-03	3.2176e-06	2.2690e+00	1.9872e-04	1.9323e+00
1.2932e-03	3.1469e-06	2.1542e+00	1.9430e-04	2.1817e+00
1.3491e-03	3.0803e-06	-5.0581e-01	1.8948e-04	-5.9433e-01
1.2610e-03	3.0397e-06	1.9649e-01	1.8427e-04	4.1264e-01

Note that the errors in the Table 16 and plots 21, associated to $\varepsilon = 5e - 2$, decrease with a second order in both norms only in the first three coarsest macro-scale meshes. Then the errors decrease slowly by decreasing H_{max} , up to reaching a value $6.38e - 04$ in the norm $\|\cdot\|_H$ and $4.994e - 02$ in the norm $\|\nabla_{-x}\|_{H,-}$. We perform in the following a error analysis in the norm $\|\cdot\|_H$ but a similar analysis is valid in the norm $\|\nabla_{-x}\cdot\|_{H,-}$. Our understanding is that the error does not decrease further since for the formula (7.35)₂, is bounded by a term $O(\varepsilon^2)$, that should be $C_1\varepsilon^2 = C_1(0.05)^2 \approx 6.38e - 04$ with $C_1 = 2.552e - 01$. This understanding is confirmed by the observation that with $\varepsilon = 1e - 02$ we have in Table 17 and plot 22 that the errors have a second order rate in more meshes (5 coarsest meshes) and reach a constant value $2.7e - 05 \approx C_2\varepsilon^2 = C_2 \cdot (1e - 04)$ with $C_2 = 2.7e - 01$ that is approximately C_1 . Using $\varepsilon = 1e - 03$ we observe in Table 18 that the error is still decreasing with the H_{max} used, and that it is maybe reaching the value $C_1\varepsilon^2 = 2.5e - 01 \cdot 1e - 06 = 2.5e - 07$. One can see also that $C_3 = 2\sqrt{C_1}$ and $C_4 = 2\sqrt{C_2}$ fit very well in the bounds of $\|\cdot\|_{H,-}$ norm. Now, observe that the errors in $\|\cdot\|_{H,-}$ does not have the same behavior as $\|\cdot\|_H$ errors, in fact the error in $\|\cdot\|_{H,-}$ looks like a ball that is thrown down and bounces on the surface. We are not able to explain this effect without determining the theoretical the analytical error bounds.

7.4 Coupled multiscale problem

In this section we propose a multiscale method for solving with an high order of convergence the one dimensional version of the coupled elliptic-parabolic multiscale problem in (2.21) that determine the cell density and pressure inside the colonic crypts with micro-domain Y distributed in the colon domain Ω .

In Chapter 2 we proved that the microscale cell problem that determine χ can be solved once in the reference domain, and then we can use this solution to obtain the

homogenized tensor for both the elliptic and parabolic equation as well as the ε^1 terms p^1 and C^1 . We propose a multiscale method defined by the following steps:

1. Solve the microproblem using the supraconvergent method with periodic boundary conditions, which means we get χ^h as before in (7.15)
2. Build a discrete version of the problem with the supraconvergent method again by replacing the homogenized tensor by q^h and use the $mean_Y$ operator where it is needed;
3. Solve first the homogenized elliptic equation and then insert the obtained homogenized pressure in the parabolic equation;
4. Build an approximation of the multiscale solutions C^ε and p^ε by using respectively $C_\varepsilon^H = C_0^H - \varepsilon \chi^H \nabla_{-x} C_0^H$ and $p_\varepsilon^H = p_0^H - \varepsilon \chi^H \nabla_{-x} p_0^H$;

We observe that, as in HMM-FEM, the computational effort of this method is quite independent of ε since we use a reference domain instead of each repeated periodic domain. Beside that at the last step, we just have to interpolate χ^h near the nodal points of Ω_H to get χ^H .

In the following we prove numerically that this multiscale scheme is convergent with order two with respect both step sizes H and h and with order 1 or 2 with respect ε depending on the norm used. On the other words we have the same convergence rates observed for the elliptic problem. The stability and convergence of this method will be proved theoretically in the near future, see the conclusions Chapter.

Example 13. Consider the coupled 1D system

$$\begin{cases} -\nabla \cdot (\mathcal{K}^\varepsilon \nabla p^\varepsilon) = \alpha(y) C^\varepsilon + f_1^\varepsilon. \\ \frac{\partial C^\varepsilon}{\partial t} + \nabla \cdot (v^\varepsilon C^\varepsilon) = \nabla \cdot (D(y) \mathcal{K}^\varepsilon \nabla C^\varepsilon) + \beta(y) C^\varepsilon + f_2^\varepsilon. \end{cases} \quad (7.38)$$

where $v^\varepsilon = -\mathcal{K}^\varepsilon \nabla p^\varepsilon$, $\mathcal{K}(y) = 1/(2 + \cos(2\pi y))$ and $D = \beta = \alpha = 1$.

Findig exact solutions for multiscale problems is not a too easy task, so we added two additional functions $f_1^\varepsilon, f_2^\varepsilon$ to make this analysis possible. In the following sets of Tables we present the convergence for the macromesh H and the micromesh h for the homogenized problem.

Table 19 – Convergence rate for H in $\|\cdot\|_H$ norm ($h \sim 1e-04$)

H_{max}	$\ e_0^{p,H}\ _H$	Rate	$\ e_0^{C,H}\ _H$	Rate
5.0418e-02	4.6760e-03	-	1.4158e-03	-
2.5394e-02	1.1363e-03	2.06	3.5631e-04	2.01
1.2621e-02	2.7990e-04	2.00	8.9569e-05	1.97
6.3111e-03	7.1025e-05	1.97	2.2393e-05	2.00
3.1760e-03	1.7668e-05	2.02	5.6170e-06	2.01
1.6773e-03	4.4003e-06	2.17	1.4133e-06	2.16

Table 20 – Convergence rate for H in $\|\cdot\|_{H,-}$ norm ($h \sim 1e-04$)

H_{max}	$\ \nabla_{-x} e_0^{p,H}\ _{H,-}$	Rate	$\ \nabla_{-x} e_0^{C,H}\ _{H,-}$	Rate
5.0418e-02	6.6174e-03	-	2.3904e-03	-
2.5394e-02	1.6164e-03	2.05	6.1236e-04	1.98
1.2621e-02	4.0135e-04	1.99	1.5451e-04	1.96
6.3111e-03	1.0128e-04	1.98	3.8663e-05	1.99
3.1760e-03	2.5248e-05	2.02	9.7034e-06	2.01
1.6773e-03	6.2922e-06	2.17	2.4422e-06	2.16

Table 21 – Convergence rate for h in $\|\cdot\|_H$ norm ($H \sim 2e-03$)

h_{max}	$\ e_0^{p,H}\ _H$	Rate	$\ e_0^{C,H}\ _H$	Rate
3.3527e-01	1.8098e-02	-	1.6986e-03	-
2.0195e-01	7.1451e-03	1.83	6.1790e-04	1.99
1.4397e-01	3.9705e-03	1.73	3.3595e-04	1.80
1.1214e-01	2.3891e-03	2.03	2.0017e-04	2.07
9.1816e-02	1.6658e-03	1.80	1.3907e-04	1.82
7.9848e-02	1.1984e-03	2.35	9.9901e-05	2.36

Table 22 – Convergence rate for h in $\|\cdot\|_{H,-}$ norm ($H \sim 2e-03$)

h_{max}	$\ \nabla_{-x} e_0^{p,H}\ _{H,-}$	Rate	$\ \nabla_{-x} e_0^{C,H}\ _{H,-}$	Rate
3.3527e-01	2.5567e-02	-	1.8509e-03	-
2.0195e-01	1.0093e-02	1.83	6.7494e-04	1.99
1.4397e-01	5.6088e-03	1.73	3.6710e-04	1.79
1.1214e-01	3.3749e-03	2.03	2.1868e-04	2.07
9.1816e-02	2.3531e-03	1.80	1.5187e-04	1.82
7.9848e-02	1.6928e-03	2.35	1.0902e-04	2.37

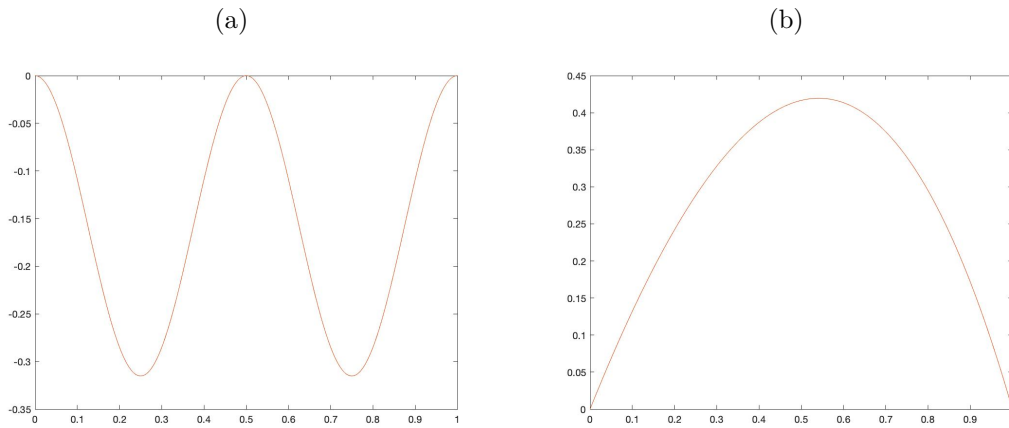


Figure 24 – 24(a) and 24(b) show us the graph of the exact homogenized solution and the numerical solution for pressure and density respectively ($H \sim 2e - 03$, $h = 1e - 04$).

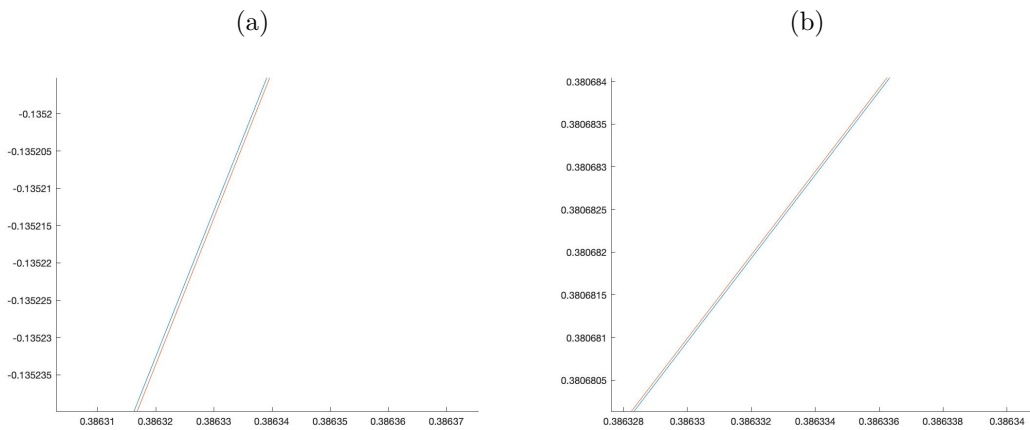


Figure 25 – Images 24(a) and 24(b) respectively with zoom applied.

The next table is one of our most interest which is the convergence for ε and as we can see the error goes to zero in a first order of convergence for the gradient.

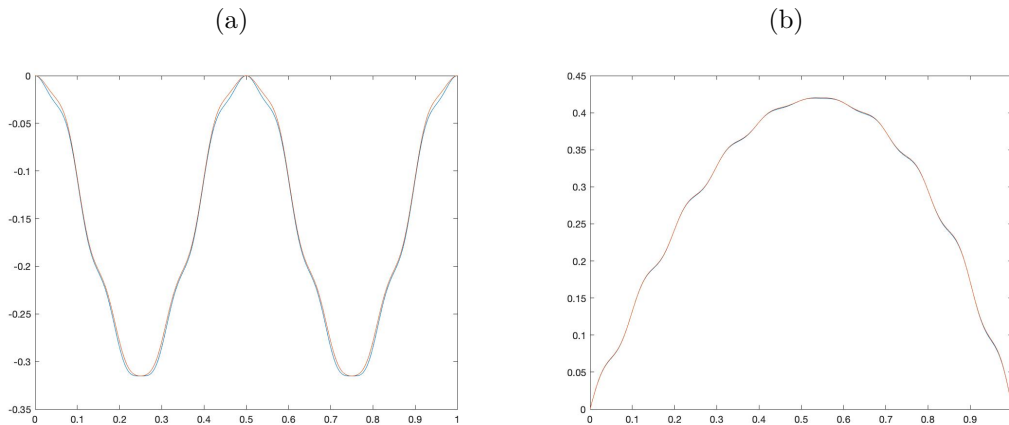
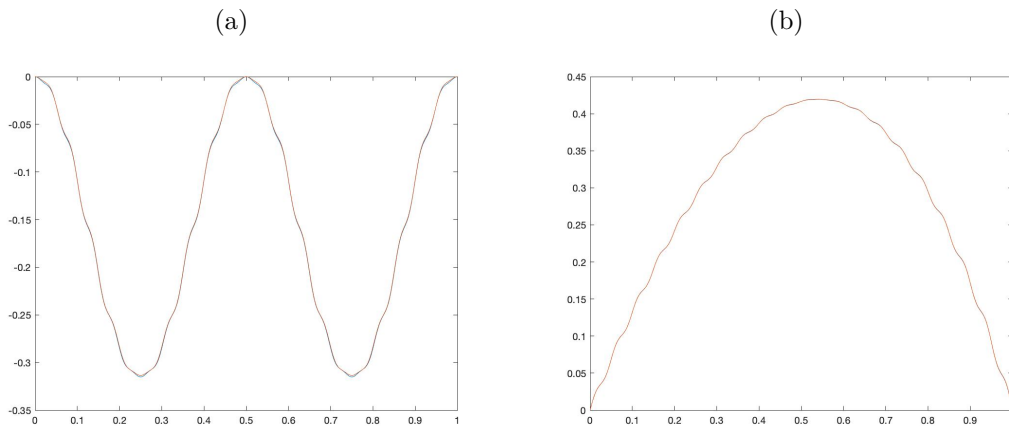
Table 23 – Convergence rate for ε in $\|\cdot\|_H$ norm ($h \sim 1e - 04$, $H \sim 2e - 03$)

ε	$\ e_\varepsilon^{p,H}\ _H$	Rate	$\ e_\varepsilon^{C,H}\ _H$	Rate
1.0000e-01	2.6331e-03	-	4.1198e-04	-
6.6667e-02	1.1420e-03	2.06	1.8319e-04	1.99
5.0000e-02	6.3743e-04	2.02	1.0306e-04	1.99
4.0000e-02	4.0681e-04	2.01	6.5964e-05	1.99
3.3333e-02	2.8230e-04	2.00	4.5810e-05	1.99
2.8571e-02	2.0749e-04	1.99	3.3657e-05	1.99

Table 24 – Convergence rate for ε in $\|\cdot\|_{H,-}$ norm ($h \sim 1e-04, H \sim 2e-03$)

ε	$\ \nabla_{-x} e_{\varepsilon}^{p,H}\ _{H,-}$	Rate	$\ \nabla_{-x} e_{\varepsilon}^{C,H}\ _{H,-}$	Rate
1.0000e-01	1.0285e-02	-	2.0415e-03	-
6.6667e-02	6.7268e-03	1.04	1.3458e-03	1.02
5.0000e-02	5.0117e-03	1.02	1.0051e-03	1.01
4.0000e-02	3.9964e-03	1.01	8.0236e-04	1.00
3.3333e-02	3.3237e-03	1.01	6.6767e-04	1.00
2.8571e-02	2.8446e-03	1.00	5.7162e-04	1.00

Note that we used the same approximation as in (7.33). A $O(\sqrt{\varepsilon})$ order of convergence was expected for $\|\cdot\|_{H,-}$ norm in the same way $O(H)$ was expected from the classical literature. We need a deeper analyze as done in Chapter 6 to conclude the exact rate of convergence.

Figure 26 – Graph of the exact multiscale solution and the numerical solution for pressure and density respectively ($\varepsilon = 0.1$).Figure 27 – Graph of the exact multiscale solution and the numerical solution for pressure and density respectively ($\varepsilon = 0.01$).

In the next 4 Tables we show the errors for H and h convergence for the multiscale problem. As we can see, the convergence rates are very similar to Tables 19-22 since $\varepsilon \sim 1e - 06$.

Table 25 – Convergence rate for h in $\|\cdot\|_H$ norm($\varepsilon \sim 1e - 06, H \sim 2e - 03$)

h_{max}	$\ e_\varepsilon^{p,H}\ _H$	Rate	$\ e_\varepsilon^{C,H}\ _H$	rate
3.3639e-01	1.7881e-02	-	1.6748e-03	-
2.0367e-01	7.0458e-03	1.85	6.0837e-04	2.01
1.4403e-01	3.9115e-03	1.69	3.3032e-04	1.76
1.1412e-01	2.4817e-03	1.95	2.0753e-04	1.99
9.1788e-02	1.6750e-03	1.80	1.3932e-04	1.83
7.7804e-02	1.1982e-03	2.02	9.9364e-05	2.04

Table 26 – Convergence rate for h in $\|\cdot\|_H$ norm($\varepsilon \sim 1e - 06, H \sim 2e - 03$)

h_{max}	$\ \nabla_{-x} e_\varepsilon^{p,H}\ _{H,-}$	Rate	$\ \nabla_{-x} e_\varepsilon^{C,H}\ _{H,-}$	Rate
3.3639e-01	2.5260e-02	-	1.8253e-03	-
2.0367e-01	9.9535e-03	1.85	6.6480e-04	2.01
1.4403e-01	5.5256e-03	1.69	3.6119e-04	1.76
1.1412e-01	3.5058e-03	1.95	2.2697e-04	1.99
9.1788e-02	2.3662e-03	1.80	1.5237e-04	1.83
7.7804e-02	1.6926e-03	2.02	1.0866e-04	2.04

Table 27 – Convergence rate for h in $\|\cdot\|_H$ norm($\varepsilon \sim 1e - 06, h \sim 1e - 04$)

H_{max}	$\ e_\varepsilon^{p,H}\ _H$	Rate	$\ e_\varepsilon^{C,H}\ _H$	Rate
5.0994e-02	4.7257e-03	-	1.4058e-03	-
3.3641e-02	1.9674e-03	2.10	6.3358e-04	1.91
2.5243e-02	1.1147e-03	1.97	3.5674e-04	2.00
2.1161e-02	7.2352e-04	2.44	2.2919e-04	2.50
1.6831e-02	4.9429e-04	1.66	1.5901e-04	1.59
1.4717e-02	3.7325e-04	2.09	1.1683e-04	2.29

Table 28 – Convergence rate for h in $\|\cdot\|_H$ norm($\varepsilon \sim 1e - 06, h \sim 1e - 04$)

H_{max}	$\ \nabla_{-x} e_\varepsilon^{p,H}\ _{H,-}$	Rate	$\ \nabla_{-x} e_\varepsilon^{C,H}\ _{H,-}$	Rate
5.0994e-02	6.5900e-03	-	2.3800e-03	-
3.3641e-02	2.8429e-03	2.02	1.0820e-03	1.89
2.5243e-02	1.6014e-03	1.99	6.1261e-04	1.98
2.1161e-02	1.0335e-03	2.48	3.9544e-04	2.48
1.6831e-02	7.0945e-04	1.64	2.7404e-04	1.60
1.4717e-02	5.2946e-04	2.17	2.0166e-04	2.28

7.5 Comments

If we take a look closer, the scheme described here is very familiar with the HMM framework (see Chapter 4). The macro solver choose is the supraconvergent method described in Chapter 6 and we supply the need data by approximate the homogenized tensor using information of the microscale. On the other hand, we take advantage of the periodicity to build a scheme that does not need to solve a microproblem around each node of the macro mesh. The micro problem is solved in a domain of reference that in some sense is independent of ε . The main idea of the scheme is lead the convergence of the micro problem to the macro problem without lose accuracy.

The numerical convergence of $O(\varepsilon)$ for the post-processing approximation was not expected and is superior in comparison with other methods as HMM-FEM. We strongly believe that it is a consequence of the supraconvergent method, but we remark that there is a finite elements equivalency so we need to go deeper to find the right answer. Note that the computational cost of this scheme is the same than solving a 1D coupled problem in Chapter 6.

8 Conclusions, contributions and future work

8.1 Conclusions

Based on some models for tumor growth in the colon, see Chapter 1, we used a system of PDE in three spatial dimensions for the dynamics of colon cell populations. The cell dynamics, differentiation and proliferation in the colon occur in three dimensional cavities wide spread in the colon epithelium and called crypts. Due to its micro-dimension (measured in micro-meters), that is very small with respect the dimension of the colon that is measured in meters, such dynamics in the colon can be modeled by using multiscales with a microscale dimension ε representing the dimension of a single crypt and a macroscale for the colon epithelium dimension. Moreover due to the large diffusion of crypts in the colon we suppose that an averaged crypt is periodically distributed in the colon, as done in Chapter 2. The averaged reference crypt is there represented by a two dimensional Riemannian manifold that permits to rewrite the three dimensional PDE system in a bidimensional PDE system whose parameters describing the proliferation, diffusion and geometry of the crypt will depend on the micro-scale dimension ε . Solving a multiscale problem with a standard FEM usually needs to use the smallest scale in all the domain. For multiscale elliptic problem

$$-\nabla(A^\varepsilon \nabla u^\varepsilon) = f \quad (8.1)$$

the following sharp a-priori error is valid

$$\|u^\varepsilon - u\|_{H^1} \leq C \frac{h}{\varepsilon} \|f\|_{H^{-1}}, \quad (8.2)$$

which means that to get a limited error the mesh size must satisfies $h < \varepsilon$ leading to a huge computational effort. To overcome this difficulty in solving multiscale problems we introduced the homogenization theory in Chapter 3 for the coupled multiscale PDE system solving the cell dynamics in the colon epithelium. The homogenization permits to analyze the multiscale problem with solution u^ε when $\varepsilon \rightarrow 0$ by using a single scale, transforming the multiscale PDE equations in a problem, called homogenized problem with solution u^0 , that is uniformly spanned in all the domain. There are known analytical forms for the homogenized problem and error estimates associated to many elliptic, parabolic and coupled problems (GOUDON; POUPAUD, 2005), however it results computationally expensive to build the associated homogenization tensors. This is the reason for introducing the HMM-FEM method in Chapter 4 that permits to approximate the homogenized solution through a FEM multiscale strategy using a limited computational and memory effort. Its computational cost is in fact independent of the dimension of the micro scale, and the associated homogenized tensor can be computed by solving the microscale cell problem

only around the quadrature points used to approximate the macro-scale integrals that depend on the FEM used. As discussed in the thesis, exists in the literature HMM error estimates with respect the homogenized solution $\|u^0 - u^{HMM}\|$ for elliptic and parabolic multiscale problems. It is known for example that the error estimates for the gradients scales with a first order of convergence with respect H , and second order with respect to $\frac{h}{\varepsilon}$. Moreover the HMM-FEM solution can be used to approximate the multiscale solution after a proper post-processing construction of a approximation of u^ε . This reconstructed approximation scales for the gradients with order 0.5 and for the solutions with order 1.

A goal of this thesis was to speed-up such convergence in solving coupled parabolic elliptic multiscale PDE problem as that associated to the colonic crypt cell dynamics in nonuniform meshes. We succeed in this by building firstly a finite difference method with a higher convergence order than to HMM-FEM for approximating the gradient of the solution of coupled PDE parabolic-elliptic system in a single scale, see Chapter 5. This supraconvergent method is proved to converge with a such high order for solutions in $C^4(\Omega)$.

We were able to relax such assumption in Chapter 6 proving that this method is equivalent to a FEM method that converges with the same order using less regular functions that are in $H^3(\Omega)$. Finally in Chapter 7 we extended this method to solve accurately, with an high order, multiscale coupled PDE systems. We proposed a multiscale strategy that uses the supraconvergent method at each scale: in the micro to solve the microscale cell problem for obtaining the homogenized matrix, and in the macro-scale to solve the homogenized equations. Such strategy combined with the post-processing of the homogenized solution $u^{\varepsilon,H} := u^{0,H} + \varepsilon u^{1,H}$ permits to have a high accurate method for the gradient that is a second order for the micro and macro scale mesh size and of first order with respect ε . This post-processing strategy is similar to that used in HMM-FEM (see Chapter 4).

8.2 Future work

In this section we give some remarks on perspectives of the thesis results that can be investigated in the future.

8.2.1 Convergence and stability analysis

In Chapter 7 we presented how to use the supraconvergent method to obtain better approximations of the multiscale solution of PDE multiscale coupled elliptic parabolic problems. Our numerical tests show a $O(H_{max}^2 + h_{max}^2 + \varepsilon + f(H, h, \varepsilon))$ order of convergence in nonuniform meshes. The next step is then to prove such orders theoretically using a

similar approach of that used in Chapter 5 and 6 but now considering also the ε scale and the interaction with the macro scale in the approximations.

8.2.2 The Hill equation

Nowadays medical doctors are interested in the physiochemical reactions of drugs with the cancer cell proliferation. A such problem is modeled nowadays by adding a reaction term represented by a Hill equation in the cell dynamics that inhibits or reduces the cell proliferation and cancer growth. A such new equation coupled with a drug release model in the colon can be considered in our mathematical modeling of colonic cell dynamics to simulate its effect in the first stage of colorectal cancer under a pharmacological therapy.

This new equation can be represented by a Hill equation that is a nonlinear relation between three parameters y_{max} , c and α :

$$y = \frac{y_{max}x^\alpha}{c^\alpha + x^\alpha}. \quad (8.3)$$

Focusing on pharmacodynamics, the Hill equation has been widely used to describe the relation between drug effect (E) and drug concentration (C). Mathematically, this model has a Hill equation form

$$E = \frac{E_{max}C^\alpha}{C_{50}^\alpha + C^\alpha}, \quad (8.4)$$

where E is the predicted effect of the drug, E_{max} is the maximum effect, C is the drug concentration at time t , C_{50} is the drug concentration for which 50% of maximum effect is obtained and α is the Hill coefficient of sigmoidicity. For more details see (GOUTELLE et al., 2009; ZHAN; GEDROYC; XU, 2014).

8.2.3 Convergence and stability analysis of the HMM-FEM method applied to a coupled problem

In Chapter 4 we applied the HMM-FEM to our coupled problem to get the first numerical solutions in a observable macro scale. We showed numerically that HMM-FEM solution converges to the homogenized solution when macro scale size goes to zero also for our coupled elliptic parabolic problem. The convergence rates obtained are similar to those obtained in (ABDULLE, 2009; ABDULLE, 2012; ABDULLE; HUBER, 2014; ABDULLE; NONNENMACHER, 2009). It is interested to prove this convergence rate theoretically, in fact this will help us to determine the exact error estimates and understand how reducing the approximation error.

8.2.4 2D analysis of supraconvergent multiscale method

Results in Chapter 7 have been obtained applying the proposed multiscale method to solve a multiscale problem in one dimension in space. Despite this, it is easy to

extend such multiscale method in a 2D domain. Preliminary results have been already obtained, see Example 14, where we prove that we can approximate the homogenized tensor with a high order by using the supraconvergent method presented in Chapters 5-6.

Example 14. Taking $\mathcal{A}(y_1, y_2) = (2 + \cos(2\pi y_1))I$, where $I \in \mathbb{R}^{2 \times 2}$ and

$$\mathcal{A}^0 = \begin{bmatrix} \sqrt{3} & 0 \\ 0 & 2 \end{bmatrix} \quad (8.5)$$

Table 29 – Numerical approximation for homogenized tensor

h_{max}	$\ \mathcal{A}^0 - \mathcal{A}^h\ _\infty$	Rate
2.0005e-01	4.7314e-02	0.0000
1.0002e-01	1.3118e-02	1.8505
5.0024e-02	3.2997e-03	1.9919
2.5002e-02	8.2611e-04	1.9967
1.2503e-02	2.0664e-04	1.9996
6.2516e-03	5.1619e-05	2.0011

Using this result it will be possible to prove a high order of convergence for the multiscale numerical solution in bidimensional domains. This will be obtained using similar demonstrations of that presented for one dimensional multiscale problems.

8.3 Contributions

8.3.1 Presentations

Some parts of this work were presented in the following events:

- CNMAC - XXXVIII Computational and applied mathematics National Congress - Campinas/SP - Brazil (2018);
- WCMNA - Workshop on Computational Modeling and Numerical Analysis - Petrópolis/RJ - Brazil(2019);
- ICIAM - International Congress on Industrial and Applied Mathematics - Valencia - Spain (2019);
- WANA - Workshop on Numerical Analysis and Applications- Imecc/Unicamp - Brazil (2019);

8.3.2 Project

I gained a CAPES-PRINT financed project for a visiting research in the University of Coimbra-Portugal under the supervision of Professor José Augusto Ferreira from September 2019 to March 2020.

The project was named *Estabilidade e Convergência de métodos numéricos multiescala aplicados a equações diferenciais acopladas* and started at 01/09/2019. During this six months we developed a numerical process to approximate the solution of a general coupled elliptic parabolic PDE system in a single scale on nonuniform meshes. The main result obtained during this research visit was the quadratic convergence in L^2 and H^1 discrete norms of the numerical method presented in Chapters 5-6 when the solutions belongs in H^3 .

Moreover during this period a small part of Chapter 7 have been developed, and I profit that period to learn numerical techniques to improve further this Chapter later on.

8.3.3 Submissions of articles

With this work we have the intention of publish up to 3 articles. The first one are the results presented in Chapter 5. It is named

- Supraconvergent method for elliptic-parabolic PDE systems

and is expected to be submitted by January.

The second will present the results of Chapter 6.

The last one will contain the results of Chapter 7 together with the future work 8.2.1 discussed above.

Bibliography

ABDULLE, A. The finite element heterogeneous multiscale method: A computational strategy for multiscale pdes. *GAKUTO Int. Ser. Math. Sci. Appl.*, v. 31, 01 2009. Citado 7 vezes nas páginas 7, 8, 53, 59, 62, 109, and 122.

_____. Discontinuous galerkin finite element heterogeneous multiscale method for elliptic problems with multiple scales. *Math. Comput.*, v. 81, 04 2012. Citado 4 vezes nas páginas 7, 8, 62, and 122.

ABDULLE, A.; HUBER, M. Finite element heterogeneous multiscale method for nonlinear monotone parabolic homogenization problems. 01 2014. Citado 5 vezes nas páginas 7, 8, 53, 62, and 122.

ABDULLE, A.; NONNENMACHER, A. A short and versatile finite element multiscale code for homogenization problem. *Computer Methods in Applied Mechanics and Engineering*, v. 198, p. 2839–2859, 08 2009. Citado 3 vezes nas páginas 56, 58, and 122.

ANDERSON, E. C.; HESSMAN, C.; LEVIN, T. G.; MONROE, M. M.; WONG, M. H. *The Role of Colorectal Cancer Stem Cells in Metastatic Disease and Therapeutic Response*. 3. ed. , 2011. Citado na página 28.

BRAMBLE, J. H.; HILBERT, S. R. Estimation of linear functionals on sobolev spaces with application to fourier transforms and spline interpolation. *SIAM Journal on Numerical Analysis*, Society for Industrial and Applied Mathematics, v. 7, n. 1, p. 112–124, 1970. ISSN 00361429. Disponível em: <<http://www.jstor.org/stable/2949585>>. Citado na página 137.

BRENNER, S. C.; SCOTT, L. *The mathematical theory of finite elements methods*. 13. ed. , 2008. Citado na página 137.

BRENNER, S. C.; SCOTT, L. R. *Convergent discrete Laplace-Beltrami operators over triangular surfaces*. , 2004. Citado na página 129.

CARMO, M. P. do. *Differential geometry of curves and surfaces*. 13. ed. : Inc.Englewood Cliffs, 1976. Citado 2 vezes nas páginas 129 and 130.

CIORANESCU, D.; DONATO, P. *An introduction to homogenization*. 1. ed. , 1999. Citado 4 vezes nas páginas 7, 8, 37, and 38.

COLLINS, E. B. B. *Bowel dysfunction : A comprehensive guide for healthcare professionals*. Springer International Publishing, 2016. Citado 2 vezes nas páginas 25 and 26.

COY, C. Colorectal cancer prevention in brazil - where are we? *Journal of Coloproctology*, v. 33, p. 111–112, 07 2013. Citado na página 17.

DRASDO, D.; LOEFFLER, M. Individual-based models to growth and folding in one-layered tissues: Intestinal crypts and early development. *Nonlinear Analysis-theory Methods and Applications - NONLINEAR ANAL-THEOR METH APP*, v. 47, p. 245–256, 08 2001. Citado na página 31.

- ENGQUIST, B.; LI, X.; REN, W.; VANDEN-EIJNDEN, E. Heterogeneous multiscale methods: A review. *COMMUNICATIONS IN COMPUTATIONAL PHYSICS Commun. Comput. Phys.*, v. 2, p. 367–450, 07 2007. Citado 3 vezes nas páginas 51, 52, and 53.
- FERLAY, J.; SHIN, H.; BRAY, F.; FORMAN, D.; PARKIN, D. Cancer incidence and mortality worldwide: Iarc cancerbase no. *International Agency for Research on Cancer.*, v. 2, 01 2013. Citado na página 17.
- FERREIRA, J.; BARBEIRO, S.; GRIGORIEFF, R. Supraconvergence of a finite difference scheme for solutions in $h^s(0, l)$. *IMA Journal of Numerical Analysis*, v. 25, 10 2005. Citado 4 vezes nas páginas 7, 8, 78, and 97.
- FERREIRA, J.; GRIGORIEFF, R. Supraconvergence and supercloseness of a scheme for elliptic equations on nonuniform grids. *Numerical Functional Analysis and Optimization - NUMER FUNC ANAL OPTIMIZ*, v. 27, p. 539–564, 09 2006. Citado na página 78.
- FERREIRA, J.; NO, E. G.; OLIVEIRA, P. de. A second order approximation for quasilinear non-fickian diffusion models. *Computational Methods in Applied Mathematics*, v. 13, 10 2013. Citado na página 78.
- FERREIRA, J.; PINTO, L. Supraconvergence and supercloseness in quasilinear coupled problems. *Journal of Computational and Applied Mathematics*, v. 252, p. 120–131, 11 2013. Citado na página 78.
- FIGUEIREDO, I.; LEAL, C.; ROMANAZZI, G.; ENGQUIST, B.; FIGUEIREDO, P. A convection-diffusion-shape model for aberrant colonic crypt morphogenesis. *Computing and Visualization in Science*, v. 14, p. 157–166, 04 2011. Citado 2 vezes nas páginas 22 and 23.
- FIGUEIREDO, I.; LEAL, C.; ROMANAZZI, G.; ENGQUIST, B. Homogenization model for aberrant crypt foci. 03 2016. Citado 7 vezes nas páginas 9, 21, 24, 27, 29, 32, and 36.
- _____. Biomathematical model for simulating abnormal orifice patterns in colonic crypts. *Mathematical Biosciences*, v. 315, p. 108221, 07 2019. Citado 2 vezes nas páginas 23 and 24.
- FIGUEIREDO, I.; ROMANAZZI, G.; LEAL, C.; ENGQUIST, B. A multiscale model for aberrant crypt foci. *Procedia Computer Science*, v. 18, p. 1026–1035, 12 2013. Citado 5 vezes nas páginas 7, 8, 18, 21, and 24.
- GARDENAL, I. *Campanha do Cecom completa cinco anos prevenindo o câncer de intestino.*, 2017. Disponível em: <<https://www.inca.gov.br/numeros-de-cancer>>. Acesso em: 08 mar 2020. Citado na página 17.
- GOUDON, T.; POUPAUD, F. Homogenization of transport equations: Weak mean field approximation. *SIAM J. Math. Analysis*, v. 36, p. 856–881, 01 2005. Citado na página 120.
- GOUTELLE, S.; MAURIN, M.; ROUGIER, F.; BARBAUT, X.; BOURGUIGNON, L.; DUCHER, M.; MAIRE, P. The hill equation: A review of its capabilities in pharmacological modelling. *Fundamental and clinical pharmacology*, v. 22, p. 633–48, 01 2009. Citado na página 122.

- HSU, E. P. *Heat Equations on Manifolds and Bismut's Formula: Contemporary Mathematics 429*. , 2007. Citado na página 129.
- INCA. *Estatísticas de câncer*. , 2018. Disponível em: <<https://www.inca.gov.br/numeros-de-cancer>>. Acesso em: 11 apr 2019. Citado na página 17.
- JIKOV, V. V.; KOZLOV, S. M.; OLEINIK, O.; YOSIFIAN, G. A. *Homogenization of Differential Operators and Integral Functionals*. , 1994. Citado na página 39.
- KHALEK, F.; GALLICANO, G.; MISHRA, L. Colon cancer stem cells. *Gastrointestinal cancer research : GCR*, p. S16–23, 11 2010. Citado na página 27.
- KING, J. R.; FRANKS, S. J. *Mathematical analysis of some multi-dimensional tissue-growth models*. 15. ed. , 2004. Citado 2 vezes nas páginas 19 and 21.
- KREISS, H.-O.; MANTEUFFEL, T. A.; SWARTZ, B.; WENDROFF, B.; WHITE, A. B. Supra-convergent schemes on irregular grids. *Mathematics of Computation*, American Mathematical Society, v. 47, n. 176, p. 537–554, 1986. ISSN 00255718, 10886842. Disponível em: <<http://www.jstor.org/stable/2008171>>. Citado na página 137.
- LEE, J. M. Introduction to smooth manifolds. Springer New York, 2003. Citado na página 131.
- LEEUWEN, I. van; BYRNE, H.; JENSEN, O.; KING, J. Crypt dynamics and colorectal cancer: Advances in mathematical modelling. *Cell proliferation*, v. 39, p. 157–81, 07 2006. Citado na página 18.
- MATLAB. *version 9.5 (R2018a)*. Natick, Massachusetts: The MathWorks Inc., 2018a. Citado na página 24.
- MENDES, C.; LEAL, R.; MOREIRA, L.; AMORIM, T.; ANDRADE, A. Colonoscopic findings in patients aged 50 years and older: a critical analysis of 1614 exams. *Journal of Coloproctology*, v. 39, 10 2018. Citado 2 vezes nas páginas 17 and 18.
- MICHOR, F.; IWASA, Y.; LENGAUER, C.; NOWAK, M. *Dynamics of colorectal cancer*. 1. ed. , 2005. Citado na página 26.
- MURAT, F.; TARTAR, L. Calculus of variations and homogenization. In: _____. *Topics in the Mathematical Modelling of Composite Materials*. Boston, MA: Birkhäuser Boston, 1997. p. 139–173. ISBN 978-1-4612-2032-9. Disponível em: <https://doi.org/10.1007/978-1-4612-2032-9_6>. Citado na página 37.
- MURRAY, P.; WALTER, A.; FLETCHER, A.; DUNLOP, C.; TINDALL, M.; MAINI, P. Comparing a discrete and continuum model of the intestinal crypt. *Physical biology*, v. 8, p. 026011, 03 2011. Citado na página 18.
- PERSSON, L.-E.; PERSSON, L.; SVANSTEDT, N.; WYLLER, J. *The homogenization method : an introduction*. [S.l.: s.n.], 1993. 86 p. Godkänd; 1993; 20071112 (evan). ISBN 91-44-37661-8. Citado 4 vezes nas páginas 14, 42, 43, and 44.
- SOCIETY, A. C. *Colorectal Cancer Causes, Risk Factors, and Prevention*. , 2018. Disponível em: <<https://www.cancer.org/content/dam/CRC/PDF/Public/8605.00.pdf>>. Acesso em: 11 apr 2019. Citado na página 17.

_____. *Treatment of Colon Cancer, by Stage.* , 2018. Disponível em: <<https://www.cancer.org/cancer/colon-rectal-cancer/treating/by-stage-colon.html>>. Acesso em: 12 apr 2019. Citado na página 18.

WALTER, A. *Comparison of Continuum and Cell-based Models of Colorectal Cancer.* , 2009. Citado 2 vezes nas páginas 19 and 20.

ZHAN, W.; GEDROYC, W.; XU, X. Mathematical modelling of drug transport and uptake in a realistic model of solid tumour. *Protein and peptide letters*, v. 21, 08 2014. Citado na página 122.

APPENDIX A – Riemannian Manifold

A.1 Differential model on a manifold

In what follows we introduce some notations, and the derivatives for functions defined on a 2D Riemann manifold. This will permit to rewrite system (2.5) in the local coordinates of the 2D manifold Γ . Briefly let $\Gamma \subset \mathbb{R}^3$ be a 2D Riemann manifold, $\{Y, \varphi\}$ a chart, and let $(y_1, y_2) \in Y$ the local coordinates that parameterize the manifold Γ . For an arbitrary $C^2(\Gamma)$ function $f : \Gamma \rightarrow \mathbb{R}$, we define $\bar{f} : Y \rightarrow \mathbb{R}$ such that $\bar{f} = f \circ \varphi$. The relation between the derivatives of the function f , defined in Γ , and derivatives of \bar{f} , defined in Y , are established using the metric g , associated to the manifold Γ (CARMO, 1976; HSU, 2007; BRENNER; SCOTT, 2004).

In the next paragraph we give the formal definitions for Riemannian Manifold, metric g , the associated function matrix g , and the matrix \mathcal{A} that are used in Chapter 2.

A.1.1 Riemannian manifold and metric

Definition 1. Let Γ be a differential manifold. A differentiable function $\alpha : (-\varepsilon, \varepsilon) \rightarrow \Gamma$ is called a (differentiable) curve in Γ . Suppose that $\alpha(0) = p \in \Gamma$, and let \mathcal{D} be the set of functions on Γ that are differentiable at p . The tangent vector to the curve α at $t = 0$ is a function $\alpha'(0) : \mathcal{D} \rightarrow \mathbb{R}$ given by

$$\alpha'(0)f = \left. \frac{\partial(f \circ \alpha)}{\partial t} \right|_{t=0}, \quad f \in \mathcal{D}. \quad (\text{A.1})$$

Since $\alpha(0) = p$, each tangent vector defined in (A.1) is also called tangent vector at p . The set of all tangent vectors to Γ at p , indicated by $T_p\Gamma$, is called Tangent Plane of Γ at p .

A Riemannian Metric g in a differentiable manifold Γ is a correspondence which associates to each point p on Γ an inner product $\langle \cdot, \cdot \rangle_p$ (that is, a symmetric, bilinear, positive-definite form) on the tangent space $T_p\Gamma$. The differential manifold Γ endowed with the metric g , that is (Γ, g) , is for definition a Riemannian manifold. If $\varphi : Y \subset \mathbb{R}^2 \rightarrow \Gamma$ is a system of coordinates around p , for each $q \in \varphi(Y)$, $q = \varphi(y_1, y_2)$, then $g_{i,j}(y_1, y_2) := \left\langle \frac{\partial \varphi(y_1, y_2)}{\partial y_i}, \frac{\partial \varphi(y_1, y_2)}{\partial y_j} \right\rangle_p$ is a differentiable function on Y . The function $(g_{i,j})_{i,j=1,2}$ is called the local representation of the Riemannian metric g in the coordinate system $\varphi : Y \subset \mathbb{R}^2 \rightarrow \Gamma$. This matrix function $(g_{i,j})$ is represented in this thesis, for abuse of notation, by the matrix function g .

We consider in our model problem a crypt as a surface in \mathbb{R}^3 , that is a Riemannian manifold thus in the next part we define the differential operators over

surfaces. Recall that a subset $\Gamma \subset \mathbb{R}^3$ is a regular surface if, for every point $p \in \Gamma$, there exist a neighborhood V of p in \mathbb{R}^3 and a mapping $\mathbf{x} : U \subset \mathbb{R}^2 \rightarrow V \cap \Gamma$ of an open set $U \subset \mathbb{R}^2$ onto $V \cap \Gamma$, such that:

- \mathbf{x} is a differentiable homeomorphism;
- The differential $(d\mathbf{x})_q : \mathbb{R}^2 \rightarrow \mathbb{R}^3$ is injective for all $q \in U$ (CARMO, 1976).

The natural inner product of $\Gamma \subset \mathbb{R}^3$ induces on each $T_{\varphi(y_1, y_2)}(\Gamma)$ of a regular surface Γ , an inner product to be denoted by $\langle \cdot, \cdot \rangle_{\varphi(y_1, y_2)}$ ($\langle \cdot, \cdot \rangle$ for convenience). In general, to this inner product, which is a symmetric bilinear form, there corresponds a quadratic form $I_p : T_p\Gamma \rightarrow \mathbb{R}$ given by

$$I_p(w) = \langle w, w \rangle_p = |w|^2 \geq 0. \quad (\text{A.2})$$

In the case of Γ is a surface, $g_{ij} = \left\langle \frac{\partial \varphi}{\partial y_i}, \frac{\partial \varphi}{\partial y_j} \right\rangle$ that are the scalar product between the derivatives $\frac{\partial \varphi}{\partial y_i} \in \mathbb{R}^3$. A Riemannian metric is important to introduce the meaning of distance on the manifold. We define by g^{-1} , the g inverse matrix, with elements g^{ij} , that is $g^{-1} = (g^{ij})_{i,j=1,2}$. This permits to define the function \mathcal{A} with elements $\mathcal{A}_{ij} = \sqrt{|\det g|} g^{ij}$, where $\det g$ denotes the determinant of g .

A.1.2 Differential operators on a Riemannian manifold

Although we can solve the problem (2.5) in that form, the implementation of numerical methods would be easier if the domain was a subset of \mathbb{R}^n , thus we firstly rewrite the original problem in local coordinates.

A.1.2.1 The gradient

Let (Γ, g) be a surface, and let $f : \Gamma \rightarrow \mathbb{R}$ be a real-valued function over Γ . For any $p \in \Gamma$ and for any $v \in T_p\Gamma$, the gradient of f in p is a vector field defined by

$$\langle \text{grad} f, v \rangle = df_p(v). \quad (\text{A.3})$$

That is, for each $p \in \Gamma$ and for any $v \in T_p\Gamma$, $\text{grad} f$ is a vector in $T_p\Gamma$ such that the inner product with v is the derivation of f by v . In local coordinates

$$\text{grad} f = \sum_{i,j=1}^n g^{ij} \frac{\partial f}{\partial y_i} \frac{\partial}{\partial y_j}. \quad (\text{A.4})$$

A.1.2.2 The divergence

The divergence of a vector field V in local coordinates is

$$\operatorname{div}V = \frac{1}{|\sqrt{\det g}|} \sum_{i=1}^n \frac{\partial}{\partial y_i} (V_i \sqrt{|\det g|}) \quad (\text{A.5})$$

where $V = \sum_{i=1}^n V_i \frac{\partial}{\partial y_i}$.

A.1.2.3 The Laplacian-Beltrami-Operator

After determining the expressions to the gradient and to the divergence, we can combine them into a way to compute the Laplace-Beltrami-Operator ($\Delta_\Gamma : C^\infty(\Gamma) \rightarrow C^\infty$) in local coordinates

$$\Delta_\Gamma f = \operatorname{div} \operatorname{grad} f \quad (\text{A.6})$$

$$= \frac{1}{\sqrt{|\det g|}} \sum_{i,j=1}^n \frac{\partial}{\partial y_i} \left(\sqrt{\det g} g^{ij} \frac{\partial f}{\partial y_j} \right) \quad (\text{A.7})$$

$$= \frac{1}{\sqrt{|\det g|}} \sum_{i,j=1}^n \frac{\partial}{\partial y_i} \left(\mathcal{A}_{i,j} \frac{\partial f}{\partial y_j} \right), \quad (\text{A.8})$$

where $\mathcal{A}_{i,j} = \sqrt{\det g} g^{ij}$. One can find more details about these operators in (LEE, 2003).

APPENDIX B – Banach Spaces, Sobolev Spaces and Periodic function in Sobolev Space

H^1

B.1 Banach space

B.1.1 Dual space

Definition 2. If E is a Banach space, the set of the linear and continuous maps from E into \mathbb{R} is called the dual space of E and is denoted E' . If $x' \in E'$, the image $x'(x)$ of $x \in E$ is denoted by $\langle x', x \rangle_{E', E}$. The bracket $\langle \cdot, \cdot \rangle_{E', E}$ is called the duality pairing between E' and E .

B.1.2 Weak convergence

Definition 3. A sequence $\{x_n\} \in E$ is said to converge weakly to x iff

$$\forall x' \in E', \langle x', x_n \rangle_{E', E} \rightarrow \langle x', x \rangle_{E', E}. \quad (\text{B.1})$$

This weak convergence is denoted

$$x_n \rightharpoonup x \text{ weakly in } E. \quad (\text{B.2})$$

B.2 Sobolev space

B.2.1 $W_p^k(\Omega)$

Definition 4. Let k be a non-negative integer, and let $f \in L_{loc}^1(\Omega)$. Suppose that the weak derivative $D_w^\alpha f$ exist for all $|\alpha| \leq k$. Define the Sobolev norm

$$\|f\|_{W_p^k(\omega)} \equiv \left(\sum_{|\alpha| \leq k} \|D_w^\alpha f\|_{L^p(\Omega)}^p \right)^{1/p} \quad (\text{B.3})$$

in the case $1 \leq p < \infty$, and in the case $p = \infty$

$$\|f\|_{W_p^k(\omega)} \equiv \max_{|\alpha| \leq k} \|D_w^\alpha f\|_{L^\infty(\Omega)}. \quad (\text{B.4})$$

In either case, we define the Sobolev space via

$$W_p^k \Omega \equiv \{f \in L_{loc}^1(\Omega) : \|f\|_{W_p^k(\Omega)} < \infty\}. \quad (\text{B.5})$$

For $p = 2$, one denotes $W_2^k(\Omega) = H^k(\Omega)$. Suppose that $\partial\Omega$ is Lipschitz continuous. Then

$$H_0^1(\Omega) = \{u | u \in H^1(\Omega), \gamma(u) = 0\}. \quad (\text{B.6})$$

The function $\gamma(u)$ is called the trace of u on $\partial\Omega$.

Definition 5. We denote by $H^{-1}(\Omega)$ the Banach space defined by

$$H^{-1}(\Omega) = (H_0^1(\Omega))' \quad (\text{B.7})$$

equipped with the norm

$$\|F\|_{H^{-1}(\Omega)} = \sup_{H_0^1(\Omega) \setminus \{0\}} \frac{|\langle F, u \rangle_{H^{-1}(\Omega), H_0^1(\Omega)}|}{\|u\|_{H_0^1(\Omega)}}. \quad (\text{B.8})$$

B.3 Periodic functions in the Sobolev space $H^1(Y)$

Here we introduce a notion of periodicity for functions in the Sobolev space H^1 . Let Y be the reference cell defined by $Y = (0, l_1)$, where l_1 is a positive number.

Definition 6. Let $C_{per}^\infty(Y)$ be the subset of $C^\infty(\mathbb{R})$ of Y -periodic functions. We denote by $H_{per}^1(Y)$ the closure of $C_{per}^\infty(Y)$ for the H^1 -norm.

Proposition 13. Let $u \in H_{per}^1(Y)$ and $u^\#$ be its extension defined by periodicity. Then $u^\#$ is in $H^1(w)$ for any bounded open subset w of \mathbb{R} .

Definition 7. The quotient space

$$\mathcal{W}_{per}(Y) = H_{per}^1(Y)/\mathbb{R} \quad (\text{B.9})$$

is defined as the space of equivalence classes with respect to the relation

$$u \simeq v \iff u - v \text{ is a constant, } \forall u, v \in H_{per}^1(Y). \quad (\text{B.10})$$

We denote by \dot{u} the equivalence class represented by u .

Proposition 14. The following quantity:

$$\|\dot{u}\|_{\mathcal{W}_{per}(Y)} = \|\nabla u\|_{L^2(Y)}, \forall u \in \dot{u}, \forall \dot{u} \in \mathcal{W}_{per}(Y), \quad (\text{B.11})$$

defines a norm on $\mathcal{W}_{per}(Y)$.

Suppose that the coefficients $a_{i,j}$ are Y -periodic. Let f be Y -periodic and consider the problem

$$\begin{cases} -\nabla(A\nabla u) & = f & \text{in } Y \\ \langle u \rangle & = 0 \\ u & Y\text{-periodic.} \end{cases} \quad (\text{B.12})$$

A natural space for the solutions is

$$\mathcal{W}_{per,0}(Y) = \{v | v \in H_{per}^1(Y), M_Y(v) = 0\}. \quad (\text{B.13})$$

Hence, for f given in $(\mathcal{W}_{per,0}(Y))'$, the variational formulation is

$$\begin{cases} \text{Find } u \in W_{per,0}(Y) \text{ such that} \\ \int_Y A \nabla u \nabla v \, dy = \langle f, v \rangle_{(W_{per,0}(Y))', W_{per,0}(Y)} \\ \forall v \in W_{per,0}(Y). \end{cases} \quad (\text{B.14})$$

Due to the Poincaré-Wirtinger inequality, $W_{per,0}(Y)$ is a Banach space for the norm

$$\|u\|_{W_{per,0}(Y)} = \|\nabla u\|_{L^2(Y)}, \forall u \in W_{per,0}(Y). \quad (\text{B.15})$$

Theorem 5. *Let A be a elliptic matrix with Y -periodic coefficients and $f \in (W_{per,0}(Y))'$. Then problem (B.14) has a unique solution.*

B.4 Homogenization in one dimensional function space

Consider the following problem

$$\begin{cases} -\frac{d}{dx}(\lambda^\varepsilon(x) \frac{\partial u^\varepsilon}{\partial x}) = f^\varepsilon, & 0 < x < 1, \\ u(0) = u(1) = 0. \end{cases} \quad (\text{B.16})$$

In the light of the properties of our model problem it is now natural to assume a two scales asymptotic expansion for the solution $u^\varepsilon(x)$. We start by introducing the new variable y , defined as $y = \varepsilon^{-1}x$, and assume that $u^\varepsilon(x)$ can be represented as

$$u^\varepsilon(x) = w_0(x, y) + \varepsilon w_1(x, y) + \varepsilon^2 w_2(x, y) + \dots \quad (\text{B.17})$$

where the function $w_i(x, y), i = 0, 1, 2, \dots$, are assumed to be periodic in the variable y over some fixed interval Y . We introduce the operator A^ε as

$$A^\varepsilon \Psi = -\frac{d}{dx}(\lambda^\varepsilon(x) \frac{d\Psi}{dx}). \quad (\text{B.18})$$

Assuming $\Psi(x) = \Phi(x, y)$, the chain rule yields

$$\frac{d\Psi}{dx} = \frac{\partial \Phi}{\partial x} + \frac{1}{\varepsilon} \frac{\partial \Phi}{\partial y}. \quad (\text{B.19})$$

Thus

$$A^\varepsilon u^\varepsilon = -\frac{d}{dx}(\lambda^\varepsilon(x) \frac{du^\varepsilon}{dx}) \quad (\text{B.20})$$

$$= -\left(\frac{\partial}{\partial x} + \frac{1}{\varepsilon} \frac{\partial}{\partial y}\right)(\lambda(y) \left(\frac{\partial}{\partial x} + \frac{1}{\varepsilon} \frac{\partial}{\partial y}\right)(w_0 + \varepsilon w_1 + \varepsilon^2 w_2 + \dots)) \quad (\text{B.21})$$

$$= (\varepsilon^{-2} A_0 + \varepsilon^{-1} A_1 + A_2)(w_0 + \varepsilon w_1 + \varepsilon^2 w_2 + \dots) = f^\varepsilon, \quad (\text{B.22})$$

where

$$A_0 = -\frac{\partial}{\partial y}(\lambda(y) \frac{\partial}{\partial y}), \quad (\text{B.23})$$

$$A_1 = -\frac{\partial}{\partial y}(\lambda(y) \frac{\partial}{\partial x}) - \lambda(y) \frac{\partial^2}{\partial x \partial y}, \quad (\text{B.24})$$

$$A_2 = -\lambda(y) \frac{\partial^2}{\partial x^2}. \quad (\text{B.25})$$

Equating in powers of ε leads us to the following three lowest order equations

$$A_0 w_0 = 0, \quad (\text{B.26})$$

$$A_0 w_1 + A_1 w_0 = 0, \quad (\text{B.27})$$

$$A_0 w_2 + A_1 w_1 + A_2 w_0 = f^\varepsilon. \quad (\text{B.28})$$

In order to solve (B.26)-(B.28) we need the following Lemma:

Lemma 7. *Let $\zeta(y) \in L^2(\Omega)$ be Y -periodic. For the boundary value problem in Y*

$$A_0 \Psi = \zeta(y), \quad , \quad (\text{B.29})$$

where $\Psi(y)$ is Y -periodic, the following holds:

1. *There exists a solution Ψ if and only if $\langle \zeta \rangle = 0$.*
2. *If there exists a solution it is unique up to an additive constant.*

Now we note that (B.26) has the trivial solution $w_0 = 0$. Since the variable x is just a parameter in (B.26), Lemma 7 yields that $w_0(x, y)$ is a solution of (B.26) if and only if w_0 is a constant with respect to the variable y , i.e., $w_0(x, y) = u(x)$, for some sufficiently differentiable function $u(x)$. Then we have

$$A_0 w_1 = \frac{\partial \lambda}{\partial y}(y) \frac{\partial u}{\partial x}(x). \quad (\text{B.30})$$

Here again x is just a parameter and the equation may be regarded as a problem depending on the variable y only. Therefore it suffices to consider the *cell problem*

$$A_0\chi = -\frac{\partial\lambda}{\partial y}, \quad \chi(y) \quad Y\text{-periodic.} \quad (\text{B.31})$$

Now, assume that a solution $\chi(y)$ of (B.31) is given. By using the linearity and the fact that A_0 not involves differentiation with respect to x , we conclude that the function

$$w_1(x, y) = -\chi(y)\frac{\partial u}{\partial x}(x) + u_1(x) \quad (\text{B.32})$$

is also a solution of (B.31) for every sufficiently differentiable $u_1(x)$. By using Lemma 7 once more we find that (B.28) has a solution $w_2(x, y)$, Y -periodic in y , if and only if

$$\langle f - A_1w_1 - A_2w_0 \rangle = 0, \quad (\text{B.33})$$

where

$$A_1w_1 = \frac{\partial}{\partial y}(\lambda(y)\chi(y))\frac{\partial^2 u}{\partial x^2}(x) - \frac{\partial\lambda}{\partial y}(y)\frac{\partial u_1}{\partial x}(x) + \lambda(y)\frac{\partial\chi}{\partial y}\frac{\partial^2 u}{\partial x^2}(x), \quad (\text{B.34})$$

and

$$A_2w_0 = -\lambda(y)\frac{\partial^2 u}{\partial x^2}. \quad (\text{B.35})$$

The Y -periodicity of $\lambda(y)$ and $\chi(y)$ implies that

$$\langle A_1w_1 + A_2w_0 \rangle = -\langle \lambda - \lambda\frac{\partial\chi}{\partial y} \rangle \frac{\partial^2 u}{\partial x^2}. \quad (\text{B.36})$$

A function $w_2(x, y)$ exists if and only if $\chi(y)$ and $u(x)$ satisfy the relation

$$-\langle \lambda - \lambda\frac{\partial\chi}{\partial y} \rangle \frac{\partial^2 u}{\partial x^2} = \langle f \rangle. \quad (\text{B.37})$$

We say that

$$q = \langle \lambda - \lambda\frac{\partial\chi}{\partial y} \rangle, \quad (\text{B.38})$$

is the homogenized coefficient of the homogenized equation (B.37).

B.5 Some theorems of functional analysis

Theorem 6 (Lax-Milgram). *Assume that H is a Hilbert space, $B : H \times H \rightarrow \mathbb{R}$ is a bilinear functional and there exist constants $\alpha, \beta > 0$ such that*

$$|B(u, v)| \leq \alpha \|u\| \cdot \|v\|, \quad u, v \in H, \quad (\text{B.39})$$

$$\beta \|u\|^2 \leq B(u, v), \quad u \in H. \quad (\text{B.40})$$

Then for every continuous functional f on H there exists a unique $w \in H$ such that

$$B(w, v) = f(v), \quad v \in H. \quad (\text{B.41})$$

For more details see (BRENNER; SCOTT, 2008).

Theorem 7 (Bramble-Hilbert). *Let F be a linear functional on $H_p^k(R)$ satisfying*

- $|F(u)| \leq C \sum_{j=1}^k \rho^{j-N/p} |u|_{j,p}$ where C is independent of ρ and u ,
- $F(q) = 0$ for $q \in P_K$.

Then there is a constant C independent of ρ and u such that

$$|F(u)| \leq C \rho^{k-N/p} \sum_{\tau \in K} \|D^\tau u\|_{p,R}. \quad (\text{B.42})$$

For more details see (BRAMBLE; HILBERT, 1970).

B.6 Supraconvergence and Superconvergence of numerical methods

A finite difference method is called supraconvergent when it has an higher convergence order than the truncation error order measured pointwise or in the L^∞ norm, (KREISS et al., 1986) Thus for example if u is a solution of a differential problem and u_h is its approximation obtained by some finite difference method having a truncation error T_h , such that $\|T_h\| \leq Ch^s$, where h is the maximum mesh size used in the grid. If the error of the method $\|u - u_h\|$ converges to zero with order greater than s , then the method is called supraconvergent. In our case we proved in Chapter 5 that in a discrete H^1 norm the error goes to zero with order two for any non uniform mesh, even if the truncation error is of order one in the infinity norm. Then our method is supraconvergent in a discrete H^1 norm. When a such supraconvergence appear for a finite element method then the method is called superconvergent.